Behaviour And Fault-locating Methods

Of

A Train-line With Leakage

Khaled Sayed Abdol-Hamid

A Thesis
in the
Faculty of Engineering

Presented in Partial Fulfillment of the Requirements for
the Degree of Master of Engineering at
Concordia University
Montreal, Quebec

August 1983

Behaviour And Fault-locating Methods

Of

A Train-line With Leakage

Khaled Sayed Abdol-Hamid

Abstract

This research work is divided into two parts. In Part One, experiments and theoretical investigations are carried out to study the behaviour of a train-line with leakage. A mathematical model is introduced to simulate the train-line. Two numerical schemes are proposed to provide the solution. The implicit scheme is found to be better than the explicit for providing an accurate and faster solution. The investigations show that the steady-state and transient behaviour of the train-line is dependent on the leakage size and leakage location among other factors. In Part Two, two methods are formulated for fault location. One method is known as the pressure-ratio method for multiple faults, the viability of which is established by a theorem. The other method is known as the pressure-difference method, for which a theorem is formulated only for a single fault. However, experiments show that this method can be applied to multi-faults also.

ACKNOWLEDGEMENT

The author is very grateful to his thesis supervisor, Dr. R.M.H.Cheng, who so generously extended guidance, encouragement and moral support in all phases of this research.

Acknowledgement is due the late Dr. Silas Katz (1924-1982) for his contribution in the capacity of co-supervisor, his constant support, his great generosity and his proverbial kindness.

The author would like to acknowledge the contribution of Concordia University, for the facilities placed at his disposal through the Fluid Control Center, where this work was conducted.

Thanks should also go to the Natural Sciences of Engineering Research Council of canada for the partial financial support of this research.

The author would like to thank his colleagues in the Department of Mechanical Engineering for providing a conducive environment for this research. Special thanks to Mrs. C. Nadeau who skilfully and graciously participated in typing this thesis, making its preparation less of a chore.

Also many thanks are due my parents and my wife for their encouragement and moral support.

TABLE OF CONTENTS

LIST OF FIGURES

LIST OF TABLES

NOMENCLATURE

A	train-line cross-sectional area	, m^2
A_i	leakage flow area of the ith node	, m^2
a	local speed of sound ($\sqrt{\gamma R_g \theta}$)	, m/s
B	coefficient matrix	, -
$b_{\eta,K}$, $b_{\xi,K}$	system equation coefficient	, -
C	capacitance per unit length	, s^2
C_i	resistance characteristic ratio for the ith section, $\frac{R_i}{r_i}$	, -
D	transducer sensitivity threshold	, -
D_i	ratio of in-line resistance, $\frac{R_{i+1}}{R_i}$	, -
D_r	relative transducer sensitivity threshold, $\frac{D}{P_{r(0)}}$	, -
d_i	leakage flow diameter at the ith node	, m
d_p	train-line inside diameter	, m
E_i	pressure ratio, $\frac{P_i}{P_i'}$	, -
f	coefficient of friction	, -
$I_1(\nu)$	modified Bessel function of first kind of order 1	, -
K_j	position of faulty node j, $1 \leq K_i \leq N$	, -
L	inertance per unit length	, m^{-2}
l	total length of the train-line	, m
M_{i-1}	$M(X_{i-1})$, steady-state normalized mass flow through the ith section ($m/\rho_a a A$)	, -
N	total number of sections in the train-line model	, -

N_K	characteristic number ($a/l\ \omega_f$)	, -
$P_{i,j}$	$P(X_i,T_j)$, normalized pressure at distance X_i and time T_j ($\frac{p}{p_a}$)	, -
P_i	$P(X_i)$, steady-state normalized pressure at distance X	, -
P_o	P(0) normalized pressure at the head-end	, -
$P_r(X_i)$	changes of the steady-state pressure at the distance X_i	, -
$P_r(0)$	changes of the steady-state pressure at the head-end	, -
R_c	characteristic resistance of the train-line ($\frac{\Delta P}{U(0)}$)	, -
R_i	in-line normalized resistance to air flow through the ith section	, -
R_g	gas constant	, kJ/kg°K
R	resistance per unit length	, $m^{-2}.s^{-2}$
$\overline{R}^*$	average normalized resistance	, -
$\overline{R}$	average resistance per unit length	, $m^{-2}.s^{-2}$
Re	the Reynolds number	, -
r	total number of faulty nodes	, -
r_i	leakage normalized resistance at the ith section of the train-line	, -
T	normalized time, $\frac{t.a}{l}$	, -
T_D	time delay	, -
T_P	peak time	, -
T_s	steady-state time	, -

$U_{i,j}$	$U(X_i,T_j)$, normalized velocity at distance X_i and time T_j, $(\frac{u}{a})$	, -
U_i	$U(X_i)$, steady-state normalized velocity at distance X_i	, -
V	propagation speed	, m/s
X	normalized distance $\frac{x}{l}$	, -
α	gain coefficient $(\frac{P_r(X_i)}{P_r(0)})$	, -
β_i	$(\frac{P_{i-1}}{P_i})^2$, taking the function form of $\sigma_1(\beta_{i+1}, C_i)$	, -
β_N	$(\frac{P_{N-1}}{P_N})^2$, taking the function form of $\sigma_2(C_N)$	, -
Γ	propagation function per unit length	, m^{-1}/rad
γ	ratio of the specific heat of air (1.4),	-
Δ_i	normalized pressure difference at the ith section $(P_i - P_i')$	, -
ΔP	normalized pressure gradient $(P(0)-P(1))$	, -
δ	$(P_{i-1,j} - P_{i,j})$, the pressure difference between two neighbour nodes (see Appendix E)	, -
θ	absolute temperature	, °K
μ	mass flow removed per unit length	, kg/m.s
τ	wall shear stress	, N/m^2
ν	kinematic viscosity	, m^2/s
$\phi_{i,j}$	$\phi(X_i,T_j)$ normalized leakage flow $(\phi_{i,j} = \psi_{i,j}\Delta X)$	, -
ω_f	friction characteristic frequency	, rad/s

viscous characteristic frequency (laminar) , rad/s

NOTE: Physical parameters (C_i, D_i, P_i, R_i, r_i, β_i) are expressed in the unprimed form for the no-fault train-line, and in the primed form for the faulty train-line.

CHAPTER 1

INTRODUCTION

1.1 Train-Line (Brake Pipe)

Pneumatic transmission lines have been used for transmitting braking signals in trains for over 100 years. They are known as the brake pipe or the train-line of a train.

A schematic illustration of a train brake system is shown in Fig. 1.1. The system consists of a locomotive control unit situated at the head-end of the train and car control unit located at each car. The locomotive control unit consists of the compressor which supplies the working medium of the entire brake system at a suitable pressure. A brake valve assembly incorporates the control level, and the brake cylinders which are responsible for actuating the brake rigging and shoes at the locomotive only. The control car unit, similarly consists of ABD brake valve, with its combined emergency and auxiliary reservoir, as well as the brake rigging and shoes of that particular car. The locomotive control unit and the car control unit are connected together in a chain like manner by the train-line.

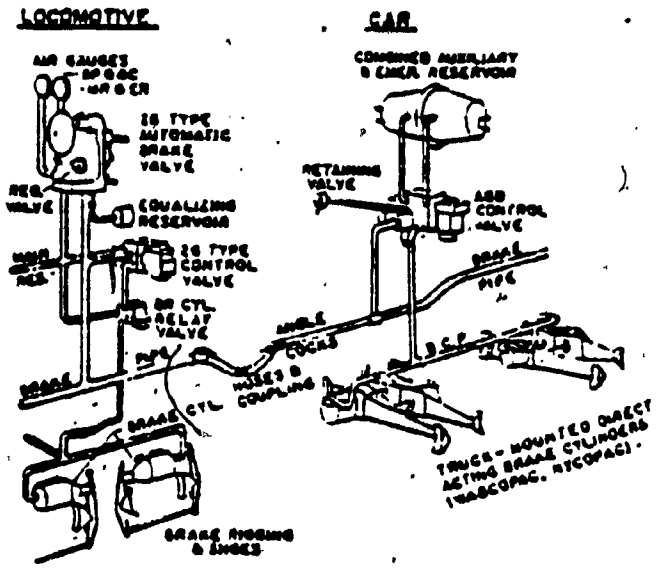

Fig. 1.1 Schematic of the Air Train-line System [Ref. 1]

The train-line, is connected by hoses at the end of each car and locomotive unit in the train, and furnishes the means of operating the automatic air brake system. The train-line provides the functions of a conduit through which the engineer communicates his commands for various degrees of brake operations to all cars in the train.

The air brake system is charged with compressed air by means of the train-line when the locomotive brake valve is in "release" position. Compressed air is stored in the reservoirs on each car. When braking is required, the locomotive control valve at the head-end of the train is opened to reduce the pressure by a controlled amount. This negative step change in pressure travels down the train-line, causing the control valve of each car to apply the brakes in succession.

Very often air brake systems have leakage to some degree. Leakage occurs primarily at the various pipe joints and fittings, gaskets and seals in devices, as well as at the hoses and hose couplings. A typical freight car has from 40 to as many as 100 joints and seals [1].

Leakage existing throughout the train reduces train-line pressure as the distance from the locomotive increases. The difference in pressure in the train-line at the rear-end point of the train and that at the locomotive

(feed valve or regulating valve setting) or the head-end is called train-line pressure gradient.

1.2 Serial Action, 'Pressure Gradient' and Leakage

In practice leakage is unavoidable, standards of acceptable amount of leakage are provided by the AAR Rules [3]. For a train to be satisfactory for road movement at an initial terminal, the AAR Rules specify that "all cars have operative brakes and that the train-line leakage not exceed 5. psi/min (34. kPa/min). Rear end train-line pressure must be within 15 psi (103 kPa) of the locomotive feed valve train-line setting (but not less than 515 kPa (60 psig))".

It has to be understood that the train-line plays the vital role of supplying pneumatic power to operate the brake cylinders, and to transmit the control signal (brake signal) from the locomotive all the way to the last car of the train. This is known as "serial action". As a result of that, the brakes on each vechile apply in succession as the train-line reduction progresses through the train.

Brake action transmission speed (which will be referred to as propagation speed, V) is faster than 400 ft/s (130 m/s) [1]. In service application, this is accomplished by the initial quick service. Initial quick

service action travels through the train at speed of approximately 130 to 200 m/s (400 to 600 ft/s). In emergency, rapid venting of the train-line pressure at each car results in transmission speed of 300 to 315 m/s (900 to 950 ft/s). In all cases the speed is less than the acoustic speed, i.e.sub-acoustic. Noruma et al [2] argue that this sub-accoustic speed is due to attenuation of the pressure signal, the relation between propagation speed and the several contributing factors has not been developed into a usable closed-form. The important factors are however the direction of the pressure step at the head-end (discharging or charging) and the mimimum pressure change detectable by the sensory portion of the brake valve, before braking action can take place (in other words, the threshold sensitivity of the transducer). But, one of the most significant factor is the presence of the leakage (size and distribution). A train-line leakage over 344 kPa/min (5 psi/min) or pressure gradient over 103 kPa(15 psi) on a train can cause erratic brake response, because this may exceed the ability of the brake valve to maintain control of the train-line pressure, undesired applications and releases may result or brakes may not respond satisfactory.

If leakage is concentrated toward the rear of the train, the effect on gradient will be significantly greater.

There is a need for a mathematical model for the train-line to quantify the relationships between leakage size, leakage distribution, charging, discharging, threshold sensitivity of the brake valve, propagation speed, peak velocity flow rate, peak time, air supply and pressure gradient. These relationships may be established by studying the transient behaviour and the steady state behaviour of the train-line. In this research, the propagation speed, peak velocity and peak time are used to study the transient behaviour of the train-line, whereas the pressure gradient and the air supply flow rate are used to study the steady state behaviour of the train-line. There is also a need for a quick and efficient method to locate excessive leakages, wherever they exist, which is based on an analytical understanding of the interplay between pressure gradient in a train-line and the train-line leakages.

It is important at this juncture to define the terms "no-fault" and "fault". In the context of this research, a train-line that exhibits an acceptable amount of leakage is, in a "no-fault" condition to begin with. Subsequently, a faulty situation, which developes additional leaks or if some existing leaks become more severe, arises as a result of either normal usage or mishandling of the train.

1.3 Review of Previous Work

This Section reviews the previous research work done on the transient behaviour of fluid transmission lines and the fault detection in networks.

1.3.1 Transient Behavior of Fluid Transmission Lines

The transient behaviour of fluid transmission lines has been the subject of many investigations. One of the earliest investigations into transient response is that of Schuder and Binder [4]. They developed a theory and performed experiments for the step response of long pneumatic lines terminated by volume or blockage. Their theory does not consider heat transfer effects and assumes a constant laminar friction. The experimental results lag behind the theoretical and showed more attenuation. Nichols [5] included the effects of heat transfer and the change of the laminar velocity profile shape with frequency, to derive a frequency dependent propagation function. Simultaneously, Brown [6, 7], developed the propagation operator in terms of Laplace transforms. The propagation operator given by Nichols and Brown has been verified by numerous experiments with frequency signals. However, the transient response of a blocked line is quite a complicated function of the propagation operator, Cheng,

Katz and Abdol-Hamid [8] showed that the semi-infinite line solutions can be used to predict the transient response of the blocked line. They also modeled the brakepipe as a blocked pneumatic RLGC (Resistance, Inductance, Conductance, Capacitance) transmission line to demonstrate that the propagation of the braking signal is caused by cutting off the high-frequency components of the signal, and to predict the propagation speed for various pipe parameters and working conditions. A complete description of Ref. [8] can be found in Appendices F, G and H. This analysis is only applicable if the leakage is concentrated at the rear-end.

For a matched line (semi-infinite line) several solutions have been presented. Kantola [9] obtained an infinite series representation for the impulse and step response and Karam [10] transformed a simplified frequency domain model into the time domain. Brown and Nelson [11] found the step response solution of liquid lines from the frequency response. Katz [12] developed the direct conversion of the exact frequency response for terminated transmission lines into transient response.

The method of characteristics has also been used by many researchers to solve the transients in fluid transmission lines. Zielke [13] and Brown [14] have presented a quasi-method of characteristics that takes into

account frequency dependent shear and heat transfer. This method has been applied by Krishner and Katz [15] to find the step and pulse response of blocked lined. Ho [16] applied this method to find the transient behaviour of the train-line.

It is difficult to employ any of the methods mentioned above to predict the transient behaviour of the train-line with leakage, because of the complex boundary condition (the presence of leakage).

Funk and Robe [17] developed the method of lines for solving the governing, one-dimensional partial differential equations. They used the finite difference technique in the space coordinate, X, to reduce the governing one-dimentional partial differential equations to a set of differential-difference equations which are solved using a Kutta-Fehlberg algorithm. Their mathematical model takes into account the changing of the wall shear stress and the flow is assumed to be quasi-steady for the purpose of estimating friction pressure losses. Calculations were performed to compare with the data and analytical results presented by Schuder and Binder [4]. The calculations are in good agreement with these data as well as with their data. It is more convenient to use the finite difference technique to solve the train-line problem, because the ease in formulating the leakage boundary condition. The method

of lines has been used by Ho [16]. He assumed that the friction factor is constant during the entire transient, that the influence of the acceleration term $\frac{\partial u}{\partial t} + u \frac{\partial u}{\partial x}$ can be neglected. Because of these assumptions, he found that the percentage error between the experimental and theoretical result, is within 10%. In this thesis, the mathematical model takes into account the change of the friction factor, f, during the entire transient and contains the acceleration term $\frac{\partial u}{\partial t} + u \frac{\partial u}{\partial x}$.

These considerations reduce the percentage error between the experimental and the theoretical result to a value of 3%.

1.3.2 Fault Diagnosis of Networks

Substantial work has been done in fault detection and analysis in ladder networks. In 1977, Katz and Cheng [18] first proposed a ladder network model for the train-line for the purpose of studying the pressure distribution in steady state conditions with the head-end (locomotive) of the line held at a constant pressure level. The network consists of a number of concatenated sections, each made up of an in-line nonlinear flow resistance, and shunt resistance. In 1979, Katz, Cheng and Aula published their work in connection with the fault-location in linear resistor network [19] and non-linear network [20],

culminating in an ASME paper in the same year describing a number of methods of fault locating for a train-line provided that there is only one fault leak [21].

While considerable progress has been made in the area of fault diagnosis of networks, many of the papers concentrate on general principles and do not consider specific networks. The readers may refer to such work as Saeks and Liberty [22]. The bibliography by Rault et alias [23] review the 193 papers of fault detection and location of analog circuits. Other researchers, including Berkowitz [24], Shekel [25], Gefferth [26], and Trick and Chien [27], make significant contribution to different types of networks.

Berkowitz [24] derives the conditions for the single-fault solwability. When applied to ladder networks, this implies completely specifying the network by measurement of the potential variable at each ladder section or node, or, in the case of the pneumatic train-line, by pressure readings at the individual cars, or groups thereof. Shekel [25], Gefferth [26] suggest using two network functions to locate the single fault, a technique which proves to be worth pursuing. Trick and Chien [27] take a more quantitative approach, stating categorically that in a single-fault network, the potential change at the faulty impedance is almost as high in

magnitude as at any other circuit element.

In the specific area of location of faulty leaks of a train-line, Aula, Cheng and Katz [20] proposed several methods, which are applicaple to single faults, and there is no rigorous proof given. They suggested the extension of single fault location methods to multiple fault location. Developement of a method to locate multiple faulty leaks however is a rather complicated task.

1.4 Scope of the Thesis

This research is divided into two parts. The First part (Chapters 2, 3 and 4) is an investigative and theoretical analysis of a train-line model in the Fluid Control Center of this University to study the transient behaviour and the steady-state behaviour of the train-line with leakage. Two schemes are developed to solve the governing one-dimensional partial differential equations. The Second part (Chapter 5) deals with the development of 2 methods to locate multiple faulty leaks in the train-line. A proof is provided for each method to substantiate its viability.

This entire thesis is divided into six chapters. The first Chapter briefly introduces the train-line, the air brake of the freight train and its operation. It also

reviews the previous work has been done in the area of transient response of fluid transmission lines as well as detection and location of fault in pneumatic train-line model.

The second Chapter gives a description of the train-line laboratory model and formulation of the train-line mathematical model. Then, two finite difference schemes are completely developed. Firstly, the method of lines (explicit scheme), which is proposed by Funk and Robe [17]. But, they apply this model for no leakage along the train-line. Secondly, the implicit scheme is formulated in such a way that the requirement to maintain a certain relationship between the time increment t and the length increment x is relaxed. This feature offers the opportunity for a more flexible scheme than the previous method. Finally, the computational results, using both finite difference schemes are performed to compare with the data and analytical results presented by Funk and Robe [17] as well as the train-line laboratory model experimental results. The calculations are in better agreement with their data than their analytical results (the method of lines) and the computation time is more or less half their computation time, same observations are made to the laboratory results. Because of these reasons the implicit scheme is preferred for solving the train-line mathematical model.

In the third Chapter, two test set-ups are descriped to investigate the effects of the leakage location and size on the train-line behaviour. In this Chapter, the steady state behaviour of the train-line is discussed in detail. The inlet velocity and the pressure gradient are chosen to represent the train-line.

In the fourth Chapter, three experimental tests are employed to study the transient behaviour of the train-line, adding three more factors to the leakage factor. The peak velocity and peak time as well as the propagation speed are chosen to represent the train-line in this study. The mathematical and the laboratory models have been used to quantify the relationships between, leakage distribution, leakage size, and the directions of the pressure step applied at the head-end (charging and discharging), sensitivity of the train-line control valves 6.9, 13.8 or 20.7 kPa (1,2 or 3 psi), peak velocity and peak time as well as propagation speed. A discussion, and comparison between, the experimental and analytical results are also introduced in the same Chapter.

The fifth Chapter deals with formulation of the nonlinear model of the train-line, and two methods are developed for locating multiple faulty leaks. Theorem 1 (the ratio method) has been formulated with rigorous proof. Similarly, Theorem 2 (the difference method) is formulated

with proof for the train with single faulty leakage only. The difference and the ratio methods are demonstrated to be applicable to the nonlinear train-line model both by simulation and experimentation on the laboratory train-line model.

The last Chapter briefly summarizes the entire research and presents some suggestions for further work.

PART ONE

CHAPTER 2

NUMERICAL SOLUTIONS

OF

THE TRAIN-LINE MATHEMATICAL MODEL

2.1 Introduction

The transient response of fluid transmission lines has been intensively studied by many researchers during the past twenty years and more. Liquid transmission lines have been studied by Brown [6] and Kantola [9] among others. Pneumatic transmission lines have been studied by Schuder and Binder [4], Nichols [5], Karam [10], Katz [12], Funk and Robe [17], Shute, Wrigh, Taft and Banister [28] and others.

In many of the analytical descriptions of transient gas flow in tubes, investigators normally make certain simplifying approximations in order to obtain linear equations. Usually these involve neglecting the convective acceleration term in the Momentum Equation [4] & [10] and the spatial variation of density in the Continuity Equation [4] & [5]. In these analyses the friction losses are often described by Poiseuille's Law which implies a quasi-steady flow approximation. In fact frictional losses depend on the velocity gradient at the wall which, in turn, depends on the transient radial velocity distribution, and may be properly

accounted for with a two-dimensional problem of the transient flow [6]. In this study, the train-line can be treated as one-dimensional flow problem as suggested by Cheng, Katz and Abdol-Hamid [8], Ho [16], and Funk and Robe [17].

Sec. (2.2) generally describes the train-line laboratory model. Different arrangements for this model will be used in the subsequent section. Then, the one-dimensional equations describing the unsteady flow and pressure in a train- line mathematical model (as suggested by [8], [16] & [17]) are formulated in Sec. (2.3). The train-line governing equations are a system of nonlinear hyperbolic partial differential equations. In Sec. (2.4), two finite difference schemes are employed to solve these equations. Those schemes are the explicit scheme, referred to as method of lines, and the implicit scheme. The method of lines has been used by Funk and Robe [17] for predicting the transient response of no-leakage pneumatic transmission line. The broadest of the implicit scheme applications is in unsteady flow calculations [29], because it is more stable than any other finite difference scheme. Finally, in Sec. (2.5), the implicit scheme, the method of lines and the experimental results are compared with one another. These comparisons demonstrate the validity of the implicit scheme over the method of lines for solving the train-line mathematical model, Sec. (2.6) briefly summarizes the result of this chapter.

2.2 Train-Line Laboratory Model

The train-line laboratory model is shown in Fig. 2.1. This model consists of a number of sections of steel pipes approximately 17.2 m (56.4 ft) in length. Each of the sections is made up by five pipes of 3.05 m (10 ft) in length and 6.4 mm (1/4 in) inside diameter, connected together by plastic tubes of 1/2 m (1.5 ft) in length, each bent into a semi-circle. The leakage in each section is simulated by an orifice of known size. A cross is fitted at the end of each section so that a toggle valve and an orifice may be located. The purpose of the toggle valve is to permit the measurement of transient or steady state pressure at each node.

A regulated supply air 608 kPag (88 psig) is provided at the head-end of the model. The pressure transducers have an accuracy of 0.5%. A digital multimeter of 0.04% accuracy is used to provide the steady state pressure read out. A storage oscilloscope is used to obtain the transient pressure output of the transducers. A solenoid valve is used to change the pressure level at the head-end (Charging or Discharging).

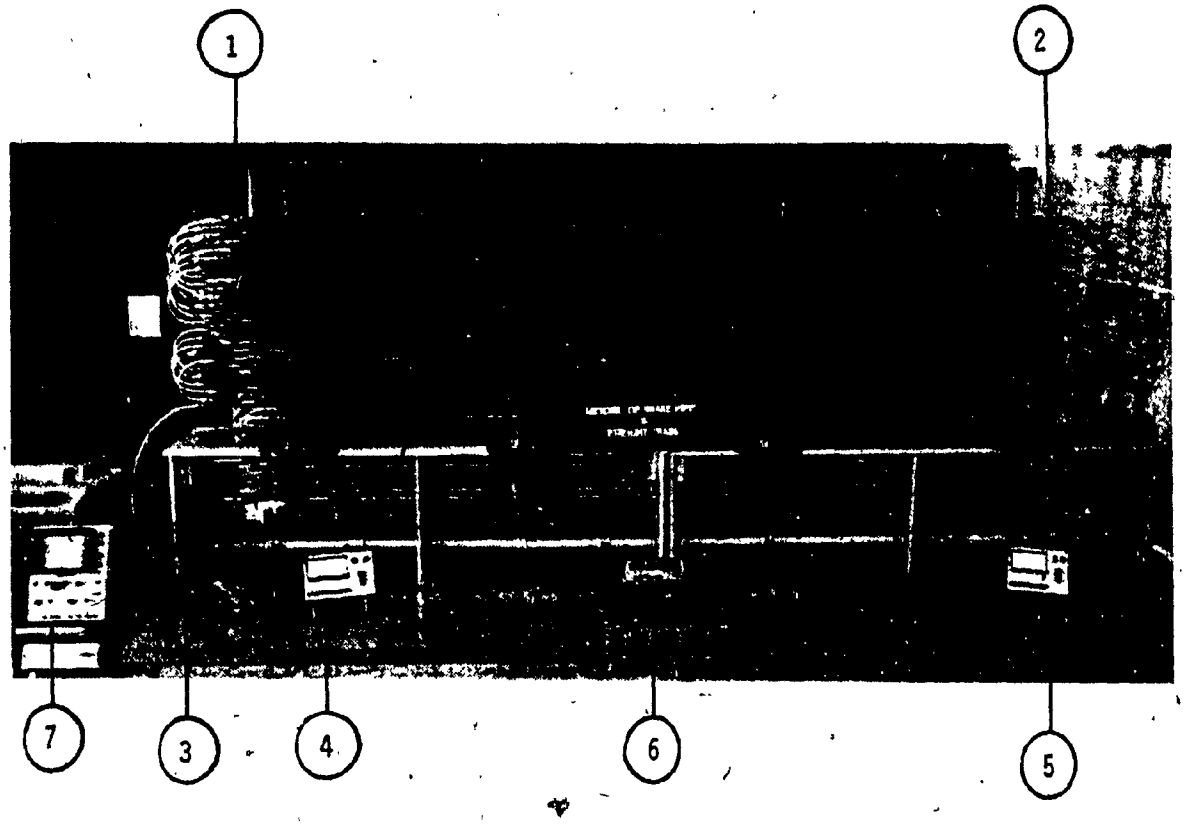

1- Head-end, H.E.

2- Rear-end, R.E.

3- Regulator

4- H.E. Transducer

5- R.E. Transducer

6- Digital Multimeter

7- Storage Oscilloscope

Fig. 2.1 Train-line Laboratory Model

2.3 Train-Line Mathematical Model

The laws of Conservation of Mass, Momentum and Energy precede the governing equations (the derivation of these equations is available in Ref. 30 as well as in Appendix A). The governing equations , combined with an Equation of State for the train-line mathematical model with mass flow removed per unit length (leakage flow μ) are described as follows:

Continuity Equation

$$\frac{\partial \rho}{\partial t} + u \frac{\partial \rho}{\partial x} + \rho \frac{\partial u}{\partial x} + \mu/A = 0 \qquad (2.1)$$

where

$\rho = \rho(x,t)$ is the air density inside the train-line (kg/m^3) as a function of distance x (m) and time t (s). where x is measured from the head-end of the train-line.

$u = u(x,t)$ is the air velocity inside the line as a function of distance x, and time t, m/s.

A = cross-sectional area of the train-line, m^2

μ = leakage flow per unit length, kg/(s.m).

Conservation of Momentum

$$\frac{\partial u}{\partial t} + u\frac{\partial u}{\partial x} + \frac{1}{\rho}\frac{\partial p}{\partial x} + 4\frac{\tau}{\rho d_p} = 0 \qquad (2.2)$$

where,

$p = p(x,t)$ is the air pressure inside the line as a function of distance x, time t, kPa

Where τ is the wall shear stress, which is defined in a number of standard texts [31] & [32] as:

$$\tau = \frac{f\rho u^2}{8}\frac{u}{|u|} \qquad (2.3)$$

where f is the wall friction factor. $\frac{u}{|u|}$ in Eqn. (2.3) is included to account for the "opposing motion" quality of friction. d_p is the internal diameter of the train-line.

But the friction factor f is a function of the Reynolds number Re.

where,

$$Re = \frac{ud_p}{\nu} \qquad (2.4)$$

ν is the kinematic viscosity of the air m^2/s

$\propto \frac{1}{p}$

Therefore

$$f = F\ (\rho, u, d_p) \tag{2.5}$$

(See Appendix B for the relationship between the friction factor f and the Reynolds Number Re)

Equation of State (for perfect gas)

$$\rho = \frac{p}{R_g \theta} \tag{2.6}$$

where

R_g = gas constant, kJ/(kg.°K)

θ = local temperature (assumed constant for isothermal flow), °K.

The governing equations are nondimensionalized by means of the following definitions.

$$U = \frac{u}{a} \qquad P = \frac{p}{p_a} \qquad \Psi = \frac{\mu}{\mu_a}$$
$$X = \frac{x}{l} \qquad T = \frac{t \cdot a}{l} \tag{2.7}$$

where,

a = the local speed of sound, m/s.

l = train-line total length, m,

$\mu_a = (\rho_a\ a\ A)/l$, kg/m.s.

p_a = local atmospheric pressure, kPa.

The final nondimensional equations are obtained after eliminating ρ from Eqns. (2.1) and (2.2), using Eqn. (2.6), and τ from Eqn. (2.2), using Eqn. (2.3), may be rewritten as

$$\frac{\partial P}{\partial T} + U \frac{\partial P}{\partial X} + P \frac{\partial U}{\partial X} + \Psi = 0 \qquad (2.8)$$

$$\frac{\partial U}{\partial T} + U \frac{\partial U}{\partial X} + \left(\frac{R_g \theta}{a^2}\right) \frac{1}{P} \frac{\partial P}{\partial X} + \left[f \frac{1}{2d_p} \cdot \frac{U}{|U|} \right] U^2 = 0 \qquad (2.9)$$

The Continuity Eq. (2.8) and Momentum Eq. (2.9) form a pair of nonlinear partial differential equations in terms of two dependent variables, velocity U and pressure P, and two independent variables, distance along the pipe line X and time T.

At this point, let us describe the train-line mathematical model as shown in Fig. 2.2. The train-line is a continuous network model, consisting of N sections of equal lengths (ΔX). Let $P_{i,j}$ and $U_{i,j}$ be defined as the nondimensionalized dependent variable P and U at grid points $X=X_i$ ($0 \le X_i \le 1$) and $T=T_j$ ($0 \le T_j \le \infty$) (see Sec. (2.4)). The nondimensionalized leakage flow $\Psi_{i,j}$ may be absent from node i

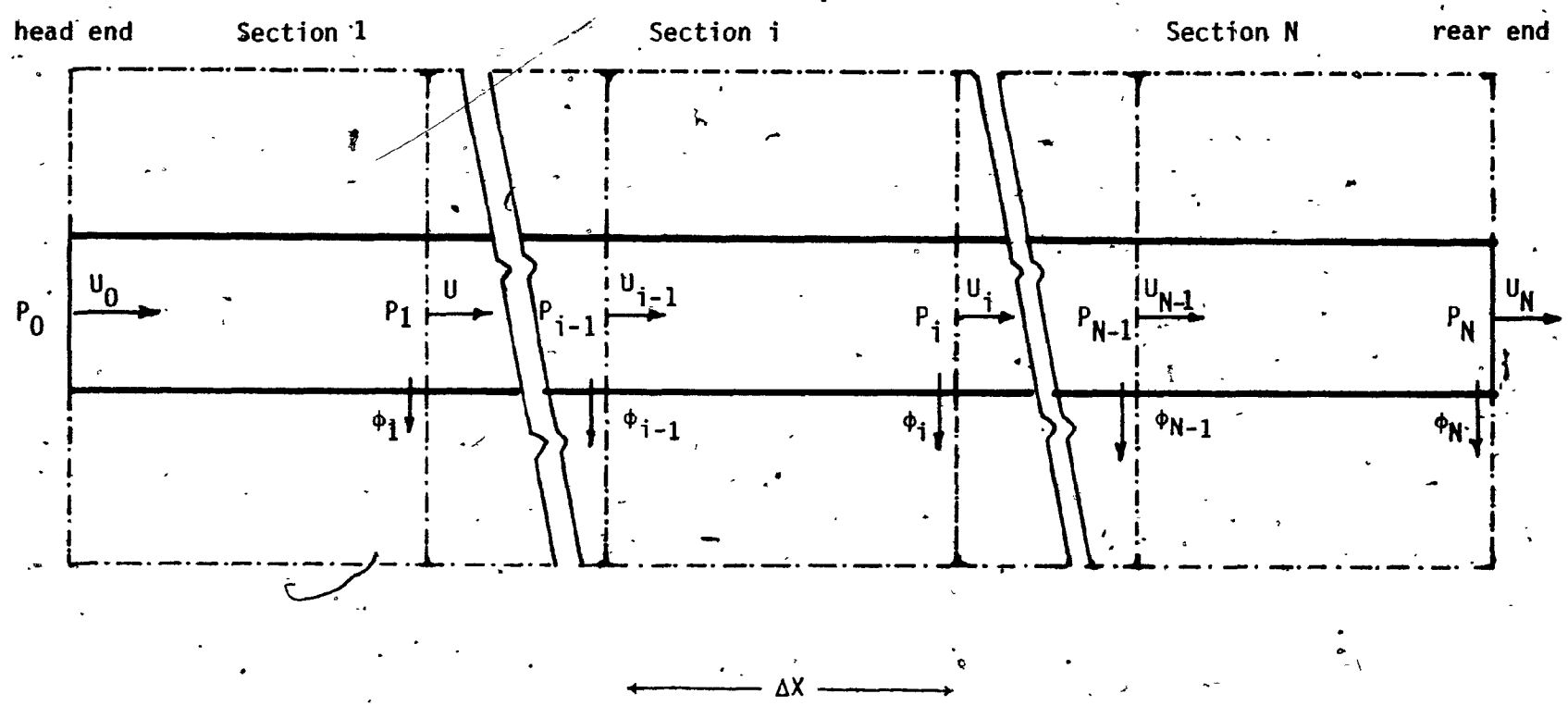

Fig. 2.2 Train-line Mathematical Model at T_j

where,

$$\Psi_{i,j} = \frac{\phi_{i,j}}{\Delta X} \tag{2.10}$$

and $\phi_{i,j}$ is a function of the leakage pressure at the ith node $P_{i,j}$ and the leakage size A_i for subsonic flow, and a function of the leakage size only for sonic flow (see Appendix C).

Funk and Robe [17] have used the method of lines to solve the mathematical model Eqns. (2.8) and (2.9) -this method is completely described in Sec. (2.4.1)- but the description of their mathematical model does not include,

1- leakages along the pneumatic transmission line,
2- $\frac{U}{|U|}$, which is used in this study to account for the "opposing motion". However, Funk and Robe might have included it in the computer program.

Ho [16] has also used the method of lines to solve the mathematical model equations. But he assumed that,

1- the friction factor, f, is constant during the entire transient period,

2- the influence of the acceleration term $\frac{\partial u}{\partial t} + u \frac{\partial u}{\partial x}$ in Eqn. (2.2) can be neglected.

Because of these assumptions, he found that the percentage error between the experimental and theoretical results was within 10%. In this study, the effects of the friction factor by not assuming f to be constant during the entire transient period, and the acceleration term $\frac{\partial u}{\partial t} + u \frac{\partial u}{\partial x}$, are taken into account to reduce the discrepancy between the experimental and theoratical results. The friction factor is evaluated at each time step, using Eqn. (2.5).

Appendix F describes an analytical model for blocked pneumatic RLC transmission line with leakage concentrated at the rear-end, which was previously proposed by Cheng, Katz and Abdol-Hamid [8]. The relation between the semi-infinite line and the blocked line is shown in Appendix G

2.4 Numerical Method Solution of Equations (2.8) and (2.9)

As mentioned in Sec. (1.4.1) finite difference method is the most appropriate method which can be used to solve Eqns. (2.8) and (2.9). The two finite difference schemes

commonly used are the explicit scheme (referred to as method of lines hereafter) and the implicit scheme. Both schemes provide a stable and accurate solution (the accuracy is established in Sec. (2.5)). These schemes will be compared with one another (refer Sec. (2.5)) and the implicit scheme will be shown to be the most appropriate.

In order to approximate the solution of Eqns. (2.8) and (2.9) by the finite difference techniques, a network of grid points is first established throughout the region of $0 \leq X_i \leq 1$ and $0 \leq T_j \leq \infty$, as shown in Fig. 2.3 with grid spacing ΔX and ΔT. where

ΔX = the normalized distance step size.

$= 1/N$

ΔT = the normalized time step size.

N = the number of train-line sections.

Referring to Fig. 2.3, the line $X = X_i$ and $T = T_j$ are called the grid lines and their intersections are called the grid points (mesh points).

Before proceeding to solve Eqns. (2.8) and (2.9), it is very important to consider the following:

(a) Differential Equation

$$\frac{\partial P}{\partial T} + U \frac{\partial P}{\partial X} + P \frac{\partial U}{\partial X} + \psi = 0 \qquad (2.8)$$

$$\frac{\partial U}{\partial T} + U \frac{\partial U}{\partial X} + \frac{G_1}{P} \frac{\partial P}{\partial X} + G_2 U^2 = 0 \qquad (2.9)$$

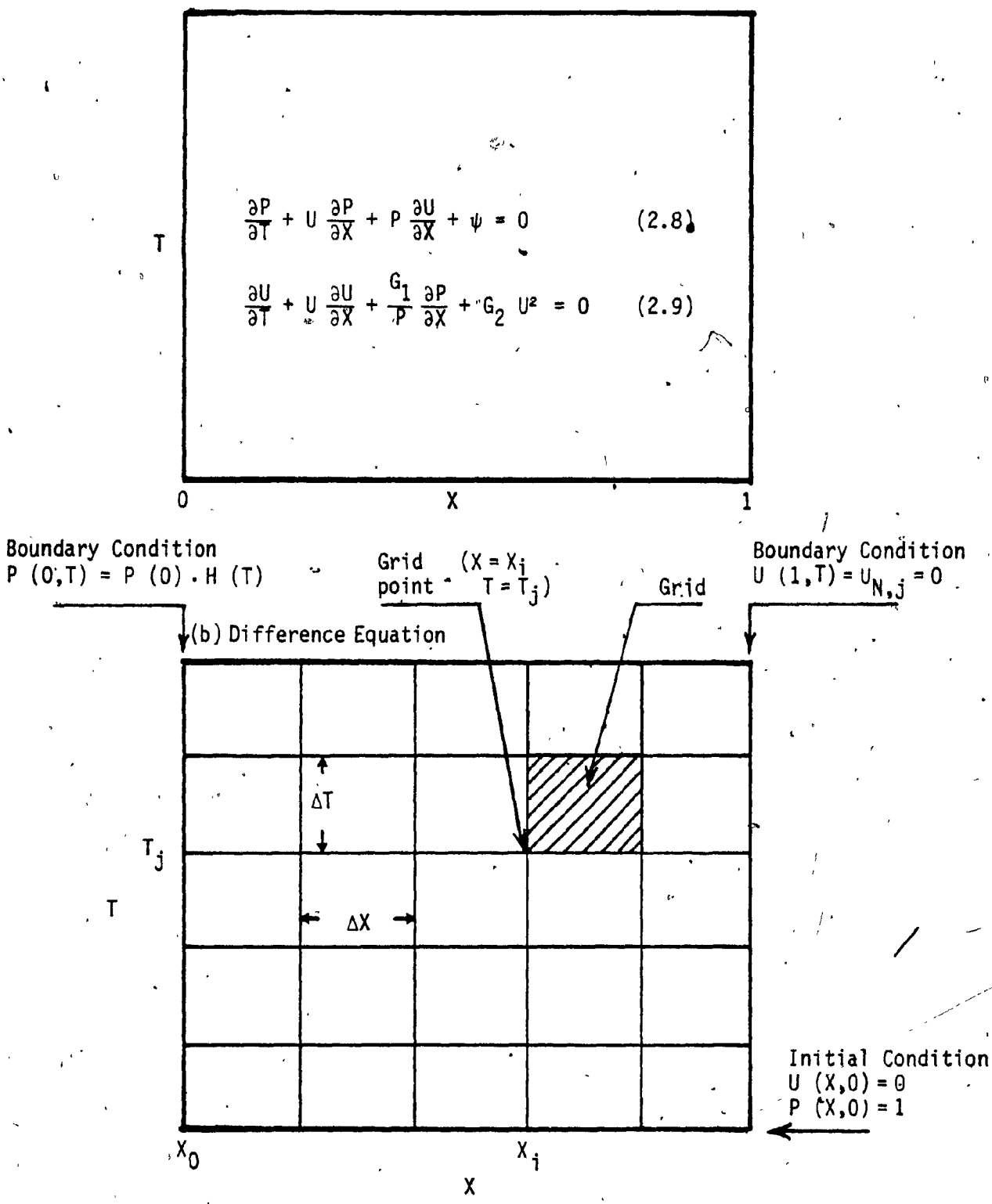

Fig. 2.3 Numerical Simulation of Eqns. (2.8) and (2.9)

1- the finite difference in space has to be either backward difference or central difference [29]. Because, the pressure information is always transmitted from the head-end to the rear-end of the train-line.

2- the highest time increment ΔT which may be chosen to speed-up the computational time is

$$\left.\begin{aligned} \Delta T &= \Delta X \\ &= \frac{1}{N} \end{aligned}\right\} \quad (2.11)$$

because the information of the pressure disturbance in the train-line are transmitted with the local speed of sound [29]. The effect of the continuum speed $U(X,T)$ on the information speed may be neglected during the entire transient ($U(X,T) \ll 1$, $T > 1$)- see Sec. 2.4.

Before proceeding any further, it is necessary to describe the boundary and initial conditions for the train-line problem. The boundary conditions of this problem are the pressure at the head-end $P(0,T)$ and the velocity at the rear-end $U(1,T)$ during the entire transient period.

$$\left.\begin{aligned} P(0,T) &= P(0)\,H(T) \\ U(i,T) &= 0 \end{aligned}\right\} \quad (2.12)$$

$$\text{where,} \quad \left.\begin{aligned} H(T) &= 1 \qquad T \geq 0 \\ &= 0 \qquad T < 0 \end{aligned}\right\} \quad (2.13)$$

Any simulation procedure will assuming the following initial conditions [1]:

$$\left.\begin{aligned} U_{i-1,0} &= 0 \qquad 1 \leq i \leq N \\ P_{i,0} &= 1 \end{aligned}\right\} \quad (2.14)$$

2.4.1 Method of Lines

Funk and Robe [17] have proposed the method of lines to solve equations (2.8) and (2.9) for pipe line without leakages ($\Psi = 0.0$).

The method of lines consist of approximating a set of

---

[1] Note that any computational simulation always starts from these fictitious initial conditions for the pressure and the velocity. Pressure boundary condition is applied at the head-end P(0,T) till the train-line reaches its steady-state $P(X,T_0)$ & $U(X,T_0)$ (actual intial conditions). Then the actual simulation is started from $T = T_0$.

partial differential equations by a system of ordinary differential equations. This is achieved by keeping one coordinate continuous (T) and approximating the derivatives in the other coordinate (X) by finite difference. The approximate solutions to the partial differential equations are thus obtained along lines parallel to the axis of the continuous coordinate, using the backward difference in space (as suggested in this chapter) for the terms $\frac{\partial P}{\partial X}$ and $\frac{\partial U}{\partial X}$ from Eqns. (2.8) and (2.9) as follows:

$$\frac{\partial P_{i,j}}{\partial X} = \frac{P_{i,j} - P_{i-1,j}}{\Delta X} \tag{2.15}$$

$$\frac{\partial U_{i,j}}{\partial X} = \frac{U_{i,j} - U_{i-1,j}}{\Delta X} \tag{2.16}$$

Substituting Eqns. (2.15) and (2.16) into Eqns. (2.8) and (2.9), and $\Psi_{i,j}$ by $\frac{\phi_{i,j}}{\Delta X}$ from Eqn. (2.10) (the relationship between $\phi_{i,j}$ and $P_{i,j}$ is described in appendix C as $\phi_{i,j} = K_{i,j}(\frac{d_i}{d_p})^2 P_{i,j}$) leads to the 2N first-order ordinary differential difference equations as follows:

$$\frac{dP_{i,j}}{dT} = \frac{1}{\Delta X} \left\{U_{i,j}(P_{i-1,j} - P_{i,j}) + P_{i,j}(U_{i-1,j} - U_{i,j}) - K_{i,j}(\frac{d_i}{d_p})^2 P_{i,j}\right\} \qquad 1 \le i \le N \tag{2.17}$$

$$\frac{d\,U_{i-1,j}}{dT} = \frac{1}{\Delta X} \left\{ U_{i-1,j}\,(U_{i-1,j} - U_{i,j}) + \frac{G_1}{\bar{P}_{ij}}\,(P_{i-1,j} - P_{i,j}) - G_2\,U^2_{i-1,j}\,\Delta X \right\} \qquad 1 \leq i \leq N \qquad (2.18)$$

where,

$$G_1 = \frac{R_g\theta}{a^2}, \qquad G_2 = \frac{f1}{2d_p}\,\frac{U_{i-1,j}}{|U_{i-1,j}|}, \qquad \bar{P}_{i,j} = \frac{P_{i,j} + P_{i-1,j}}{2} \qquad (2.19a)$$

$$K_{i,j} = \sqrt{2}\left\{ \frac{[P_{i,j}]^{-\frac{2}{\gamma}} - [P_{i,j}]^{-\frac{\gamma+1}{\gamma}}}{\gamma - 1} \right\}^{\frac{1}{2}} \qquad (2.19b)$$

The Boundary Condition Equations

for i = 1 Eqn. (2.17) will be

$$\frac{dP_{1,j}}{dT} = \frac{1}{\Delta X} \left\{ P_{1,j} \left[U_{0,j} - 2U_{1,j} - K_{1,j} \left(\frac{d_1}{d_p}\right)^2 \right] + P_0 U_{1,j} \right\} \qquad (2.20)$$

for i = N Eqn. (2.18) will be

$$\frac{d\,U_{N-1}}{dT} = \frac{1}{\Delta X} \left\{ U^2_{N-1,j}(1 - G_2\Delta X) + \frac{G_1}{\bar{P}_{N,j}}(P_{N-1,j} - P_{N,j}) \right\} \qquad (2.21)$$

Before proceeding to integrate Eqns. (2.17) and (2.18), it is important to consider the stability limitation of the method of lines as an explicit method. Based on the analysis which is suggested by Ref-33, the typical stability limitation for Eqn. (2.18) without taking the friction term into account is the Courant number restriction,

$$(|\tilde{U}| + 1)\frac{\Delta T}{\Delta X} \leq 1 \tag{2.22}$$

where $|\tilde{U}| + 1$ is the information speed which carries the information in each computational time step; $\tilde{U}$ is the maximum in-line velocity $U(X,T)$, and $\frac{\Delta X}{\Delta T}$ is the computional information speed. But the maximum value for $U(X,T)$ is close to unity, which means the best integration time step for the stability of the solution is,

$$\frac{\Delta T}{\Delta X} \leq \frac{1}{2} \tag{2.23}$$

The differential Eqns. (2.17) and (2.18) may be numerically integrated by using a Kutta-Fehlberg algorithm. The Kutta-Fehlberg is one of the numerical integration schemes [30] employed to solve the simultaneous first order differential equations . This is a fourth-order integration scheme with provision to adjust the integration step size automatically to an optimum size according to specified error tolerance ε. ε is the relative error of the dependent variables between the Runge-Kutta fourth and fifth order solution methods. The metnod of lines has local truncation error $O(\Delta X + \Delta T^4)$ where ΔT is the integration step size and ΔX is the normalized length of the section.

2.4.2 Implicit Scheme

The finite difference procedure consists of approximating a set of partial differential Eqns. (2.8) and (2.9) by a system of nonlinear algebraic equations, each equation containing four unknowns. This is achieved by taking the finite difference in the X and T coordinates. In this train-line problem (30. m ≤ l ≤ 260 m), to reduce the number of unknowns from four to three and avoid the nonlinearity of these equations, the terms of Eqns. (2.8) and (2.9) may be formulated as follows:

$$\frac{\partial P_{i,j+1}}{\partial T} = \frac{P_{i,j+1} - P_{i,j}}{\Delta T} \tag{2.24a}$$

$$\frac{\partial U_{i-1,j+i}}{\partial T} = \frac{U_{i-1,j+1} - U_{i-1,j}}{\Delta T} \tag{2.24b}$$

$$P_{i,j} \frac{\partial U_{i,j+1}}{\partial X} = P_{i,j} \frac{U_{i,j+1} - U_{i-1,j+1}}{\Delta X} \tag{2.24c}$$

$$\frac{1}{\overline{P}_{i,j}} \frac{\partial P_{i,j+1}}{\partial X} = \frac{1}{\overline{P}_{i,j}} \frac{P_{i,j+1} - P_{i-1,j+1}}{\Delta X} \tag{2.25d}$$

$$U_{i-1,j} \frac{\partial P_{i,j}}{\partial X} = U_{i-1,j} \frac{P_{i,j} - P_{i-1,j}}{\Delta X} \tag{2.25e}$$

$$U_{i,j} \frac{\partial U_{i,j}}{\partial X} = U_{i,j} \frac{U_{i,j} - U_{i-1,j}}{\Delta X} \tag{2.25f}$$

$$U^2_{i-1,j+1} \cong U_{i-1,j+1} \, U_{i-1,j} \tag{2.25g}$$

For a limited number of experimental data, this scheme gives a better result in comparison with the method of lines result (see Sec. (2.5)). The time increment ΔT is chosen to be equal to ΔX (as suggested earlier in this Section) and it does not affect the stability of the solution. This time increment ($\Delta T = \Delta X = \frac{1}{N}$) decreases the computer time in the same way as the above mentioned scheme does. A complete analysis for the validation of the implicit scheme, for a wide range of the train-line dimensions (l , d_p) and working conditions, was not necessary in the present investigation. Such an analysis would be very complex and cumbersome. A similar analysis for the method of lines has not been done yet to the best of the author's knowledge. Nevertheless, the validation of the implicit scheme is provided, for a particular set-up (l = 206 m and d_p = 6.4 mm) and different working conditions by experimental work carried out in this University (see Chapters 3 and 4).

However, it is necessary to use a simultaneous solution for all the unknown (P and U) at each time step. By substituting Eqn. (2.24) into Eqns. (2.8) and (2.9) the following equations completely describe the train-line mathematical model,

$$b_{\eta,1}\, P_{i-1,j+1} + b_{\eta,2}\, U_{i-1,j+1} + b_{\eta,3}\, P_{i,j+1} = b_{\eta,4} \qquad (2.25a)$$

$$b_{\xi,1}\, U_{i-1,j+1} + b_{\xi,2}\, P_{i,j+1} + b_{\xi,3}\, U_{i,j+1} = b_{\xi,4} \qquad (2.25b)$$

where, $\eta = 2i-1$

and $\xi = 2i$

$$b_{\eta,1} = -b_{\eta,3} = -\frac{G_1}{\overline{P}_{i,j}} \qquad (2.26a)$$

$$b_{\xi,1} = -b_{\xi,3} = -P_{i,j} \qquad (2.26b)$$

$$b_{\eta,2} = 1 + G_2 \cdot U_{i-1,j}\, \Delta T \qquad (2.26c)$$

$$b_{\xi,2} = 1 \qquad (2.26d)$$

$$b_{\eta,4} = U_{i-1,j}(U_{i-1,j} - U_{i,j}) + U_{i-1,j} \qquad (2.26e)$$

$$b_{\xi,4} = U_{i,j}(P_{i-1,j} - P_{i,j}) + P_{i,j}\left(1 - K_{i,j}\left(\frac{d_i}{d_p}\right)^2\right) \qquad (2.26f)$$

The Boundary Condition Equations

for i=1

$$b_{1,4} = b_{1,4} - b_{1,1}\, P_0$$

and Eqn. (2.25a) will be

$$b_{1,2}\, U_{0,j+1} + b_{1,3}\, P_{1,j+1} = b_{1,4} \qquad (2.27)$$

and for i=N Eqn. (2.25b) will be

$$b_{2N,1}\, U_{N-1,j+1} + b_{2N,2}\, P_{N,j+1} = b_{2N,4} \qquad (2.28)$$

Eqn. (2.25) is an implicit algebraic equation set and can be represented in a matrix form as :

$$\{B\} \cdot \{Y_{j+1}\} = \{Q\} \tag{2.29}$$

where {B} is tridiagonal matrix

$$\{B\} = \begin{bmatrix} b_{1,2} & b_{1,3} & 0 \ldots & 0 & 0 & 0 \\ b_{2,1} & b_{2,2} & b_{2,3} & 0 & 0 & 0 \\ \vdots & \vdots & \vdots & \vdots & \vdots & \vdots \\ 0 & 0 & 0 \ldots & b_{2N-1,1} & b_{2N-1,2} & b_{2N-2,3} \\ 0 & 0 & 0 \ldots & 0 & b_{2N,1} & b_{2N,2} \end{bmatrix} \tag{2.30}$$

and

$$\{Q\} = \left\{b_{1,4}, b_{2,4}, \ldots\ldots, b_{2N-1,4}, b_{2N,4}\right\}^T \tag{2.31}$$

$$\{Y_{j+1}\} = \left\{U_{0,j+1}, P_{1,j+1}, U_{1,j+1}, \ldots \ldots, U_{N-1,j+1}, P_{N,j+1}\right\}^T \tag{2.32}$$

Now the coefficient matrix {B} on the left hand side of Eqn. (2.29) is a tridiagonal matrix, whose nonvanishing elements form a band of three elements wide along the diagonal. This particular set of equations can be solved by using Gaussian elimination method as described in Appendix D.

The computational process is split into two parts. The first part consists of generating the coefficient matrix {B}. The second part is done by the Gaussian Elimination method to generate the solutions of the next time step (T_{j+1}). The finite difference implicit scheme has local truncation error of order $O\,[\Delta X + \Delta T]$.

2.5 Comparison between Experimental and Computational Results [2,3]

Funk and Robe [17] proposed the method of lines to solve Eqns. (2.8) and (2.9) for pneumatic transmission lines terminated by volumes or with blocked load (without leakage). The method of lines calculations were performed to compare with the data and analytical results presented by Schuder and Binder [4] for pneumatic transmission lines with no blocked load. The calculations were in good agreement with Schuder and Binder's data.

In this section, the implicit scheme calculations are performed to compare with calculations of the method of

---

[2] All computations were carried out on the CDC CYBER 170/552 at the computer center, Concordia University.

[3] The method of lines is reprogramed (on the CDC CYBER 170/552) by the author of this thesis, based on the description of Funk and Robe [17].

lines, Funk and Robe's.[17] data and the following two sets of laboratory data. Firstly the data reported in Ref.17 were obtained at the Westinghouse Air Brake Company using a pneumatic line of 30.5 m (100 ft) length and 4.3 mm (0.17 in) diameter. Secondly the author's data were obtained from two different arrangements of apparatus at the Fluid Control Center of Concordia University The first arrangement consists of fourteen sections, each with 17.2 m (56.3 ft) in length, 6.4 mm (1/4 in) bore, without leakage. In the second arrangement, each section contains only one leakage orifice of 0.4 mm (.016 in) in diameter.

Figs. 2.4a and 2.4b show the comparisons between the numerical calculations (implicit scheme and method of lines) and Funk and Robe [17] data for charging and discharging processes, respectively. These Figs. show that the implicit scheme solution is in better agreement with Ref-17 data than the method of lines solution (especially for the discharging process data). Fig. 2.5a shows the comparison between the two numerical calculations and the no-leakage arrangement, whereas Fig. 2.5b shows the comparison for the leakage arrangement. Both Figs. show that the method of lines solution as well as the implicit solution are in good agreement with the laboratory model data. Therefore, the validity of the implicit scheme is established.

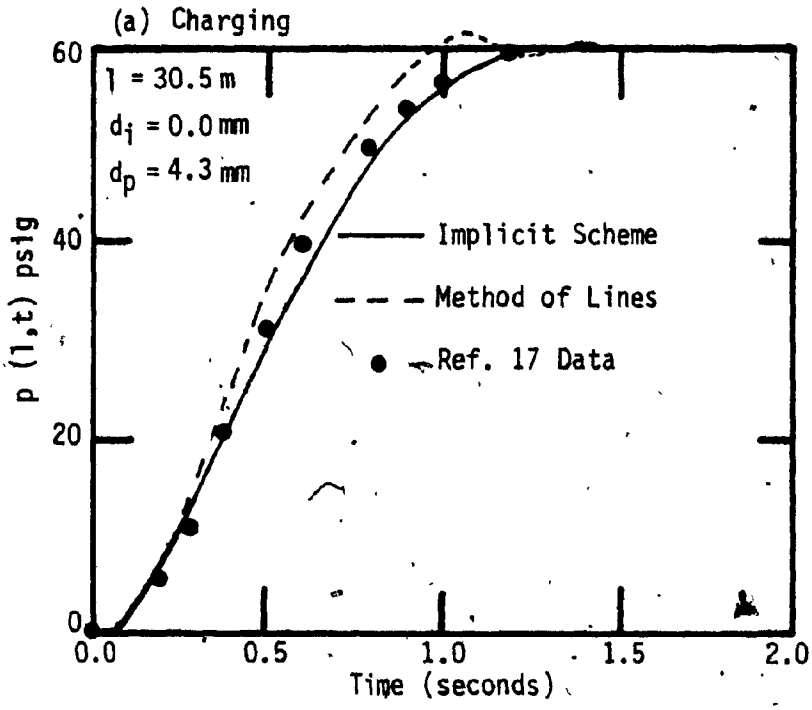

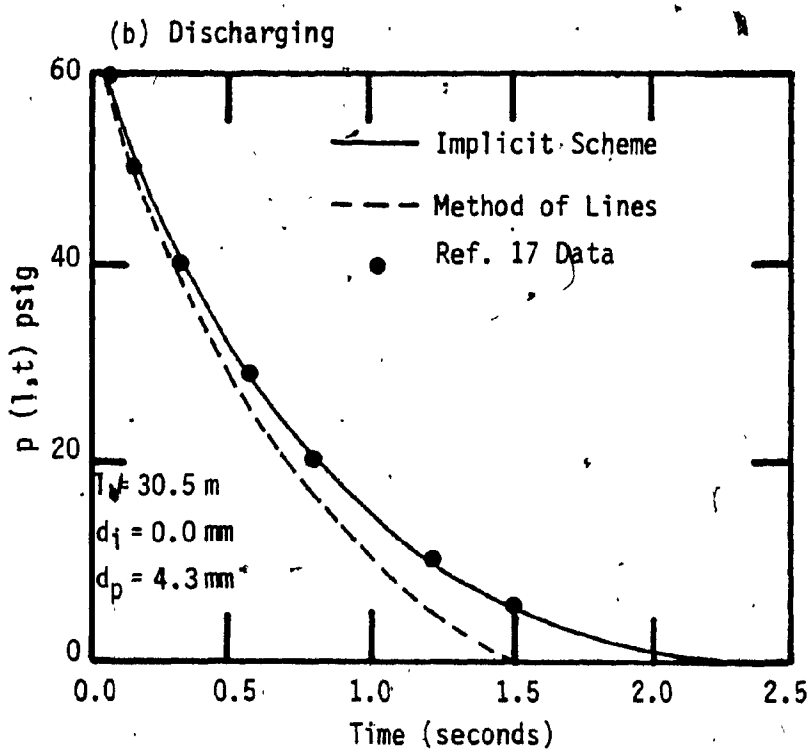

Fig. 2.4 Rear-end Pressure Transient Response

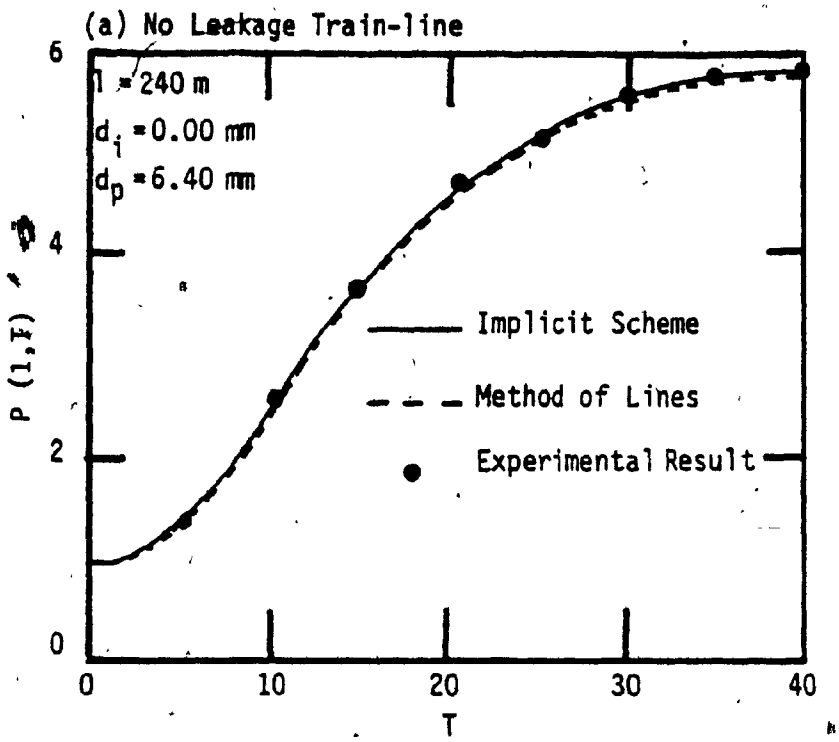

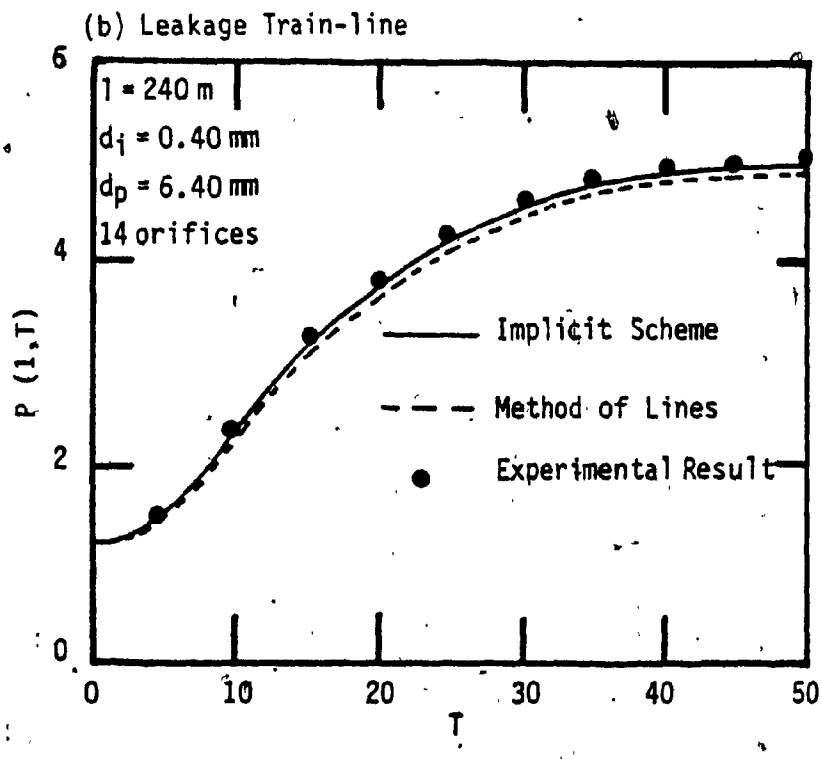

Fig. 2.5 Rear-end Pressure Transient Response

The computer time required for the implicit scheme solution and the method of line solution, presented in Figs. 2.4 and 2.5 are summarized in Table 2.1. Typically the implicit scheme takes half the computer time required by the method of lines.

Computer Solution Time (Seconds)	
Method of Lines	Implicit Scheme
5.	2.5
6.5	3.
14.	5.5
27.7	12.7

Table 2.1 Computer Time required by The Method of Lines and The Implicit Scheme

The implicit scheme has two attractive features which are not found in the method of lines. Firstly, the implicit scheme requires less computer time than other solution. Secondly, it is more accurate than the other solution.

As a conclusion, the implicit scheme is preferred and employed exclusively for solving the train line mathematical model in this study.

2.6 Summary

In this chapter, two finite difference schemes (Sec. (2.4)) were proposed to provide a solution for the train-line mathematical model (Section (2.3)). First scheme was the explicit scheme (referred to as the method of lines). This method has been used before, by Funk and Robe [17], and Ho [16]. The other method was the implicit scheme. Then, the computational results using both schemes and the experimental results, from the train-line laboratory model (Sec. (2.2)) and Westinghouse model, are compared with one another (Section (2.5)). The computational solution, using the implicit scheme, is found to be more accurate than the explicit scheme solution, and it requires less computer time because its time increment (ΔT) is larger than the explicit scheme time increment. As a result of these comparisons, the partial validation of the implicit scheme was established (Section (2.5)), then the implicit scheme is chosen to provide the solution for the train-line mathematical model in the subsequent chapters. The validation of the implicit scheme will be carried out for the various conditions of tests.

CHAPTER 3

STEADY-STATE BEHAVIOUR OF THE TRAIN-LINE

3.1 Introduction

In Chapter 2, two finite difference schemes are developed viz. the implicit scheme and the method of lines (explicit scheme). The computational results are compared with the experimental results, and the validation of the implicit scheme over the method of lines is established in Sec. (2.5). Some of the experimental results are obtained from the train-line laboratory model, and the rest are taken from Funk and Robe's [17] experiments.

In this Chapter and the subsequent Chapter, the experimental and theoretical investigations of the train-line model are carried out to demonstrate the effects of leakage (size and location) among other factors (discussed in Chapter 4), on the steady-state behaviour Sec. (3.3), as well as the transient behaviour (Secs. (4.3), (4.4) and (4.5)). The train-line laboratory model is employed to provide the experimental results and the implicit scheme is utilized to provide the theoretical results.

Sec. (3.2) describes the train-line set-ups, which are used for investigating the train-line behaviour. Then, the effects of the size and location of leakage on the steady-state pressure and velocity distribution are discussed in Sec. (3.3). In the same section, the effects of the leakage (size and location) on the the "pressure gradient" and the steady-state inlet velocity are investigated for a wide range of leakage size, relying only on the train-line mathematical model. Finally, in Sec. (3.4) the experimental and theoretical results are summarized.

3.2 Description of the Test Set-Ups

The train-line mathematical model (Fig. 2.2) and Laboratory model (Fig. 2.1), which consist of twelve sections, each of 17.15 m (56.25 ft), are used to study the effects of leakage (location and size) on the train-line behaviour (steady-state and transient). To perform this task, two set-ups are chosen. In order to investigate the effects of the leakage location on the train-line model, first test set-up is used, having a fixed leakage size with different leakage locations as follows:-

1- The head-end region (I) of the train-line (nodes 1, 2, 3 and 4).

2- The middle region (II) of the train-line (nodes ~~5, 6~~, 7 and 8).

3- The rear-end region (III) of the train-line (nodes 9, 10, 11 and 12).

where, each local leakage is expressed as a percentage of the total leakage area within these regions with respect to the train-line cross-sectional area A, and it may be defined as:

$$S = 4 \left(\frac{d_i}{d_p}\right)^2 \qquad (3.1)$$

In order to investigate the effects of the leakage size on the train-line model, another set-up is used. In this set-up, there are four assemblies, each one containing four identical sub-leakages d_i, with a fixed leakage location (rear-end region). These assemblies have the following d_i and S%

	d_i mm	S%
1-	.3	.9
2-	.4	1.6
3-	.5	2.5
4-	.6	3.57

3.3 Steady-State Pressure and Air Velocity of the Train-Line

In this section, the two set-ups are used to study the effects of the leakage location and size on the steady-state pressure P_i and velocity U_i of the train-line. The head-end pressure P(0) is maintained at 580 kPa (70 psig) and 480 kPa (55 psig). P_i and U_i are calculated for each node (mathematical model), whereas, the experimental result of the pressure at each node is recorded by using the pressure transducers and the digital multimeter (as explained in Sec. (2.2)). In the course of the experimentation the pressure ratio $\frac{P_{i-1}}{P_i}$ is always less than two. This follows the AAR rules for the rail-road application (see Sec. (1.2).

The experimental and theoretical results of the steady-state pressure are plotted against the node location i (measurement location) as shown in Fig. 3.1. From this Fig., it can be concluded that the theoretical pressure P_i agrees within 3% with the experimental pressure measurement. Thus, the validation of the mathematical model for discribing the train-line is established. Now, the mathematical model will be used to explain some of the steady-state pressure and velocity phenomena.

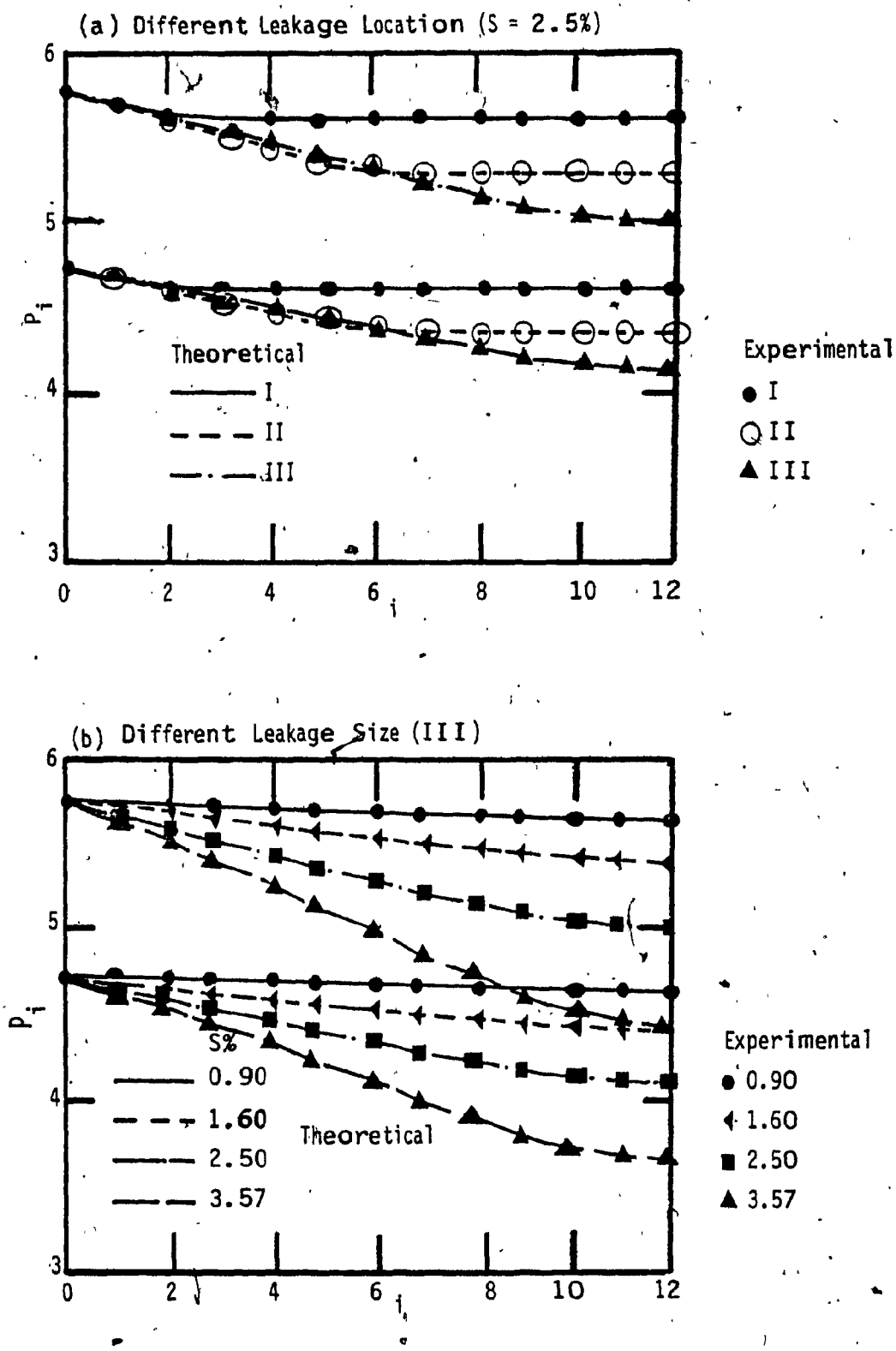

Fig. 3.1 Steady-state Pressure Distribution (Experimental and Theoretical)

Fig. 3.1a shows the following phenomenon

1- If there is a leakage in region III only, the pressure in this region will be lower than the pressure in the same region if the leakage was located in region II.

2- If the leakage is located in region III, the pressure in region I will be higher than the pressure in the same region if the leakage was located at region II.

The same phenomenon has been observed by Ho [16], but there is no explanation given. However, the following mathematical treatment provides the explanation of this phenomenon.

It may be assumed that the leakages in regions II and III, can be represented as one leakage in each region located at distances X_e equal to one third and two third of the total length of the train-line respectively. In the case of steady-state conditions, Eqns. (5.3) and (5.4) can be used to completely describe the relations between the in-line pressure and flow

$$P_{i-1}^2 - P_i = R_i^2 M_{i-1}^2 \qquad (3.2)$$

$$M_{i-1} = P_i / r_i \qquad (3.3)$$

$R_i \triangleq$ the in-line flow resistance

$$= \left[\frac{\gamma f l \Delta X}{2 d_p}\right]^{1/2}$$

$r_i \triangleq$ the leakage flow resistance,

$$= \frac{1}{K_i} \left(\frac{d_p}{d_i}\right)^2$$

But $M_i = M_{e-1} = M_0 = \frac{P_e}{r_e}$ $\quad 0 \leq i < e \quad$ (3.4)

From Eqn. C.3, it can be seen that

$$f = F(M)$$

Therefore $R_i = R_e$ $\quad 0 \leq i < e \quad$ (3.5)

In the course of this experiment, it has been noted that for any value of M_0, shown in Fig. 3.2, the flow is always turbulent. Therefore

$$R_i^2 M_{i-1}^2 = \Omega M_0^{1.86} \qquad 0 < i \leq e \qquad (3.6)$$

where $\Omega = 0.077 \Delta X \; d_p^{-0.86} \; a^{0.14}$

Eqn. (3.2), (3.4), (3.5) and (3.6) above, yield

$$P_i^2 = P_0^2 - \frac{i\Omega}{r_e} P_e^{1.86} \qquad 0 \leq i \leq e \qquad (3.7)$$

Because P_i $(0 \leq i \leq N)$ is greater than the critical pressure ratio for the air, the flow through the orifices is always sonic. The critical ratio is equal to $\left(\frac{\gamma + 1}{2}\right)^{\gamma/\gamma-1}$. For air $(\gamma = 1.4)$, this ratio is equal to 1.8. This means that the value of r_e is always constant for the same d_e.

Now for $i = e$; $P_e^2 + \left(\frac{\Omega}{r_e}\right) e \, P_e^{1.86} = P_0^2$ $\quad (3.8)$

It can be seen from Eqn. (3.8) that the pressure P_e varies inversely with the value of e. This explains the first part of the pressure phenomenon.

It can be seen from Eqn. (3.7) that the pressure P_i at any node i ($0 \leq i \leq e$) varies directly with e. This explains the second part of the pressure phenomenon.

The theoretical results of the velocity are plotted against the section location in Figs. 3.2a and 3.2b, for different leakage location and leakage size respectively. The velocity is not recorded experimentally because the introduction of sensors in this pipe (d_p = 6.4mm) could disturb the flow characteristic. However, an attempt is made to predict the velocity transient response $U(1-\frac{1}{N}, T)$ as described in Appendix E.

Fig. 3.2 shows the following velocity phenomenon

If there is a leakage at a distance X_e, the velocity U_i slightly increases as the distance X_i ($0 \leq X_i \leq X_e$) increases. Furthermore, the velocity U_i sharply decreases to zero as the distance X_i ($X_e < X_i \leq X_f$) increases, If there is no leakage at a distance greater than X_f.

The following mathematical treatment provides the

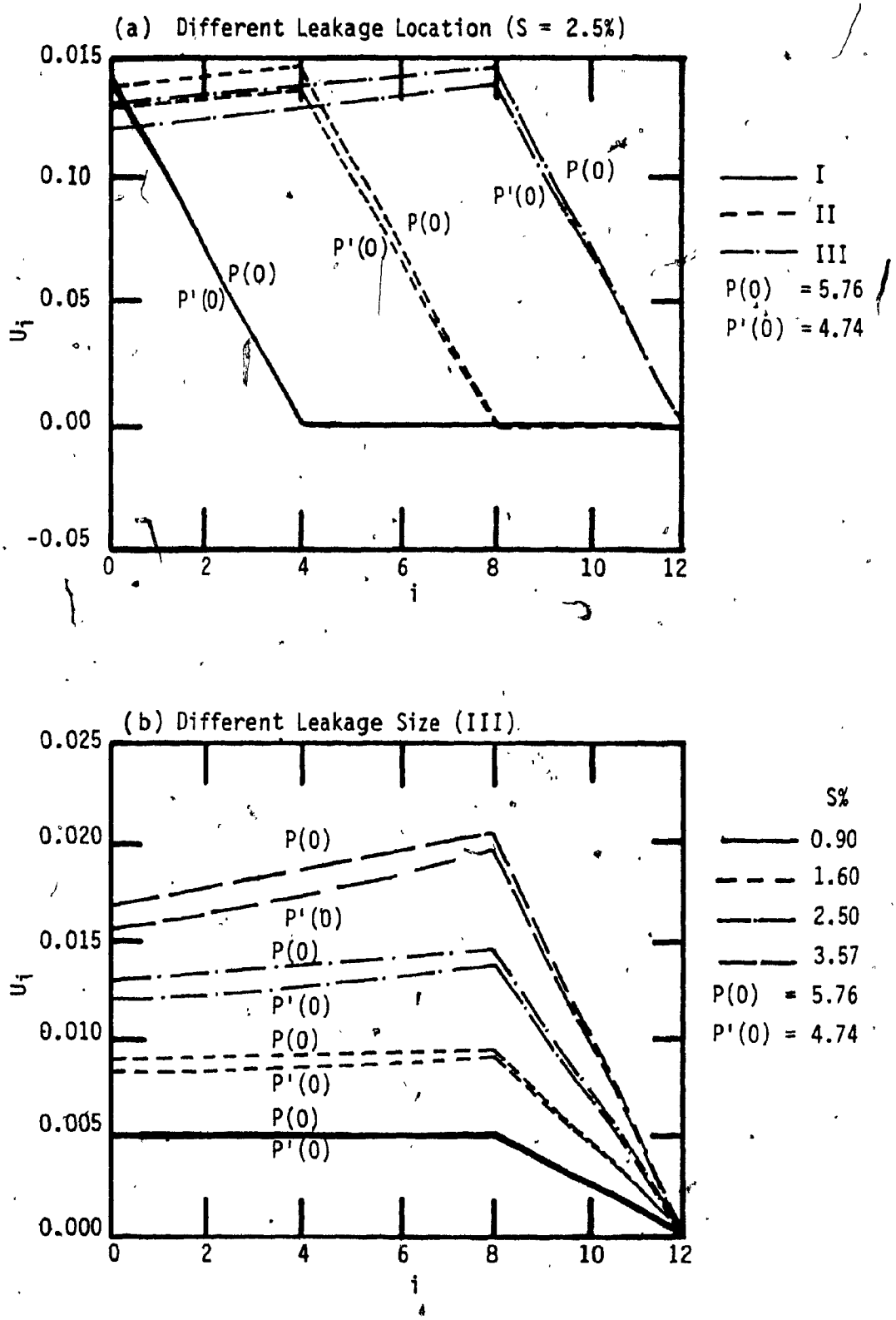

Fig. 3.2 Steady State Velocity Distribution [Theoretical]

explanation for this phenomenon.

Recalling Eqn. (2.17) and droping the dynamic term $\frac{dP_{i,j}}{dT}$, the relationship between U_{i-1} and U_i is.

$$U_{i-1} = U_i\left(2 - \frac{P_{i-1}}{P_i}\right) + K_i \left(\frac{d_i}{d_p}\right)^2 \qquad 0 < i \leq N \qquad (3.9)$$

If there is no leakage within the region $0 \leq X_i \leq X_e$

$$d_i = 0 \qquad 0 \leq i \leq e \qquad (3.10)$$

Since in the context of this thesis, relating to a train-line has

$$1 < \frac{P_{i-1}}{P_i} \ll 2 \qquad 0 < i \leq N \qquad (3.11)$$

Eqns. (3.9); (3.10) and (3.11) above, yield

$$U_{i-1} < U_i \qquad 0 \leq i < e \qquad (3.12)$$

This explains the reason for the increase of the velocity U_i with the increase of the distance X_i .

If there is a leakage within the region $X_e < X_i \leq X_f$

$$d_i > 0 \qquad (3.13)$$

For $X_i \geq X_f$, $U_i = 0$ (no leakage flow)

In particular $U_f = 0$

Hence from (3.9)

$$U_{f-1} = U_f \left(2 - \frac{P_{f-1}}{P_f}\right) + K_f\left(\frac{d_f}{d_p}\right)^2 \qquad (3.14)$$

$$= K_f \left(\frac{d_f}{d_p}\right)^2$$

But ,

$$K_i\left(\frac{d_i}{d_p}\right)^2 = K_f\left(\frac{d_f}{d_p}\right)^2 = \text{Const.} \qquad X_e \le i < X_f \quad (3.15)$$

Therefore,

$$U_{i-1} = U_i\left(2 - \frac{P_{i-1}}{P_i}\right) + \text{Const.} \qquad (3.16)$$

Eqns. (3.9), (3.11) and (3.16) above yields

$$U_{i-1} > U_i \qquad X_e < i \le X_f \quad (3.17)$$

This explains the reason for the decrease of the velocity with the increase of the distance X_i.

One can also observe from Fig. 3.2 that as the head-end pressure P(0,T) increases from 4.74 to 5.76, the inlet velocity U(0) also increases (not more than 10% from its previous value). For a fixed leakage location (III), the increase of the leakage size causes the increase in the inlet velocity (Fig. 3.1b).

Let ΔP be defined as the difference between the pressure at the head-end P(0) and that at the rear-end P(1) of the train-line as follows:

$$\Delta P = P(0) - P(1) \qquad (3.18)$$

In the case of the railroad application, the pressure gradient represents the force required to apply the brakes on the wheel in the train. On the other hand, the inlet velocity represents the amount of the air to be supplied by the compressor to maintain the pressure inside the train-line. Hence, the train-line mathematical model is used to quantitatively investigate the effects of leakage on the inlet velocity U(0) and the pressure gradient of the train-line (for d_p/l = .003%). This investigation is applicable only if the train-line model can be treated as one-dimensional flow problem.

Early in this section, different leakage locations are used to study their effects on the steady-state pressure and velocity distribution. In addition to this, two leakage locations are chosen to complete this task, and to predict the limitations of the pressure gradient (Δ P) as well as the inlet velocity. These additional locations are

1 leakage is concentrated at the rear-end, and

2 leakage is concentrated at the head-end.

Fig. 3.3 shows a plot of the train-line pressure gradient and the inlet velocity versus leakage size, for different leakage locations. This figure also shows the

railroad application zone as specified by the AAR [3]. One of the rules is that, "for a train to be fit for road movement, the rear-end pressure must not be less than 515 kPa.(60 psi) ". for this investigation, it means that the pressure gradient must not be greater than 0.68 (69. kPa or 10. psi). This figure also shows the train-line application zone which is bounded by the two extreme cases.

If leakage size is less than 2.0%, Fig. 3.3 shows that the inlet velocity varies insignificantly with the change in the leakage locations, whereas it varies significantly with the change of the leakage size. In the case of the train-line application zone (S = 20%), the flow varies significantly as the location of leakage is changed. As the location of the leakage is moved towards the front of the train-line, the pressure gradient decreases and the inlet velocity increases. Whereas if the leakage location is moved towards the rear-end, the pressure gradient increases, and the inlet velocity decreases. This is because of the fact that when the leakage is concentrated at the rear-end, the increase in the in-line resistance (R_i) causes a large pressure drop which further causes decrease in the inlet flow rate U(0). This phenomenon is discussed early in this section. For a fixed leakage location, as leakage size increases, the pressure gradient and the inlet velocity also increases. In the case of the railroad application, the pressure gradient is constant and equal to

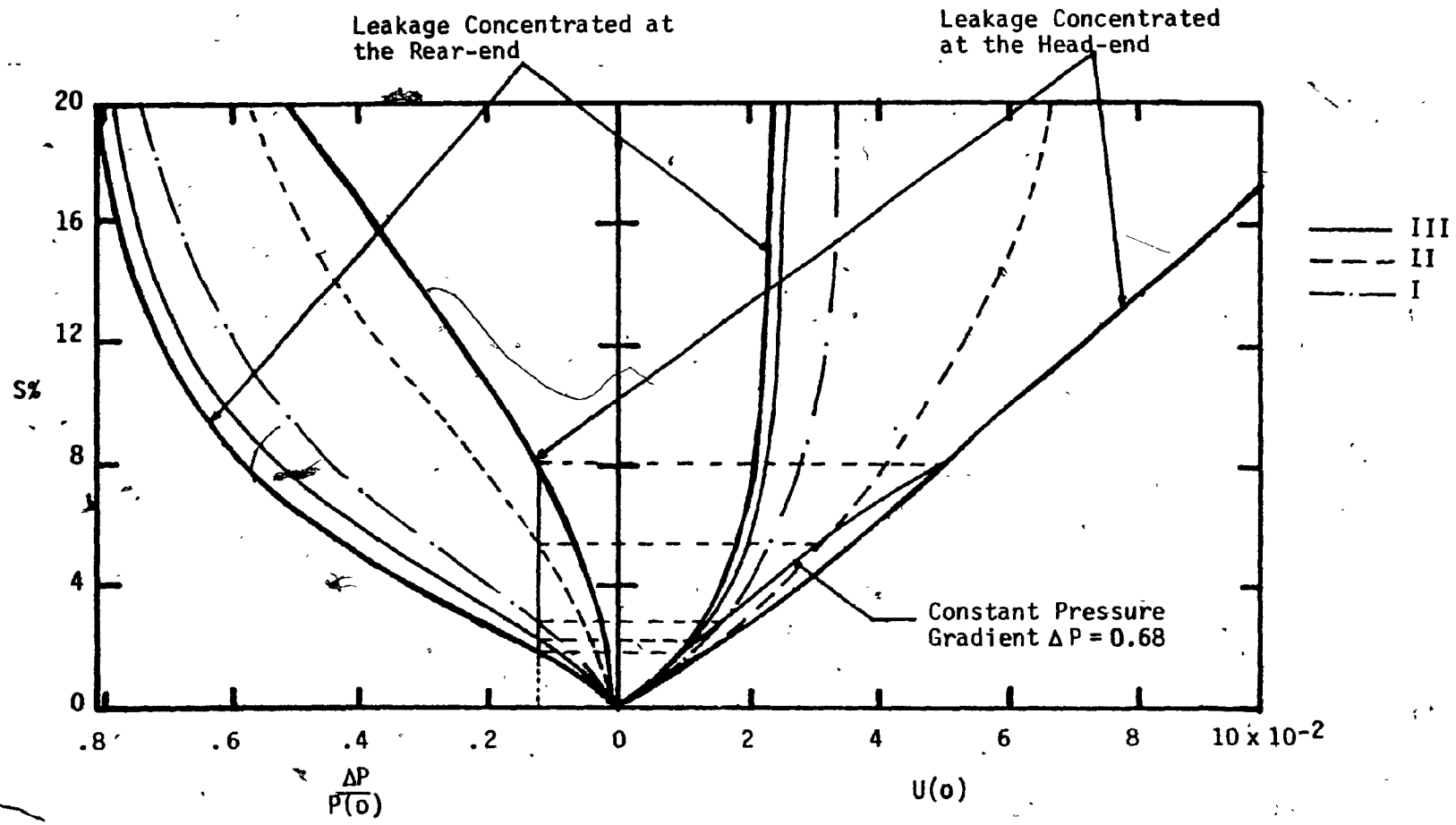

Fig. 3.3 Pressure Gradient and Inlet Flow Behaviour of the Train-line

68. Therefore to fix the pressure gradient at a certain value, as the leakage moves towards the head-end, the leakage size has to increase which causes the increase in the inlet velocity U(0). As a result, if the leakage is located in section 1, region I, region II, region III or section 12, the leakage size has to be equal to 2.1, 2.2, 3.0, 5.9 or 8.3 respectively.

3.4 Summary

In this Chapter, two test set-ups are used to study the effects of the leakage size ($S \leq 3.57\%$) and leakage location (regions I, II and III) on the steady-state pressure and velocity of the train-line. In section (2.3), train-line laboratory and mathematical model are employed to accomplish this task. Sec. (3.3) provides the validation of the mathematical model after comparing the theoretical results with the experimental results. Then, the mathematical model was used exclusively to study the effects of the leakage (location and size) on the pressure gradient (ΔP) and the steady-state inlet velocity (U(0)). Fig. 3.3 shows the steady-state characteristics of the train-line, for a particular d_p/l value (.003%). This figure shows that the train-line pressure gradient and inlet velocity vary with the change of the leakage location as well as the leakage size. But, for a small leakage size ($S \leq 2.0\%$), the inlet velocity does not vary with the leakage location, but

it varies with the leakage size. For further research work, the author suggests that Fig. 3.3 may be used to predict the location of the leakage of this particular train-line by measuring the pressure gradient and the inlet velocity. In Sec. 3.3 an attempt is made to explain the pressure and velocity distribution phenomenon. The pressure distribution phenomenon is

1- If the leakage is located in region III, the pressure in this region will be lower than the pressure in the same region if the leakage is located in region II.

2- If the leakage is located in region III, the pressure in region I will be higher than the pressure in the same region when the leakage is located in region II.

On the other hand, the velocity distribution phenomenon is If there is a leakage at a distance X_e , the velocity U_i slightly increases as the distance X_i ($0 \leq X_i \leq X_e$) increases. Furtheremore, the velocity U_i sharply decreases to zero as the distance X_i ($X_e < X_i \leq X_f$) increases, If there is no leakage at a distance greater than X_f .

CHAPTER 4

TRANSIENT BEHAVIOUR OF THE TRAIN-LINE

4.1 Introduction

In chapter 2, two numerical schemes are proposed (Sec. (2.4)) to provide a solution to the train-line mathematical model (Sec. (2.3)). Then, in Chapter 3, part of the study was carried out to investigate the effects of the leakage size and location on the steady-state pressure and velocity behaviour of the train-line. This Chapter investigates the effects of the leakage and other factors on the transient behaviour of the train-line.

Sec. (4.2) describes three test cases, which are used to study the effect of the leakage among other factors, on the transient behaviour of the train-line. Sec. (4.3) describes the transient behaviour of the pressure and the velocity due to step changes in the head-end pressure and for different initial conditions (pressure and velocity). Then, in Sec. (4.4), the mathematical model is exclusively used to study the effect of the leakage on the velocity transient behaviour of the last section in the train-line. Finally, in Sectin (4.5), the effects of some more factors

on the transient behaviour of the rear-end of the train-line are studied. These factors are the threshold sensitivity of the transducer (D) and the changes of the pressure amplitude at the head-end ($P_r(0)$). On the other hand this Section explores the relationships between the propagation speed of the head-end pressure signal and the above mentioned factors. Sec. (4.6) summarizes the result of the transient behaviour of the pressure and the velocity of the train-line.

4.2 Test Cases

This Section describes three test cases for investigating the effects of the leakage location and leakage size on the pressure and velocity transient behaviour of the train-line of the test (utilizing the test set-ups desribed in Sec. (3.2)). The first test is performed with the atmospheric pressure along the whole train-line (P(X,0)= 1.0 for all X). Then, a positive pressure step is applied at the head-end (P(0,T) = 5.76) while the pressure and the velocity (P(X,T) and U(X,T)) results are calculated. This is known as the dry charging test. Then, a negative pressure step is applied at the head-end (from 5.76 to 4.74), when the in-line pressure reaches steady-state (P(X,T)= P(X, ∞)= P(X)). This is known as the discharging test. Finally, a positive pressure

step is applied at the head-end (from 4.74 to 4.76). This is known as the recharging test.

At this point, let us define the following parameters as illustrated in Fig. 4.1.

α $\triangleq$ gain coefficient.

$\triangleq$ the ratio between the change of the pressure level at the rear-end $P_r(1)$ and the pressure step size at the head-end $P_r(0)$.

U_P $\triangleq$ the peak value of the last node in-line velocity, $\dot{U}$ (X, T) during the entire transient.

T_P $\triangleq$ the peak time.

T_S $\triangleq$ steady-state time.

$\triangleq$ time required for the last node pressure to reach its steady-state condition.

V $\triangleq$ propagation speed with respect to the acoustic speed

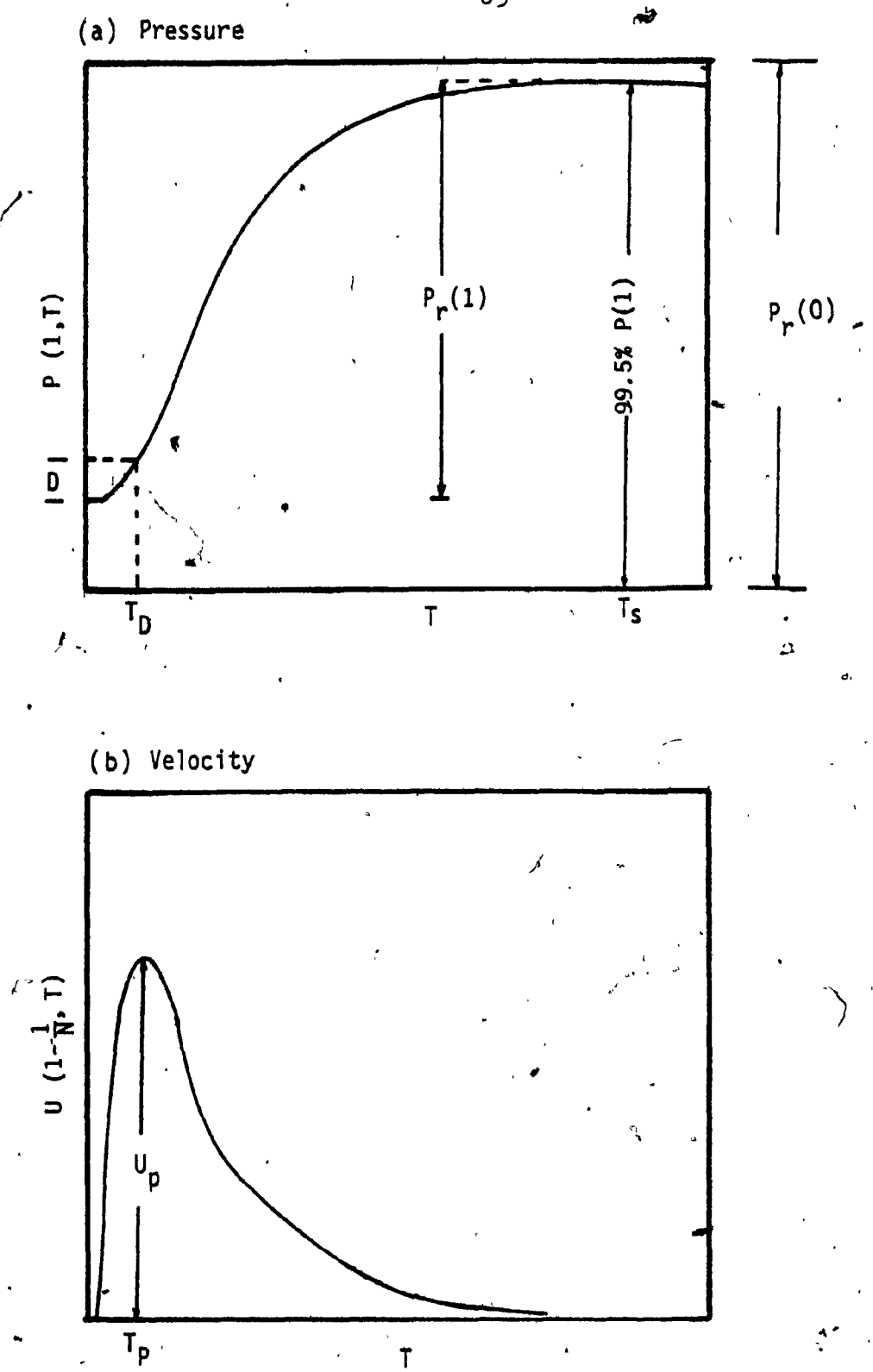

Fig. 4.1 Illustration for the Rear-end Transient Behaviours of the Train-line

T_D ≜ time required for the pressure signal to reach the threshold sensitivity of the transducer (D)

4.3 Pressure and Velocity Transient Response

The experimental and theoretical results of the rear-end pressure transient response P(1,T) are plotted against time, T, in Fig. 4.2. This figure shows that for $T \geq 4$, the discrepancy between the theoretical result and the experimental result goes as low as 3%. But, for $T \leq .4$, the discrepancy goes up to 10%. This provides the validation of the implicit scheme to solve the train-line mathematical model. Hence, the mathematical model can be utilized to complete the investigation for a wide range of leakage size and different working conditions (see Secs. 4.4 and 4.5).

In the case of the dry charging, it has been observed that as the leakage location goes towards the rear-end (Fig. 4.2a) or as the leakage size increases (Fig. 4.2b),

1- the gain coefficient decreases

2- the steady-state time increases

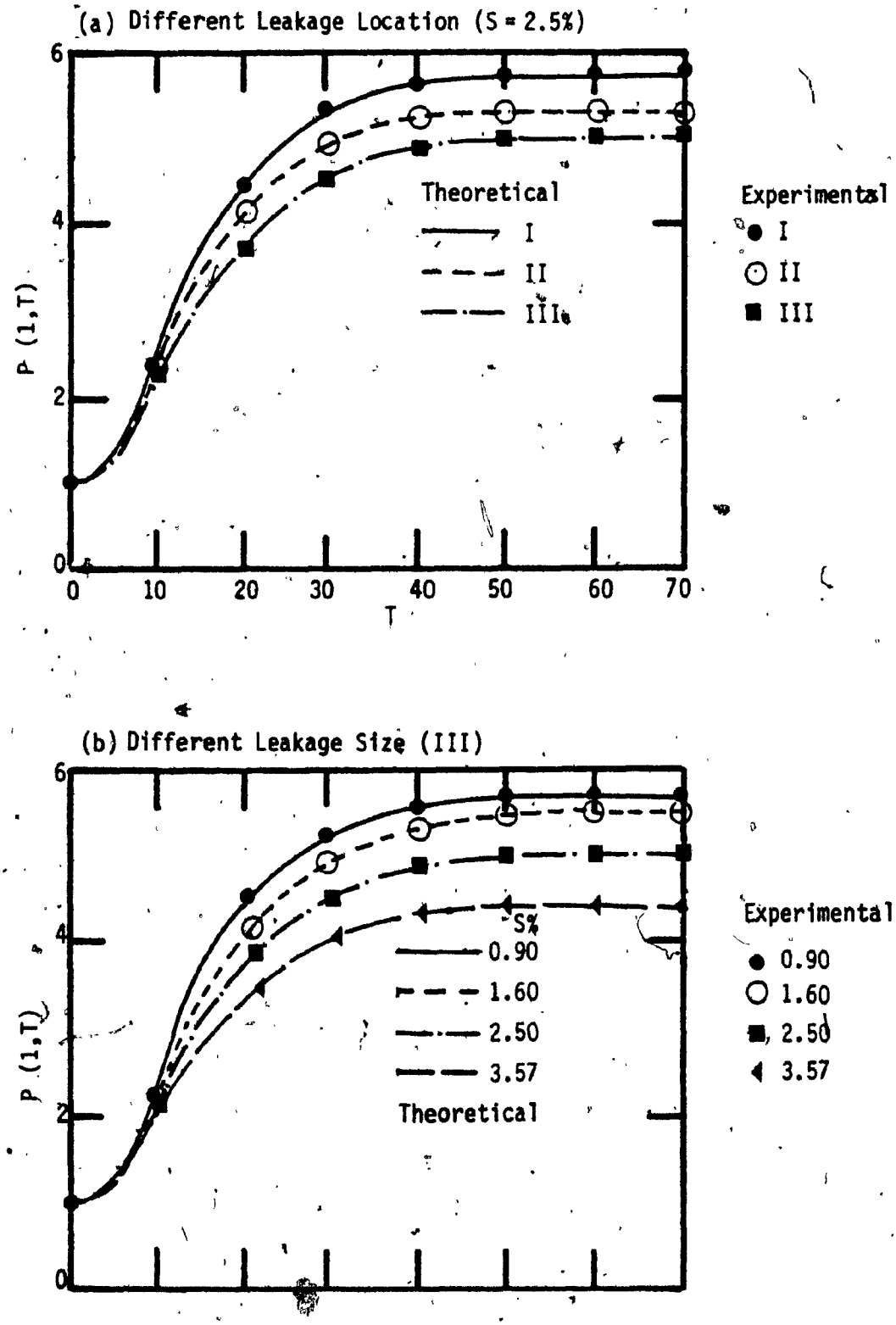

Fig. 4.2 Rear-end Pressure Transient Response due to Dry Charging Test (Experimental and Theoretical)

(a) Different Leakage Location (S = 2.5%)

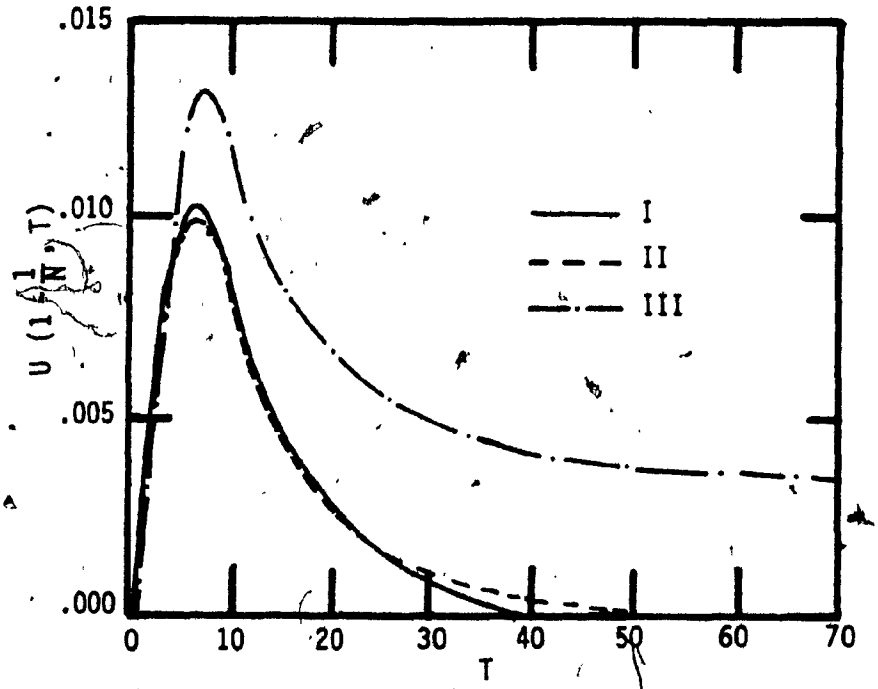

(b) Different Leakage Size (III)

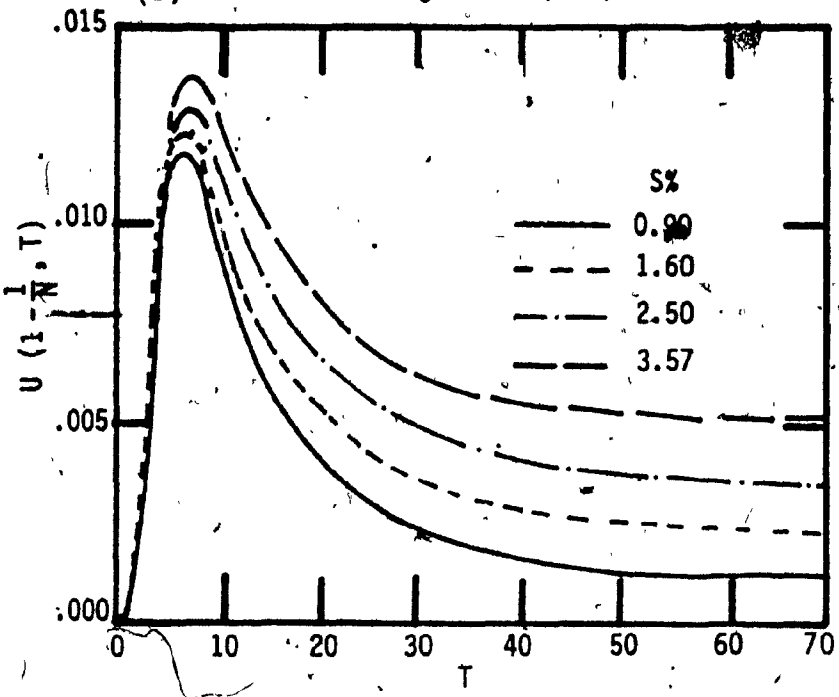

Fig. 4.3 Rear-end Velocity Transient Response due to Dry Charging Test [Theoretical]

(a) Different Leakage Location (S = 2.5%)

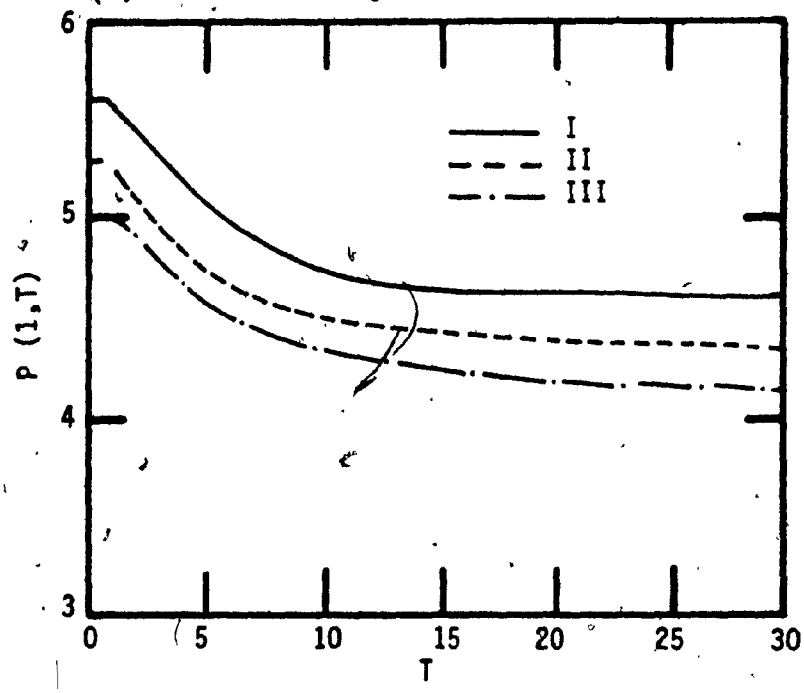

(b) Different Leakage Size (III)

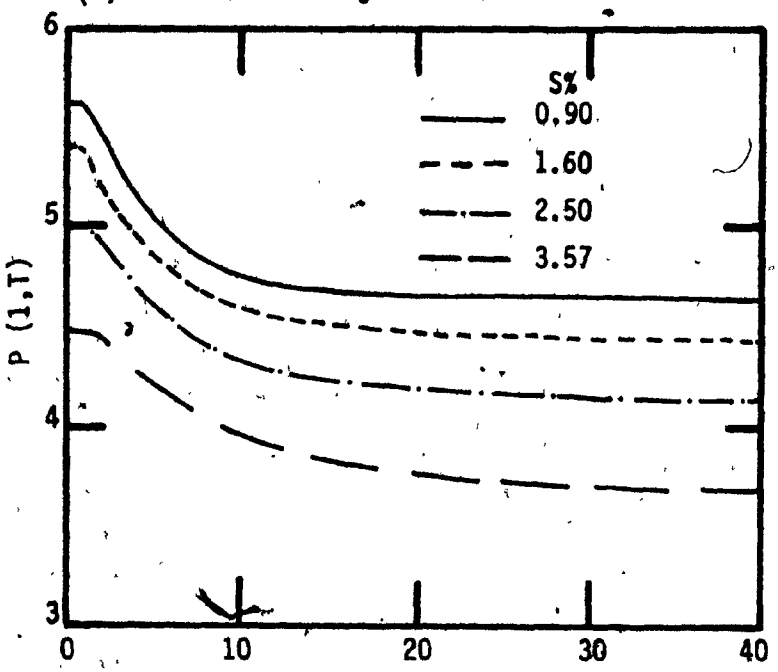

Fig. 4.4 Rear-end Velocity Transient Response due to Discharging Test [Theoretical]

3- the difference between $P_{N,j+1}$ and the $P_{N,j}$ decreases

One can also make the same observations for the discharging and the recharging tests. For the same pressure amplitude at the head-end and the same leakage size and location, the recharging test result is compared with the discharging test result. This comparison shows that the recharging steady-state time is greater than the discharging time.

Fig. 4.5b shows the transient response of the in-line velocity of the last section, $U(1-\frac{1}{N}, T)$, for the discharging test. It is noticed that the direction of velocity changes (opposing motion) only if the leakage size is less than a certain minimum value. This minimum leakage size for the model under study is 1.6%. This phenomenon may have some effect on the propagation speed, V, which is discussed in Sec. (4.5).

The theoretical result of the velocity is verified experimentally on the train-line laboratory model as shown in Fig. 4.6. But, due to the difficulty in measuring velocity inside the pipe of 6.4 mm (1/4 in) diameter, the pressure between two neighboring points along the last section was measured to determine the velocity, assuming that the flow through the rear-end of the line to be laminar. The relation between velocity and pressure difference δ is $U(1-\frac{1}{N}, T_j) = 0.37\,\delta$ (4.1)

(a) Different Leakage Location (S = 2.5%)

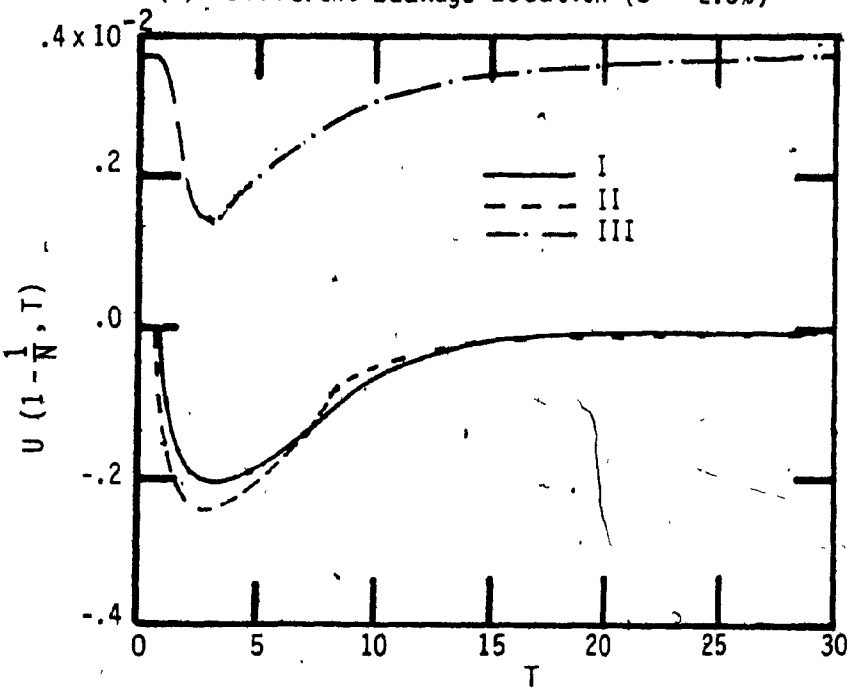

(b) Different Leakage Size (III)

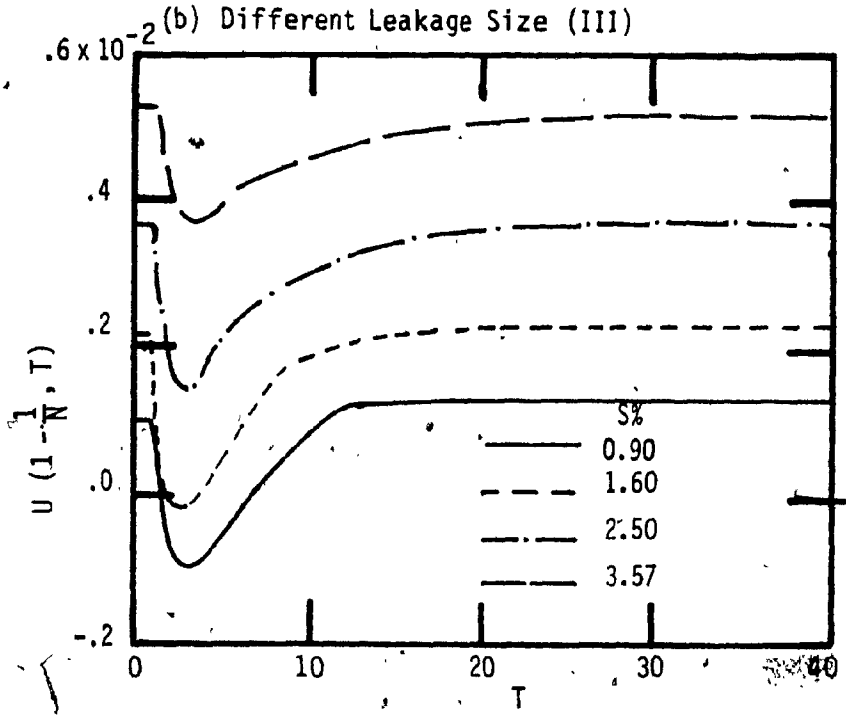

Fig. 4.5 Rear-end Velocity Transient Response due to Discharging Test [Theoretical]

(a) S = 0.9%

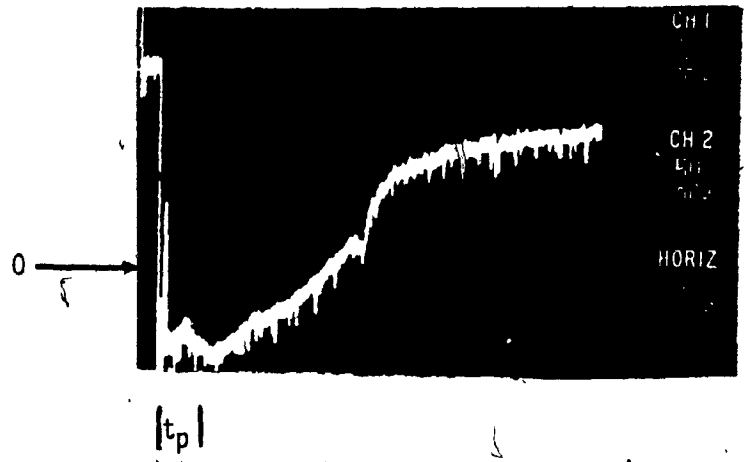

(b) S = 1.6%

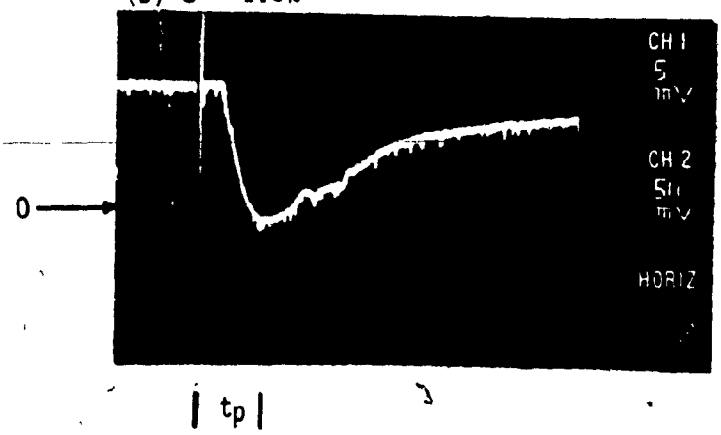

(c) S = 3.57%

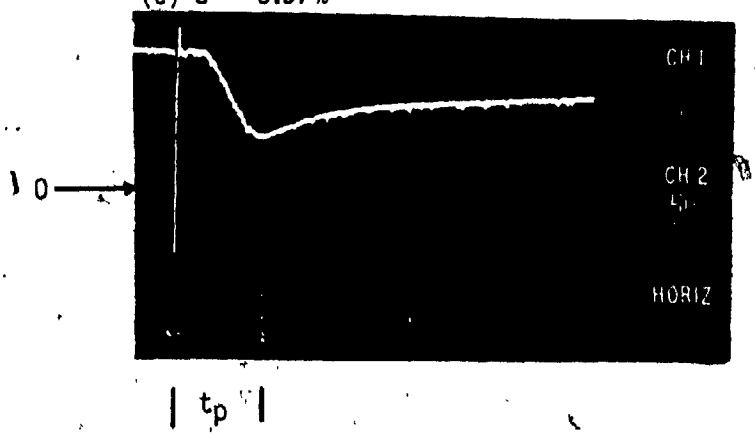

Fig. 4.6 Experimental Results of the Velocity Transient Response due to Discharging Test

(a) Different Leakage Location (S = 2.5%)

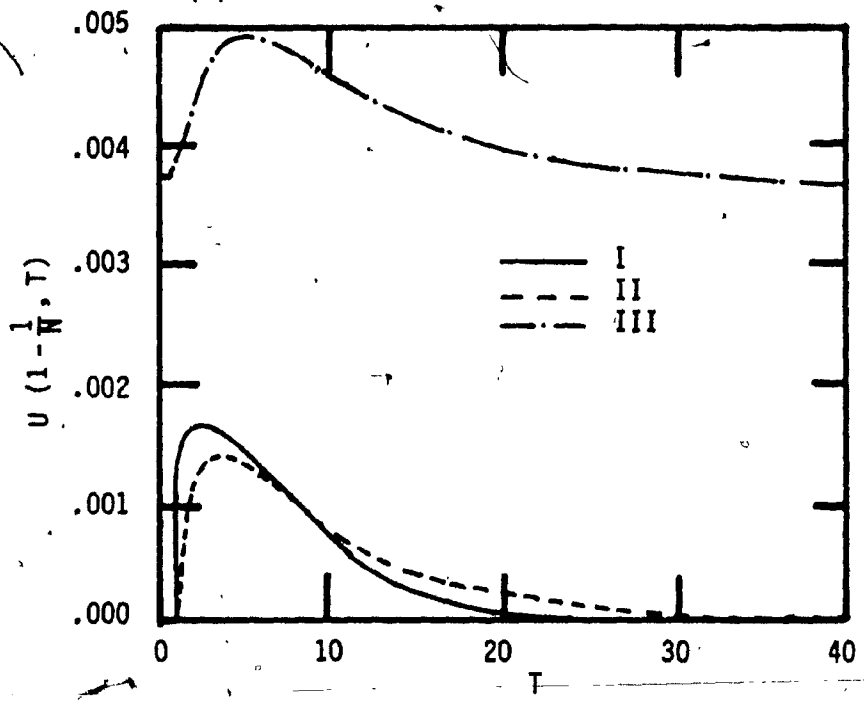

(b) Different Leakage Size (III)

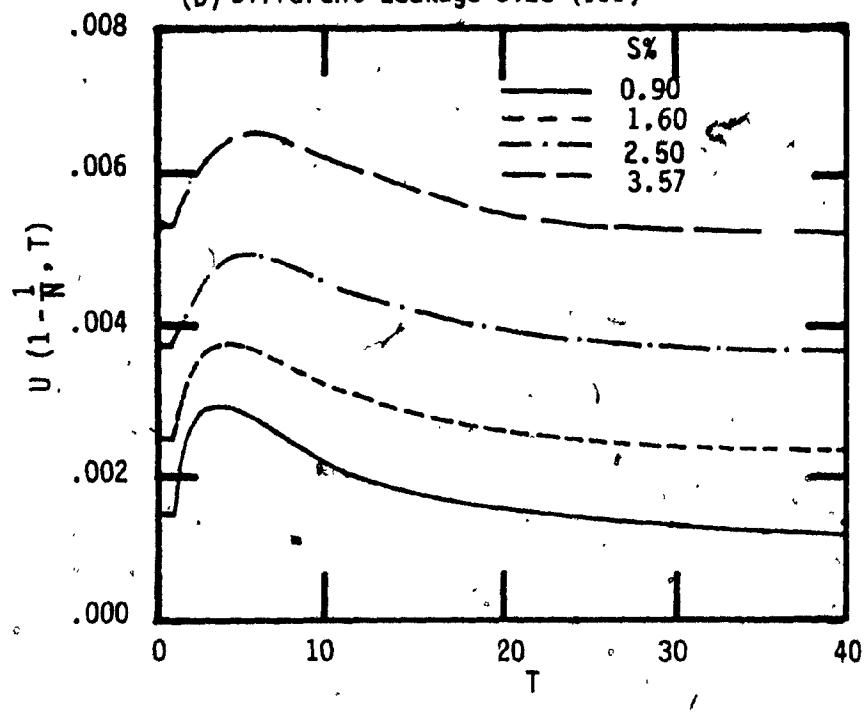

Fig. 4.7 Rear-end Velocity Transient Response due to Rechanging Test [Theoretical]

where, $\delta = P_{N-1,j} - P_{N,j}$ (4.2)

A full derivation of this relationship is described in Appendix E.

At this point, the mathematical model is exclusively used to calculate the pressure P(X,T) -Figs. 4.8A and 4.9A- and the velocity U(X,T) -Figs. 4.8B and 4.9B- (for all X). Fig. 4.8 (a) shows the transient response of the no leakage train-line, whereas Fig. 4.8 (b, c & d) show the transient response for a fixed leakage size (S = 2.5% or d_i = .5 mm) and different leakage locations (I, II and III). Fig. 4.9 (a, b, c &d) show the transient response for a fixed leakage location (III) and different leakage sizes (S = .9, 1.6, 2.5 and 3.57% or d_i = .3, .4, .5 and .6 mm).

These three dimensional representations show the wave effects in the train-line pressure or velocity response (especially, the results shown in Fig. 4.9 for different leakage locations).

From the in-line velocity transient response U(X,T) shown in Fig. 4.9, it can be concluded that for any leakage location (I, II or III), the velocity of the part of the train-line in front of the region ($k/3 \geq X \geq 1.0$) will approach its steady-state condition faster than the velocity of this region ($0 \geq X \geq k/3$). where k = 1, 2, 3 depends on

Legend 1 for Figs. 4.8 and 4.9

(1)

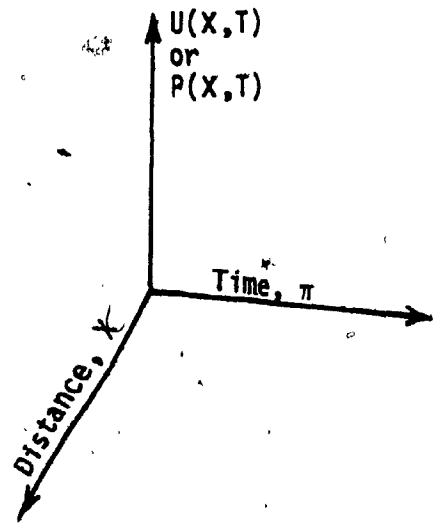

(2) H.E. Head-end of the Train-line

R.E. Rear-end of the Train-line

(3) + ve Step Pressure (1 to 5.76) at T = 0

(4) - ve Step Pressure (5.76 to 4.74) at T = 60

(for all cases, except for S = 3.57% or d_i = 0.6 mm)

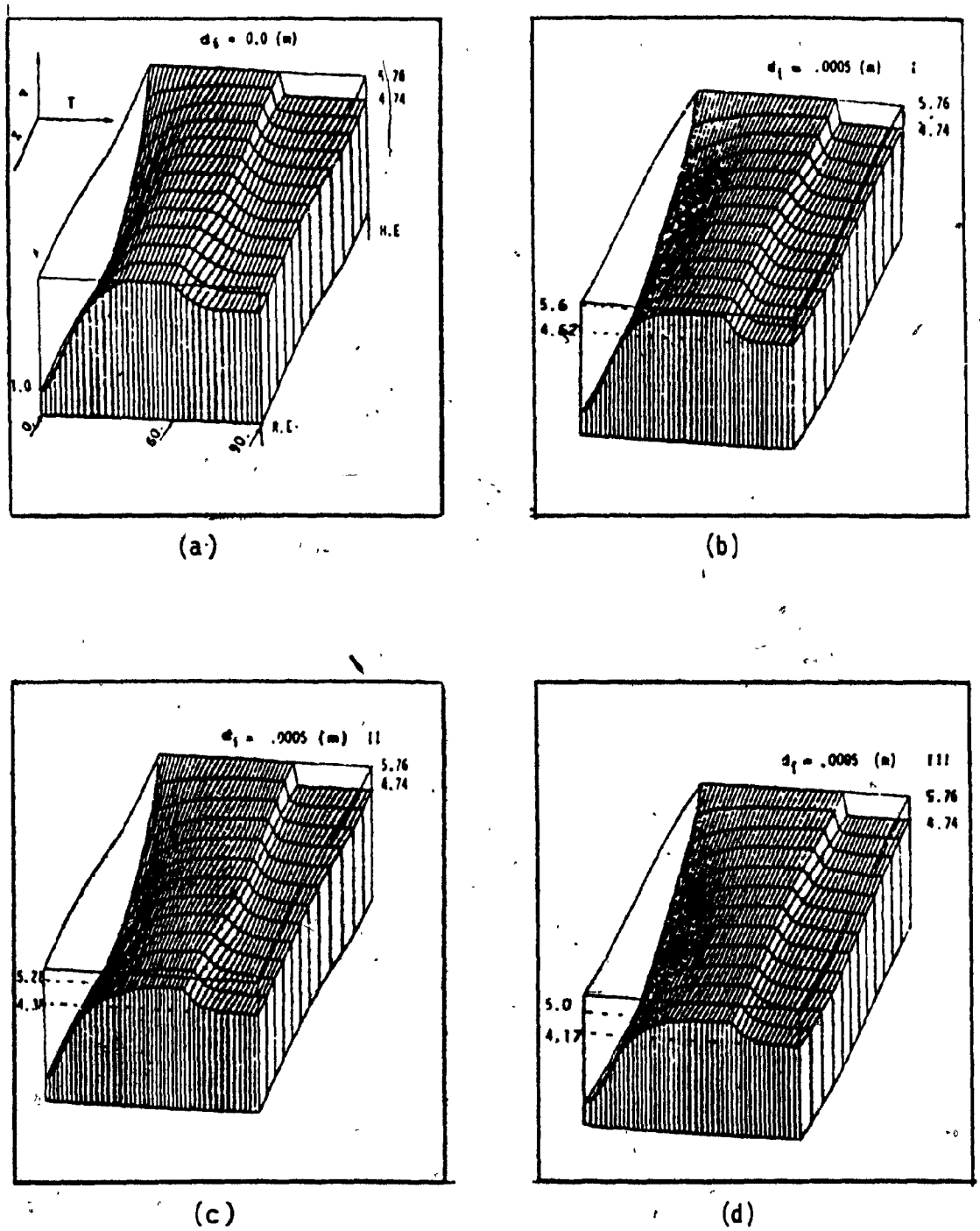

Fig. 4.8A Pressure Transient Response along the Train-line P(X,T)
[(a) No Leakage, (b),(c)&(d), Different Leakage Location]

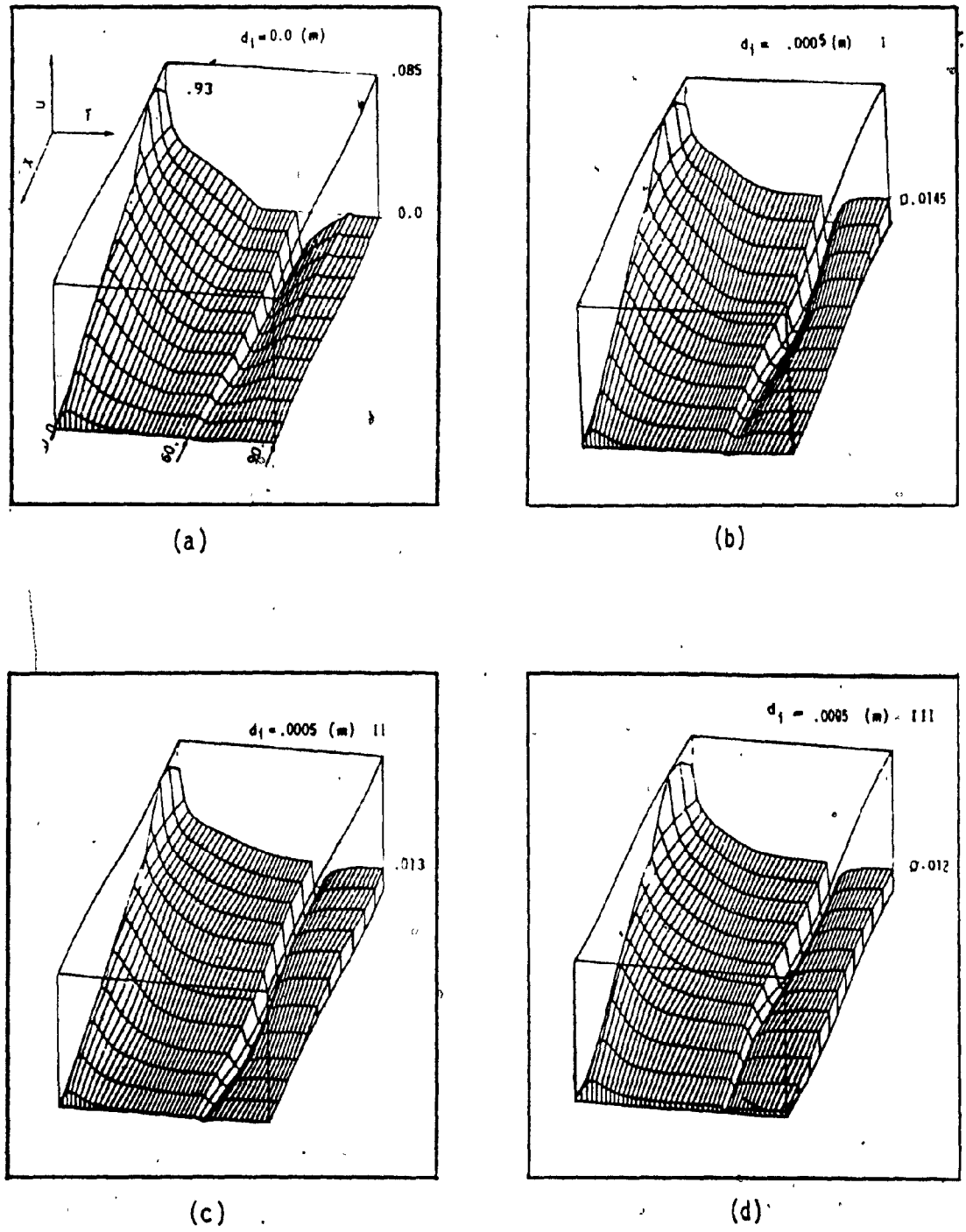

(a) (b)

(c) (d)

Fig. 4.8B Velocity Transient Response Along the Train-line U(X,T)
[Same as Fig. 4.8A]

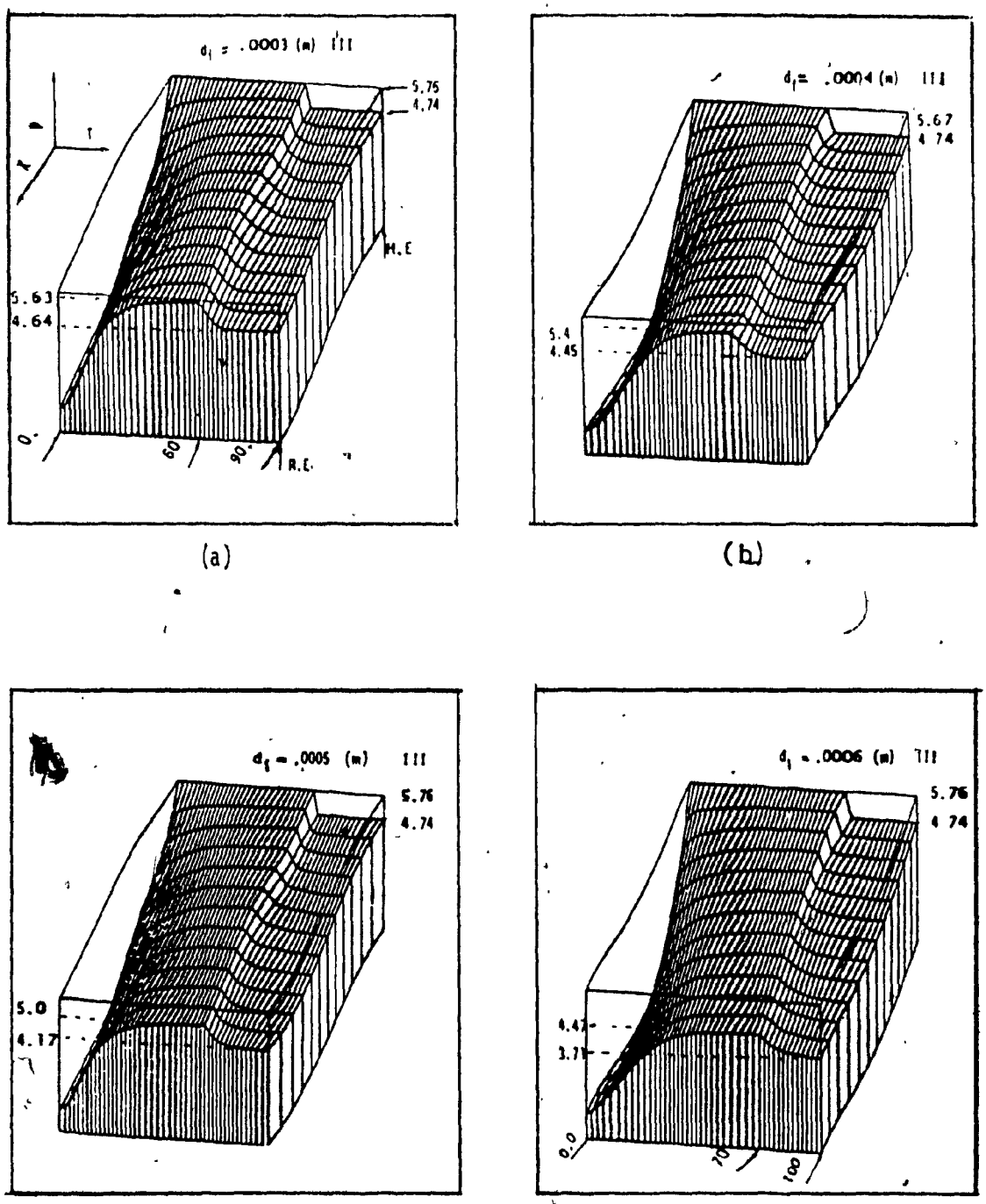

(a) (b) (c) (d)

Fig. 4.9A Pressure Transient Response along the Train-line P(X,T) [(a),(b),(c)&(d), Different Leakage Size]

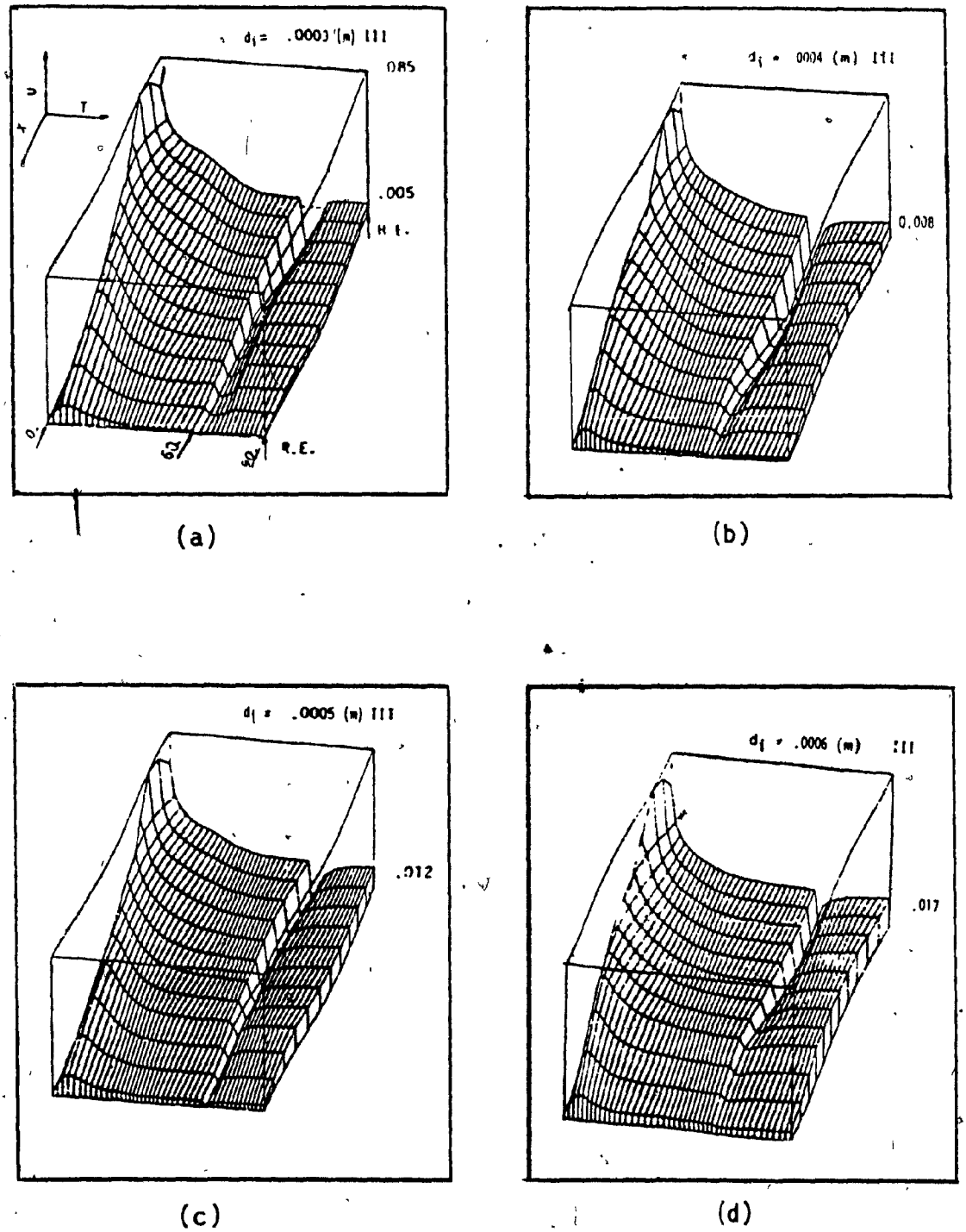

(a) (b) (c) (d)

Fig. 4.9B Velocity Transient Response Along the Train-line U(X,T) [Same as Fig. 4.9A]

the leakage location in region I, II or III. From Fig. 4.9B, it has been observed that the reverse flow phenomenon in the last region III does not occur for $S \leq 1.6\%$.

4.4 Peak Velocity and Peak Time

The peak velocity and the peak time can represent the velocity transient behaviour of the last section in the train-line. The discussion on this section is valid for any train-line with $1/d_p = .003\%$ as well as the train-line problem can be described as one-dimensional. The peak velocity and the peak time will be dependent on the leakage size and location, and the kind of test applied on the train-line. In Sec. (4.3), three tests are conducted to study the effect of these factors on the train-line transient response.

For dry charging test, Fig. 4.10 shows a plot of the peak velocity and the peak time versus the leakage size (S) and for different leakage locations (I, II and III). For a fixed leakage size, the maximum peak velocity occurs if the leakage is located in region III, and the minimum peak velocity occurs if the leakage is located in region II. As the leakage goes towards the rear-end of the line, the peak time increases. If the leakage is located in region I or II, the increase in the leakage size causes the decrease in

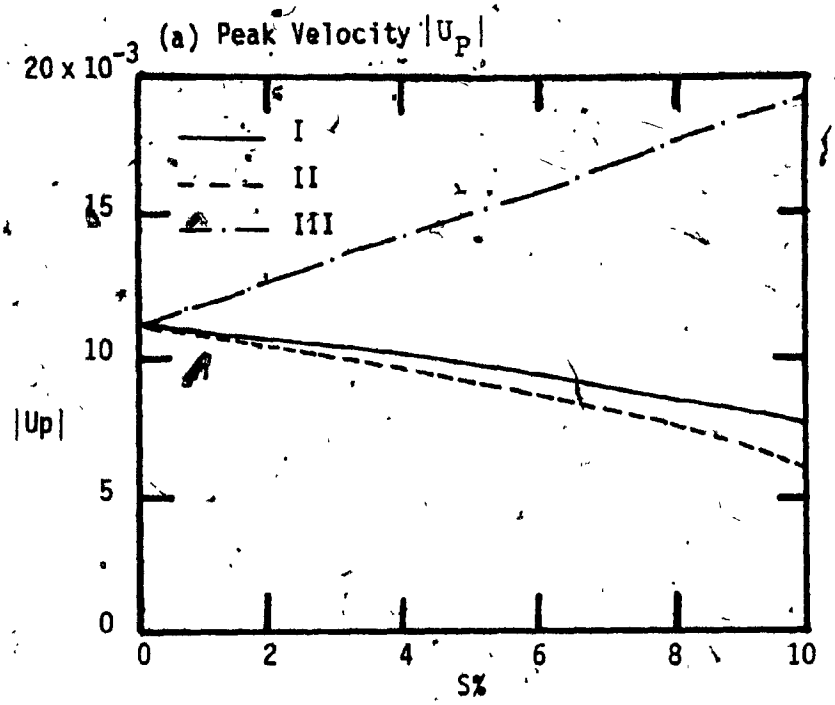

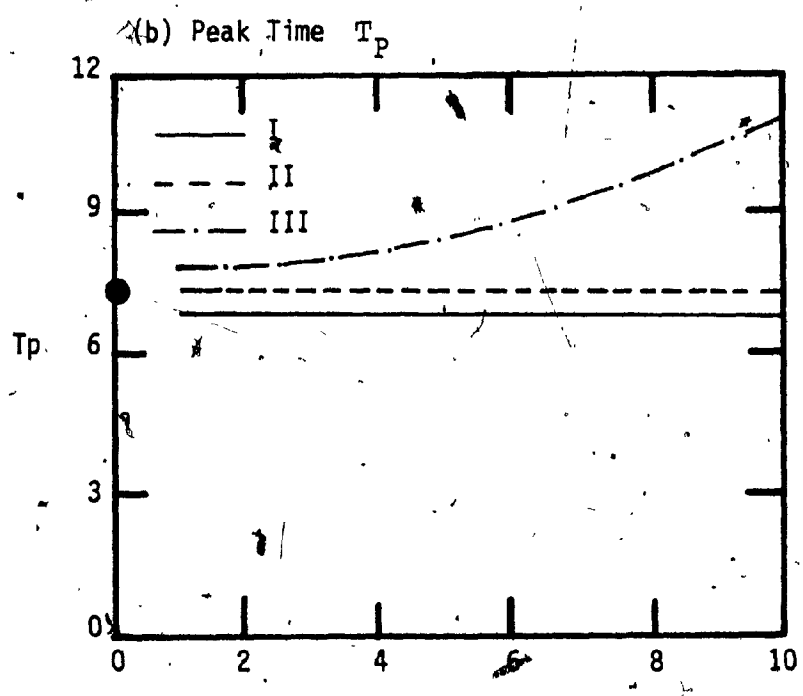

Fig. 4.10 Rear-end Velocity Transient Behaviour due to Dry Charging Test

the peak velocity and the change in the peak time is insignificant. But if the leakage is located in region III, the increase in the leakage size causes the increase in the peak time as well as the peak velocity.

The peak velocity and time obtained from the discharging test are shown in Fig. 4.11. For $S \leq 2\%$ and for fixed leakage location, the peak velocity increases with the leakage size independent of the location of the leakage (region I or II or II). However, the peak time decreases if the leakage is located in region I or II and increases if the leakage is located in region III. For a fixed leakage size, as the leakage goes towards the rear-end, the peak velocity increases and the peak time decreases. From Eqn. (2.20a), the steady-state velocity of the last section of the train-line can be written as follows.

$$U_{N-1} = U\left(1 - \frac{1}{N}\right) = K_N \left(\frac{d_N}{d_p}\right)^2 \qquad (4.3)$$

But the peak velocity is the maximum change of velocity of the last section from its initial value. Fig. 4.11a shows if the leakage is located in region III, as the leakage size increases, the peak velocity increases which might cause the occurrence of the reverse flow phenomena. But as the leakage size becomes greater than 2%, the initial value of the velocity of last section also increases, while the peak velocity decreases. Because of this reason, the occurrence

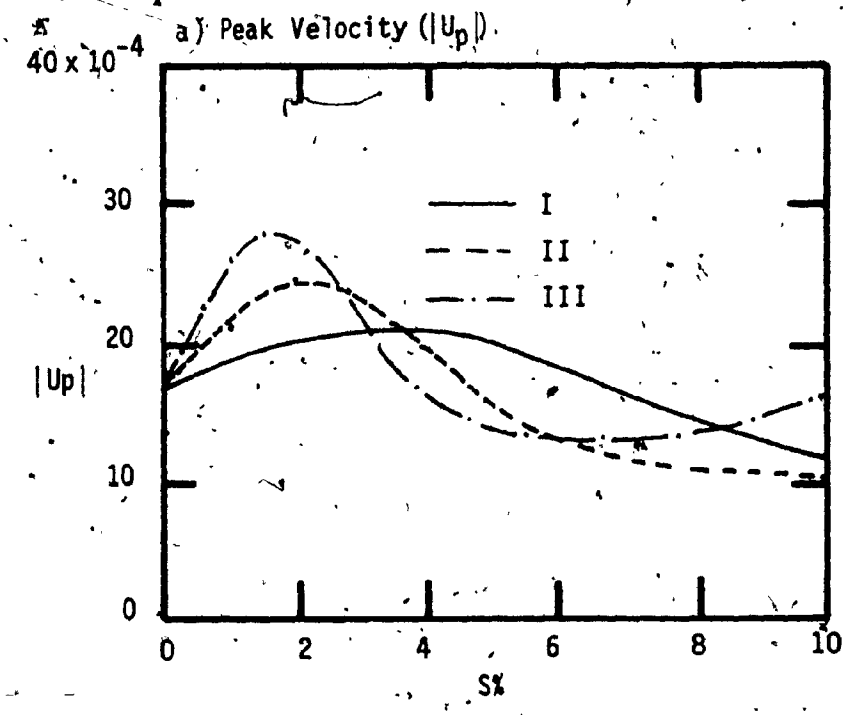

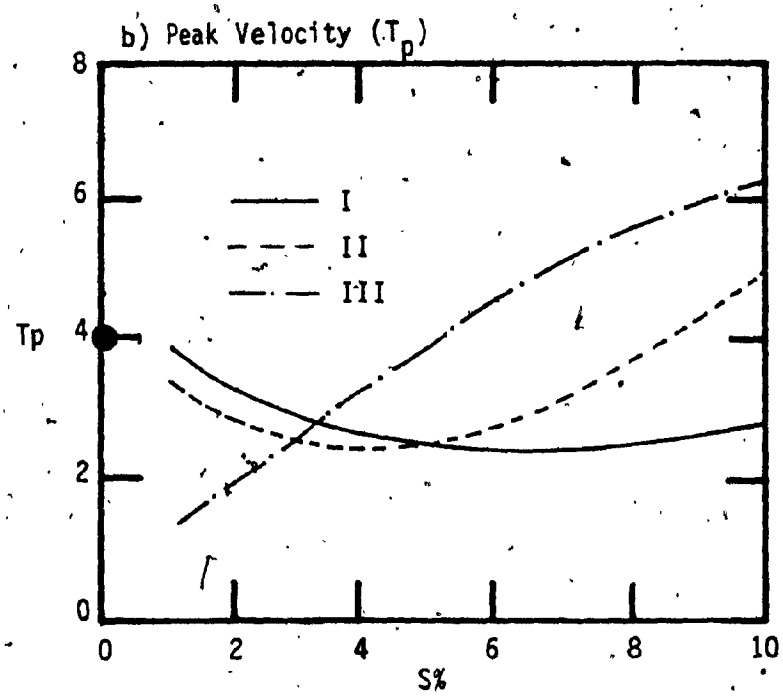

Fig. 4.11 Rear-end Velocity Transient Behaviour due to Discharging Test

of the reverse flow phenomena becomes impossible. If $4\% \leq S \leq 6\%$, for a fixed leakage location, as the leakage size increases, the peak velocity decreases and the peak time increases. There is an exception when the leakage is located in region I. For a fixed leakage size, as the leakage goes towards the rear-end, the peak velocity decreases and the peak time increases.

In general, from the result of the dry charging or discharging test, one can state that the peak velocity and the peak time will decrease with the increase in the leakage size. The peak velocity will decrease and the peak time will increase, as the leakage goes towards the rear-end of the train-line.

Finally, Fig. 4.12 shows the results of the third test (recharging test). For a fixed leakage location, as the leakage size increases, initially the peak velocity decreases till the leakage size reaches a certain value and then it increases. If the leakage is located in region II or III, the peak time increases with the increase in leakage size. However, if the leakage is located in region I instead, the variation in peak time is insignificant. For $S \leq 5\%$ and for a fixed leakage size, as the leakage goes towards the rear-end, the peak velocity decreases and peak time increases.

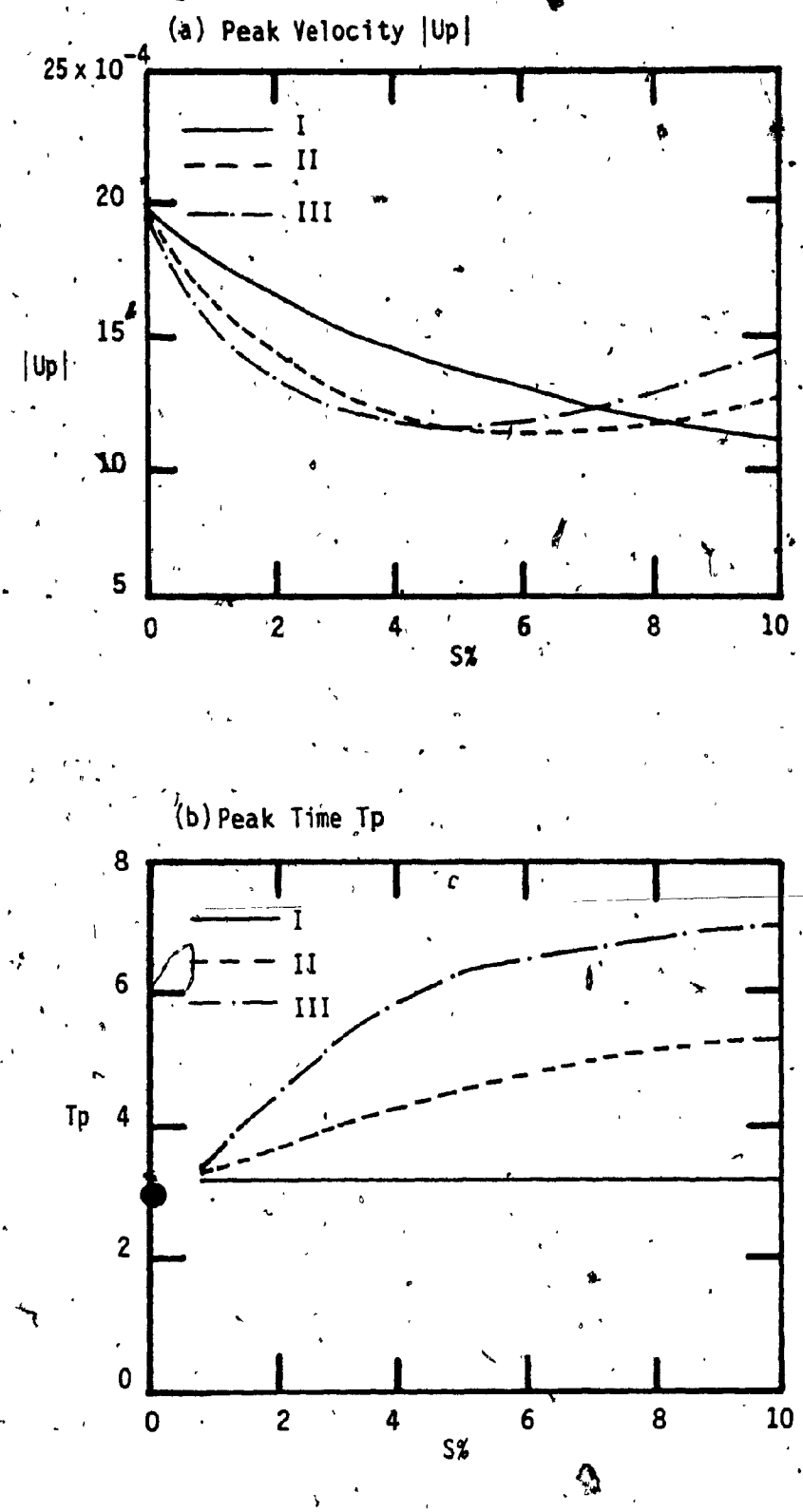

Fig. 4.12 Rear-end Velocity Transient Behaviour due to Recharging Test

4.5 Propagation Speed

The propagation speed represents the transient pressure behaviour of the rear-end of the train-line. The discussion on this section is only valid for a train-line with d_p/l = .003%. The train-line plays the essential part of supplying pneumatic power to operate the brake cylinder, and to transmit the control signals (brake signals from the locomotive to the last car of the train). The result of this action is that, the brakes on each car are applied in sequence as the brake-pipe pressure reduction progresses through the train. In this study the propagation of this action is refered to as the propagation speed, V. In train handling, this speed must be at least 130 mps (400 fps) [1]. Different operating factors are introduced in this section to accomplish this investigation. These factors can be summarized as :

1- leakage size and location.

2- the change in direction of the pressure step applied at the head-end (+ve pressure step or -ve pressure step).

3- threshold sensitivity of the transducer,

D, .2, .13 and .068 , which is equivalent to 20.7, 13.8 and 6.9 kPa or 3., 2. and 1. psi , respectively.

4- amplitude of the pressure applied at the head-end 1.02, .68 and .34, which is equivalent to 103, 69 and 34.5 kPa or 15, 10 and 5 psi respectively.

The theory developed in Chapter 2 is dependent on the direction of the pressure step. In the experiments, to produce a negative change simulating a pressure reduction in brake application, a valve at the head-end is suddenly opened to change the air supply from one regulator valve (P(0)= 5.76) to another (P(0)= 4.74). The time delay, T_D, is obtained experimentally by displaying the output of the 2 pressure transducers on a storage oscilloscope. The time is scaled directly from the oscilloscope for different thresholds D as mentioned above, with an accuracy of 10%. The propagation speed is then calculated from the definition of the time variable T_D:

$$\frac{V}{a} = \frac{1}{t_d\ a} = \frac{1}{T_D} \qquad (4.4)$$

Figs. 4.13, 4.14 and 4.15 show the experimental and theoretical results of the normalized propagation speed,

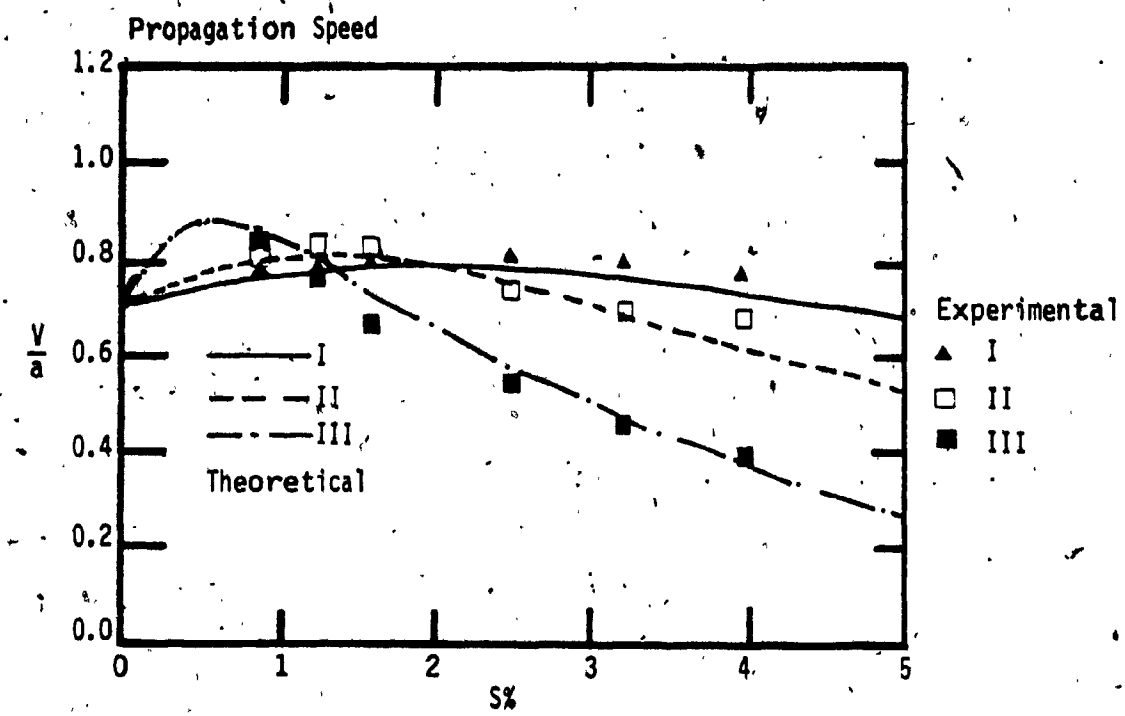

Fig. 4.13 Pressure Transient Behaviour of the Last Section of the Train-line for D = 1 psi (Experimental and Theoretical)

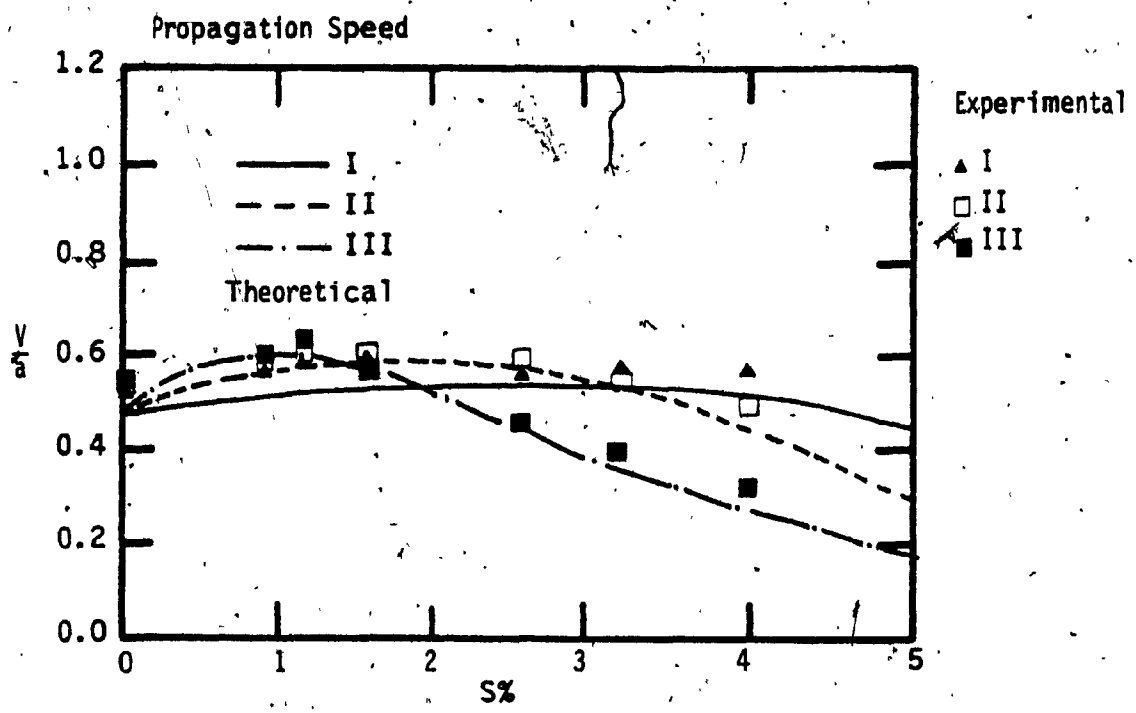

Fig. 4.14 Pressure Transient Behaviour of the Last Section of the Train-line for D = 2 psi (Experimental and Theoretical)

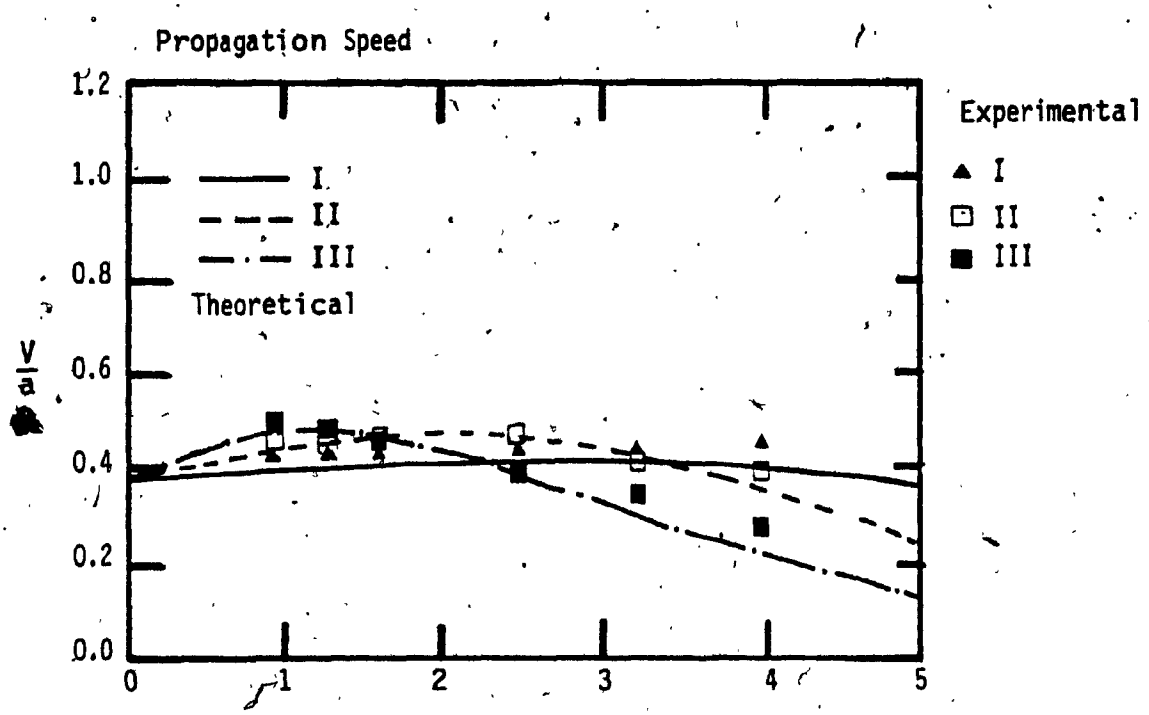

Fig. 4.15 Pressure Transient Behaviour of the Last Section of the Train-line for D = 3 psi (Experimental and Theoretical)

V/a, versus the leakage size, S, for different leakage locations (I, II and III) and threshold sensitivity (1, 2 and 3 psi). The experimental results of the propagation speed are in good agreement with the corresponding theoretical results as shown in Figs. 4.13, 4.14 and 4.15. The discrepancy between the theoretical and experimental results goes as low as 10%. When the leakage is located in region II or III, as the leakage size increases, the propagation speed also increases and then decreases as it reaches a certain leakage size (1.% or 1.5%). In case of leakage located in region I, with the increase of leakage size, the propagation speed increases. For a fixed leakage size, S, and if S is greater than 2%, as the leakage goes toward the rear-end, the propagation speed decreases, whereas for a leakage size less than 2%, as the leakage goes towards the rear-end the propagation speed increases. For fixed leakage size and location, as the threshold sensitivity increases the propagation speed decreases as shown in Figs. 4.17, 4.18 and 4.19.

If the leakage is not located in region I, it has been observed in the course of this study that the propagation speed depends on the initial conditions of the in-line pressure and the velocity or the characteristic resistance, R_c. The characteristic resistance may be defined as:

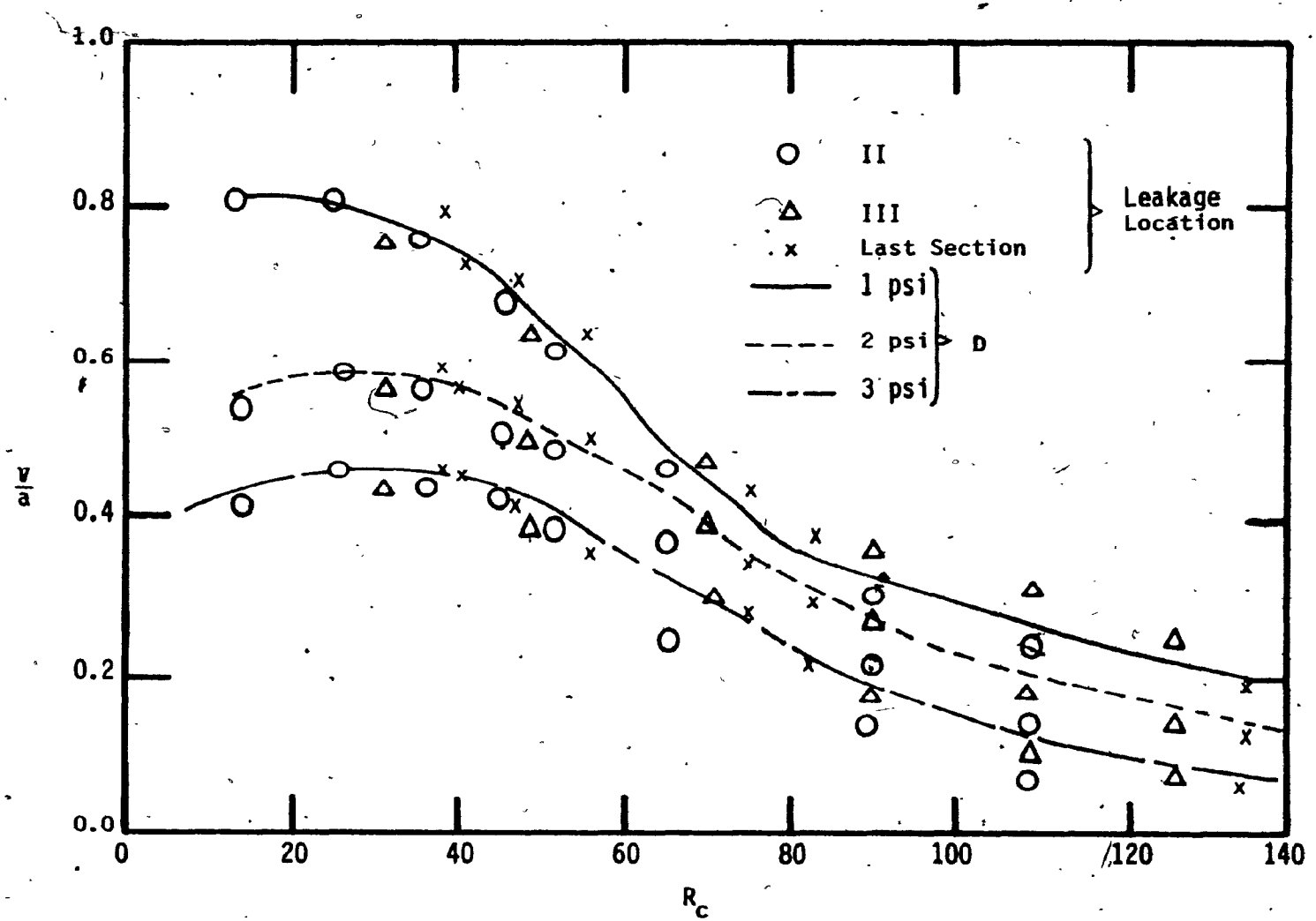

Fig. 4.16 Propagation Speed ($\frac{V}{a}$) vs. Characteristic Resistance (R_c)

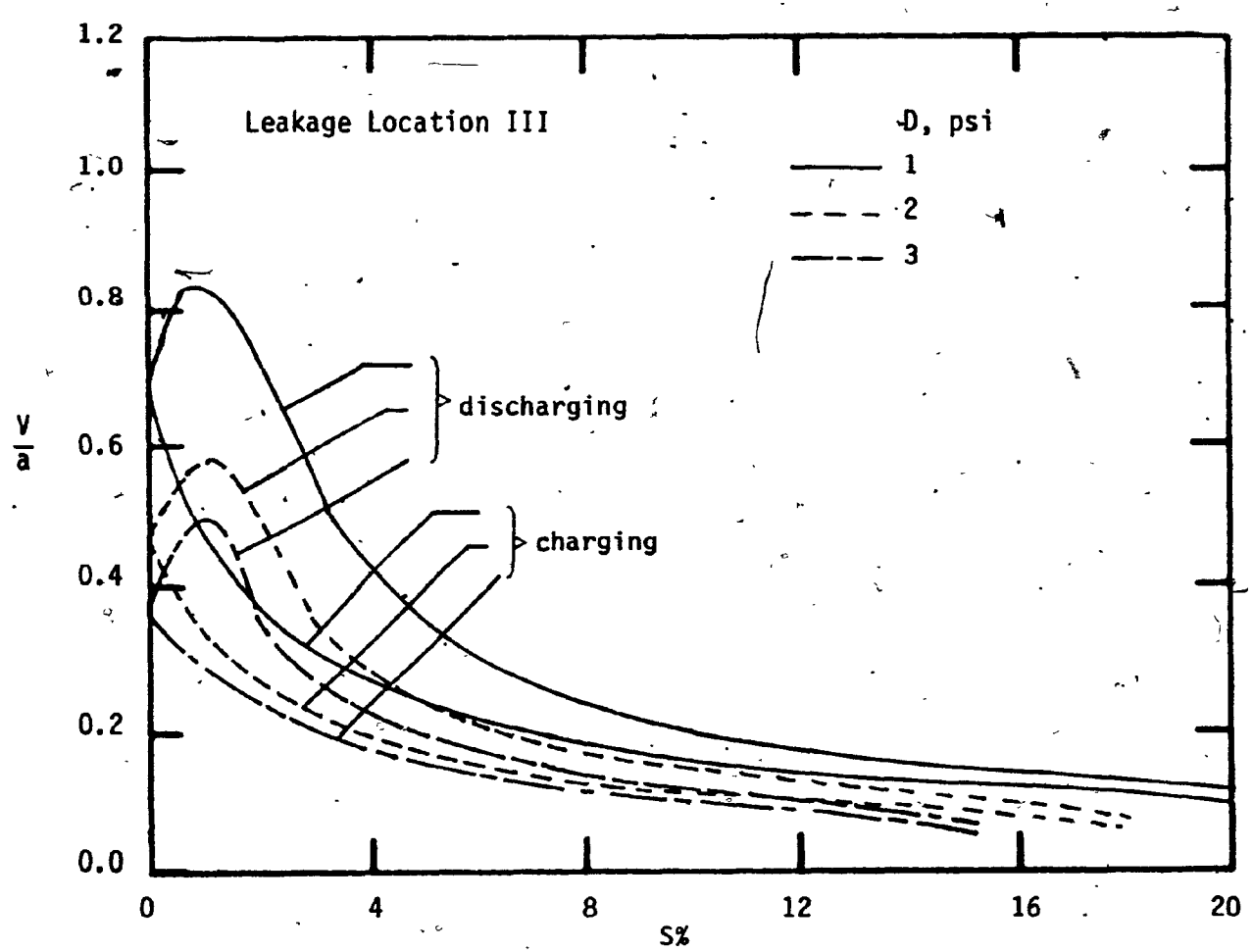

Fig. 4.17 Propagation Speed vs. Leakage Size for Different Sensitivity [D = 1,2, and 3 psi]

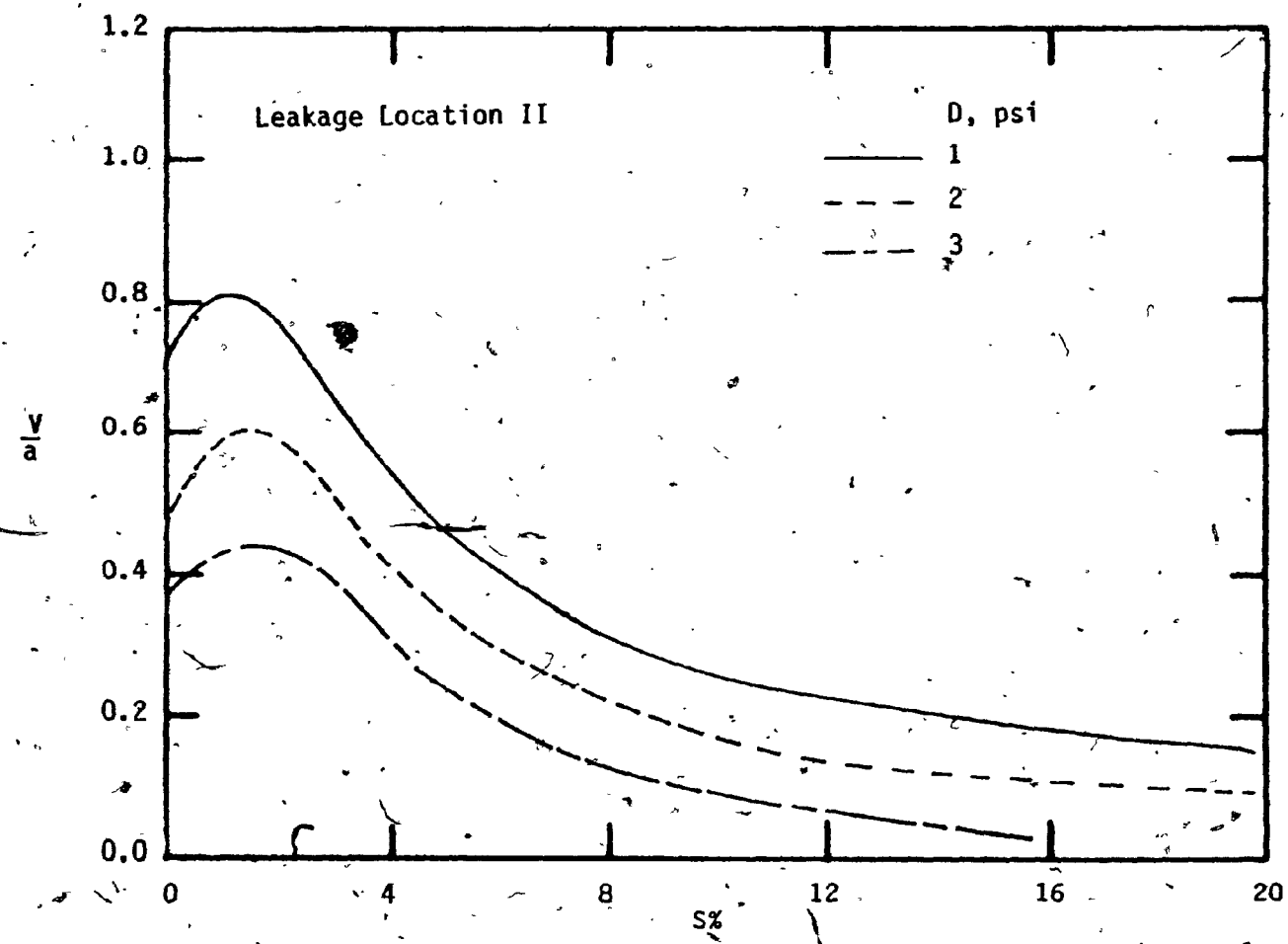

Fig. 4.18 Propagation Speed vs. Leakage Size for Different Sensitivity [D = 1, 2 and 3 psi]

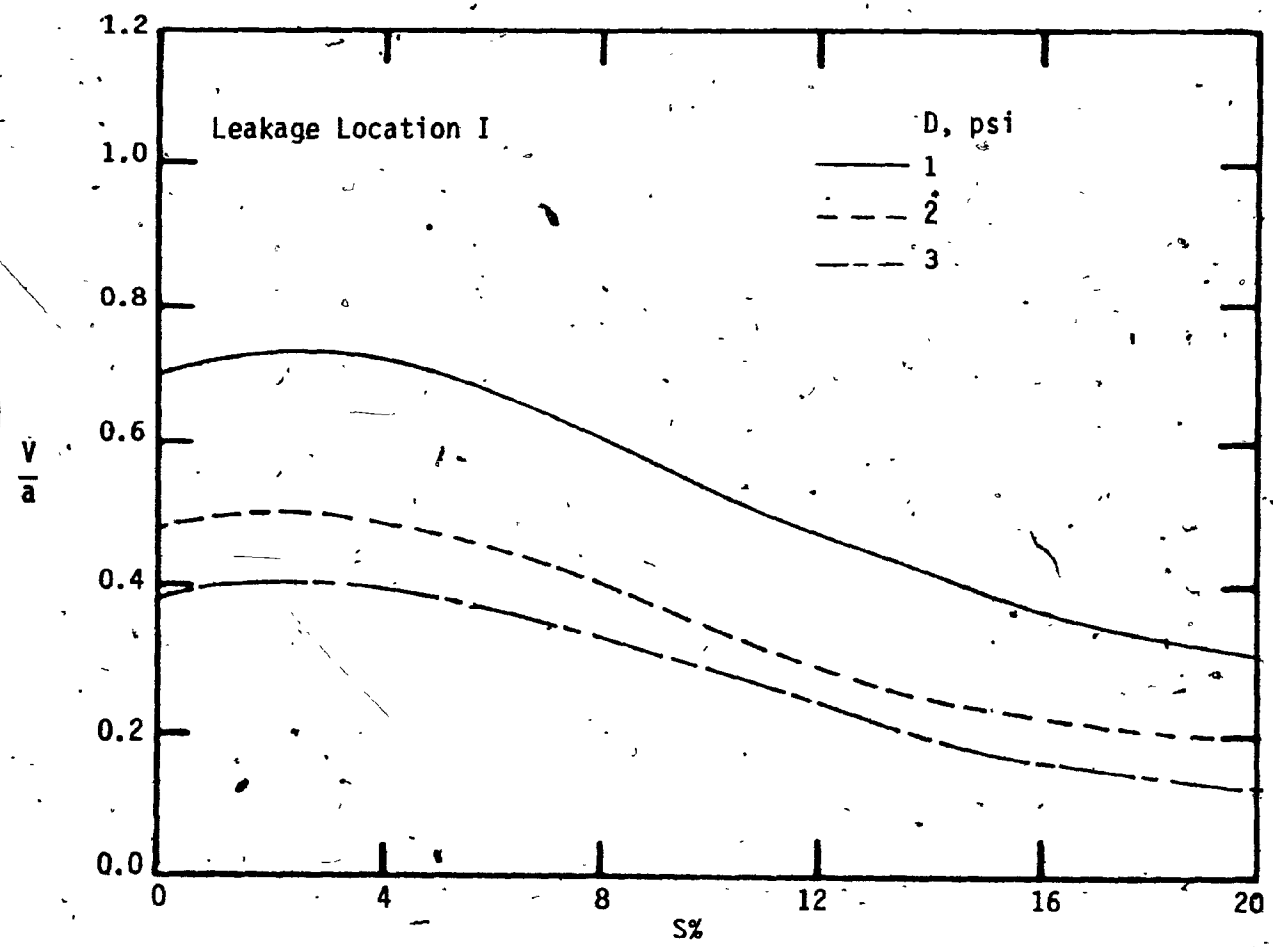

Fig. 4.19 Propagation Speed vs. Leakage Size for Different Sensitivity [D = 1, 2 and 3 psi]

$$R_c \triangleq \frac{\Delta P}{U(0)}$$

Fig. 4.16 shows that, as the characteristic resistance increases, the propagation speed decreases. The result shown in this figure may be used as a basis for a fitness test for the train-line. As an example, the propagation speed will be greater than 130 mps (V/a= .4), as suggested by the Ref. 1, only if R_c has the following values for different D.

D (psi)	R_c
1	54.4
2	68.8
3	76.0

Table 4.1 Maximum Characteristic Resistance values for a Fixed Propagation Speed (V/a = .4).

Fig. 4.17 shows the difference between the propagation speed due to the discharging and recharging tests. In the case of the recharging test (Fig. 4.17), as the leakage size increases, the propagation speed decreases. In the case of the discharging test, as the leakage size increases, the propagation speed initially increases and then decreases (S ≥ 1.0%). A similar observation has been made for the peak velocity.

In Sec. (4.3), it is mentioned that as the leakage size increases, the gain coefficient decreases until it reaches a value which is less than the threshold sensitivity in this study (.2, .13 and .067). The corresponding values of the leakage sizes are 16%, 20% and 23% respectively as shown in Fig. 4.17.

Finally, Fig. 4.20 shows the effect of change of the pressure amplitude at the head-end, $P_r(0)$, on the propagation speed (1.02, .6802 and .34). It is observed from this figure that as $P_r(0)$ increases, the propagation speed also increases. This figure also shows three different cases (1, 2 and 3). Each of these cases presents a train-line having the same relative threshold sensitivity (D_r = .2), but different $P_r(0)$. It has been noted that, as the leakage size increases the discrepancy between the propagation speed for second and third cases becomes less. Therefore, the train-line can be linearized, as suggested by Cheng, Katz and Abdol-Hamid [8]. This approach can be applied only if the leakage is located at the last car. The train line mathematical model is linearized and solved analytically in Appendixes F and G. This approach reduces the number of train-line parameter (1, d_p, d_i) to only one parameter N_K (Appendixex F and G). In Appendix H, the mathematical model and the train-line laboratory model, are employed to correlate the propagation speed with the relative threshold sensitivity (D_r = .001 P(0)) and the

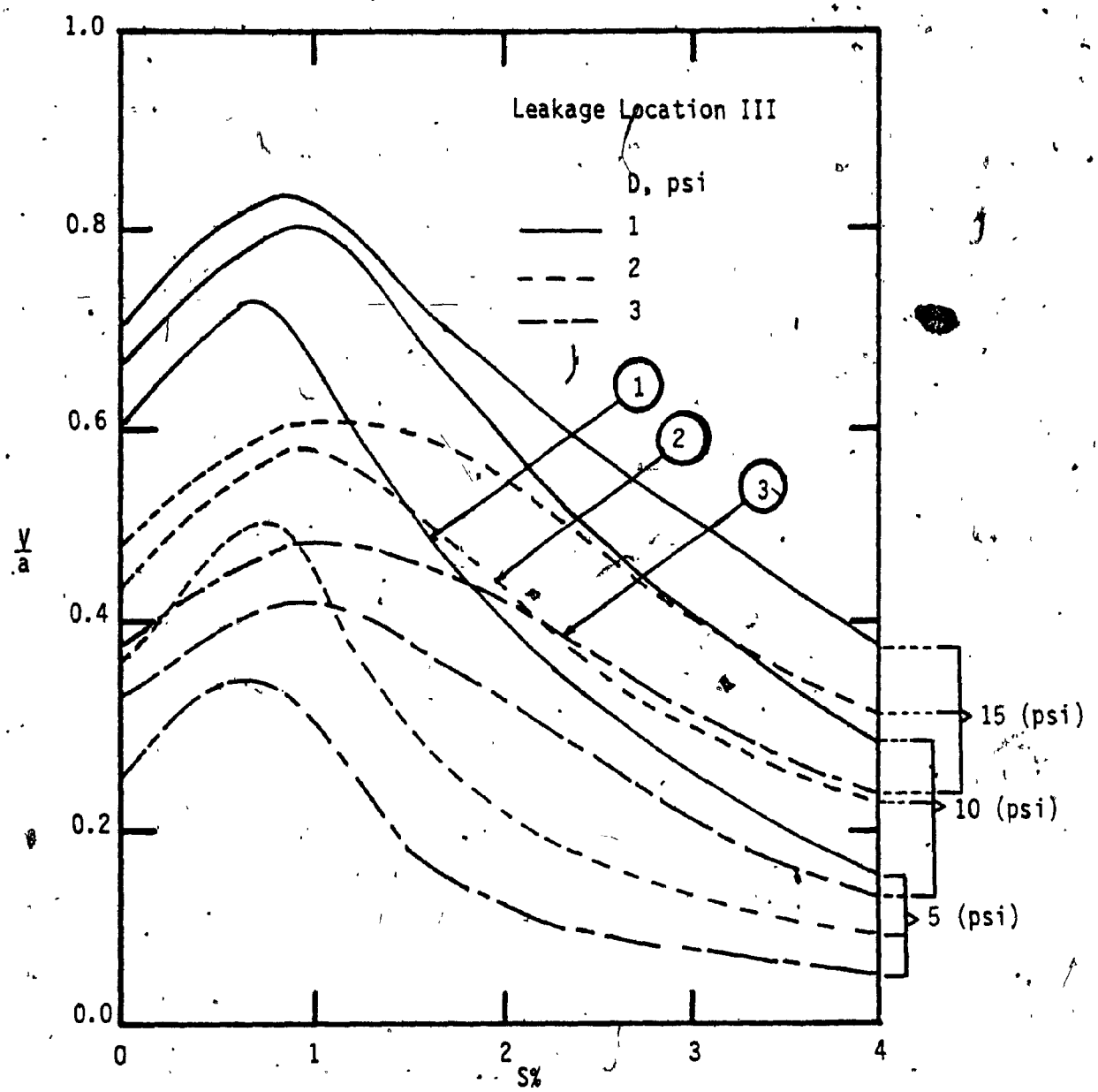

Fig. 4.20 Propagation Speed vs. Leakage Size for Different Sensitivity (D = 1, 2 and 3 psi) and Different Head-end Pressure Amplitude, $P_r(0)$

non-dimensional characteristic number N_K, which incorporates the physical and fluid dynamic properties of the line.

4.6 Summary

This Chapter investigates the effects of leakage and other parameters on the rear-end pressure and velocity transient behaviour of the train-line. These factors were

1- leakage size and location ($S \leq 3.57\%$ for the experimental investigation, and $S \leq 20\%$ for the theoretical investigation).

2- the change in direction of the pressure applied at the head-end (+ve pressure step or -ve pressure step).

3- threshold sensitivity of the transducer .2, .13 and .067 , which is equivalent to 20.7, 13.8 and 6.9 kPa or 3., 2. and 1. psi . respectively.

4- amplitude of the pressure applied at the head-end 1.02, .68 and .34 , which is equivalent to 103, 69 and 34.5 kPa or 15, 10 and 5 psi respectively (only for the

theoretical investigation)

Sec. (4.2) described three tests which were used to investigate the effects of the leakage on the transient behaviour of the train-line. Sec. (4.3) discussed in general the effects of the leakage size and the leakage location on the pressure and velocity transient response. The discussion concluded that for any of the tests as the leakage size increases or the leakage goes towards the rear-end, the steady-state time increases and the gain coefficient decreases. Then, Sec. (4.4) discussed in detail the effects of the leakage size, leakage location and the change of the pressure step direction applied at the head-end on the transient behaviour of the last section velocity ($U\,(1-\frac{1}{N},T)$) of the train-line which was refered as the peak time, T_p, and peak velocity, U_p. Finally, in Sec. (4.5), the effects of these factors on the transient pressure behaviour at the rear-end pressure have been discussed in detail. In general, one can conclude that the decrease of the propagation speed may be caused by the existence of one of the following terms:-

1- The increase of the leakage size, S.
2- The presence of the leakage at the rear-end.
3- The increase of the threshold sensitivity, D.
4- The decrease of the head-end pressure amplitude, .

This study shows the effects of the leakage on the propagation speed. However, instead of attempting to

achieve the virtually impossible task of eliminating the leakage absolutely, trains are allowed to leave the yard even if they are known to be leaking, provided that they pass stringent leak tests beforehand (Shute, Wright, Taft and Banister [28], and Blaine and Hengel [1]).

PART TWO

CHAPTER 5

MULTI-LEAK LOCATING METHODS APPLIED TO A TRAIN-LINE

5.1 Introduction

Chapter 1 describes how the train-line plays the vital role of supplying pneumatic power to operate the brake cylinders, and to transmit the control signal (brake signal) from the locomotive all the way to the last car of the train. Whereas Chapters 3 and 4 show how the train-line characteristics do depend on, among a large number of parameters and working factors, the existence of the leakage. However, in the case of the brake pipe application, because of the numerous number of joints and fittings found in each control valve that is connected to the train-line, "plumbing leakage" is unavoidable. Instead of attempting to achieve the virtually impossible task of eliminating the leakage absolutely, trains are allowed to leave the yard even if they are known to be leaking, provided that they pass the leakage tests. A brake system which passes these tests can be described as "faultless" as far as leakage is concerned.

In the specific area of location of faulty leaks of a train-line, while Aula, Cheng and Katz [21] proposed several

methods, those methods are applicable to a single fault, and there is no rigorous proof given. On the other hand this Chapter proposes two methods, each of which is suitable for locating multiple faulty leaks. Sec. (5.2) describes the steady state model of the train-line. This development of this model is extracted from the train-line mathematical model which is described in Sec. (2.2). Then, a complete proof of the pressure-ratio method for multiple leakage location (Theorem 1) is provided in Sec. (5.3). Whereas Sec. (5.4) presents a formal proof of the pressure-difference method (Theorem 2) for a single faulty leak. Then this method is extended to multiple leakage locations, without proof. Sec. (5.5) summarizes the result of this chapter.

It is important at this juncture to define the terms "no-fault" and "fault". A train-line that exhibits an acceptable amount of leakage is, in the context of this research, in a no-fault condition to begin with. Subsequently, a faulty situation, if it develops additional leaks or if some existing leaks become more severe, arises as a result of either normal usage or mishandling of the train. The two multiple-leak detection methods as proposed in this Chapter make use of some comparisons of pressure measurement of this train-line between the no-fault and the faulty condition of the train-line in question. Thus, by regularly monitoring the train-line, it is possible to detect and locate the existence of the faulty leaks as soon as they develop.

5.2 Steady State Mathematical Model for the Train-Line

The leakage location methods as proposed in this Chapter are to be applied during steady state conditions of the train-line. For the steady state conditions, one can apply Eqns. (2.8) and (2.9) after droping the unsteady state terms from these equations ($\frac{\partial P}{\partial T} = \frac{DU}{DT} = 0$). Thus Eqns. (2.8) and (2.9) can be rewritten in the form:

$$\frac{\partial M}{\partial X} = - \Psi \tag{5.1}$$

$$\frac{\partial P^2}{\partial X} = -\gamma \frac{fl}{d_p} M^2 \tag{5.2}$$

where,

M $\triangleq$ the normalized in-line mass flow rate.

$$= \frac{m}{\rho_a A a}$$

m $\triangleq$ the in-line mass flow rate.

$$= \rho u A$$

When applying the backward finite difference scheme in the space "X" in Eqns. (5.1) and (5.2). Now these equations can be written in the form:-

$$\left.\begin{aligned} M_i - M_{i-1} &= -\Psi_i \Delta X = -\phi_i \\ &= -K_i \left[\frac{d_i}{d_p}\right]^2 P_i \\ &= -\frac{P_i}{r_i} \end{aligned}\right\} \quad (5.3)$$

$$\left.\begin{aligned} P_i^2 - P_{i-1}^2 &= -\gamma \frac{f1}{d_p} \Delta X M_{i-1}^2 \\ &= -R_i^2 M_{i-1}^2 \end{aligned}\right\} \quad (5.4)$$

where,

R_i $\triangleq$ The normalized in-line flow resistance of section (i).

r_i $\triangleq$ The normalized leakage flow resistance at the node (i).

$\Psi \Delta X$ $\triangleq$ The normalized leakage flow from section (i).

P_i $\triangleq$ The normalized air pressure at the ith node.

$M_{i-1} \triangleq$ The normalized in-line airflow through the ith section of the train-line.

From Eqns. (5.3) and (5.4), the train-line may be modelled as a ladder resistance network, Fig. 5.1, of N sections. Each typical section contains an in-line non-linear resistance to air flow R_i through that section of the train-line, and a leakage resistance r_i. Let

$$\left.\begin{aligned} \beta_i &\triangleq \left(\frac{P_{i-1}}{P_i}\right)^2 \\ C_i &\triangleq \frac{R_i}{r_i} \\ D_i &\triangleq \frac{R_{i+1}}{R_i} \end{aligned}\right\} \quad (5.5)$$

It may be shown from Eqns. (5.3), (5.4) and (5.5) that

$$\left.\begin{aligned} \beta_i &= \sigma_1 (\beta_{i+1}, C_i) \\ &= 1 + \left[\frac{1}{D_i}\left(1 - \frac{1}{\beta_{i+1}}\right)^{1/2} + C_i\right] \end{aligned}\right\} \quad (5.6a)$$

and that,

$$\left.\begin{aligned} \beta_N &= \sigma_2 (C_N) \\ &= 1 + C_N^2 \end{aligned}\right\} \quad (5.6b)$$

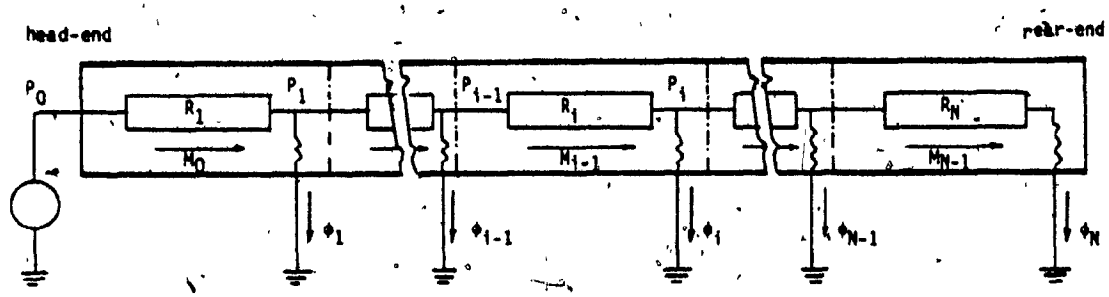

Fig. 5.1 Steady-state Model of the Train-line

Note that the following quantities are all positive in magnitude:-

$$\left.\begin{aligned} \frac{\partial \beta_i}{\partial C_i} &= \frac{\partial \sigma_1}{\partial C_i} \\ \frac{\partial \beta_i}{\partial \beta_{i+1}} &= \frac{\partial \sigma_1}{\partial \beta_{i+1}} \end{aligned}\right\} \text{ for } 1 \leq i \leq N \qquad (5.7a)$$

and,

$$\frac{\partial \beta_N}{\partial C_N} = \frac{\partial \sigma_2}{\partial C_N} \qquad (5.7b)$$

It may further be shown that

$$\frac{P_i}{P_0} = \prod_{j=1}^{i} \frac{1}{\sqrt{\beta_j}} \qquad (5.8)$$

where P_0 = head-end pressure and that,

$$\left.\begin{aligned} E_i &\triangleq \frac{P_i}{P_i'} \\ &= \frac{(P_i/P_0)}{(P_i'/P_0)} \\ &= \prod_{j=1}^{i} \left(\frac{\beta_j'}{\beta_j}\right)^{1/2} \end{aligned}\right\} \qquad (5.9)$$

where,

P_i, P'_i = the pressure measurements of the same section of train-line with no-fault initial condition and in the faulty condition, respectively.

All other variables and parameters are similarly differentiated from each other (primed for faulty and unprimed for no-fault initial conditions).

Let r be the total number of faulty leaks in the train-line, and let them be identified by the numbers 1, 2, ..., r so that leak 1 is closest to the head-end of the train-line, and leak r closest to the rear-end. Also, let leak j be located in section K_j of the train-line.

Obviously $1 \leq K_j \leq N$, $1 \leq j \leq r$ (5.10)

5.3 Pressure-Ratio Method for Multiple-Leak Location

Theorem 1

"In a faulty train-line, the ratio between the no-fault pressure reading at a section and the faulty pressure reading of the same section is smaller than, or at most equal to, the pressure-ratio of any other section downstream of it ..."

Expressed mathematically, Theorem 1 may be simply stated as,

$$E_{i-1} \leq E_i \qquad 1 \leq i \leq N$$

While Theorem 1 stipulated that E_i is a monotonic function of i (that is, one that never decreases with increasing i), by itself it is not very useful for formulating a leak location method.

However, by examining Fig. 5.2 which shows the function E_i for a train-line with different number and distribution of major leaks, it is evident that whereas the curve E vs.i is perceivably continuous throughout, at the section where a faulty leak occurs, there is a noticeable bend, signifying a discontinuty of the first derivative of the function at that section of the train-line.

Thus a second part may be addended to Theorem 1:

"....Furthermore, the curve E_i exhibits an abrupt change in slope (a bend) at a section of the train-line where there exists a faulty leak."

The proof of Theorem 1 consists of 3 parts :-

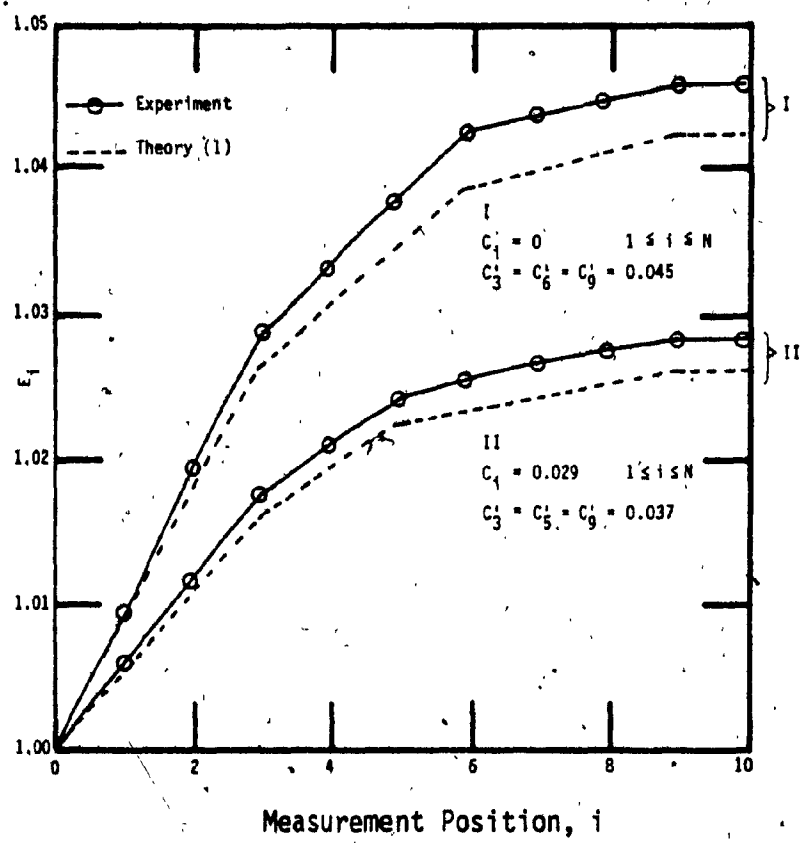

Fig. 5.2 Experimental and Simulated Results of the Ratio Method

a- to prove that $\beta'_i \geq \beta_i$ for all i

b- to prove that $(E_{i-1})_0 \leq E_i$

where $(E_{i-1})_0$ is the value of E_{i-1} provided that there is no faulty leak at section i.

c- to prove that $(E_{i-1})_1 < (E_{i-1})_0$, where $(E_{i-1})_1$ is the value of E_{i-1} if there is a faulty leak at section i.

Proof (a)

According to Eqn (5.6) $\beta_i = \sigma_1(\beta_{i+1}, C_i)$ is a recursive function of β.

Consequently

$$\beta_i = \beta\ (\beta_{i+1}, \beta_{i+2}, \ldots, \beta_N, C_i, C_{i+1}, \ldots, C_N) \quad (5.11)$$

Suppose that the last faulty leak occurs at section K_r , where $K_r < N$

I- Consider the case of $K_r < N$.

then $C'_N = C_N$. Since $\beta_N = \sigma_2(C_N)$ therefore $\beta'_N = \beta_N$.

Similarly, provides that $K_r < N-1$ (i.e. $C'_{N-1} = C_{N-1}$)

$$\left.\begin{aligned} \beta'_{N-1} &= \sigma_1\ (\beta'_N\ ,\ C'_{N-1}) \\ &= \sigma_1\ (\beta_N\ ,\ C_{N-1}) \\ &= \beta_{N-1} \end{aligned}\right\} \qquad (5.12)$$

Thus, proceeding upstream up to and before K_r,

$$\beta'_N = \beta_N \qquad (5.13)$$

However at K_r, $r'_{K_r} < r_{K_r}$, and referring to the definition of C_i in Eqn (5.5),

$$C_K = \frac{P_K}{r_K}$$

Therefore $C'_{K_r} > C_{K_r}$

$$\beta'_{K_r} = \sigma_1\ (\beta'_{K_r+1},\ C'_{K_r})$$

$$= \sigma_1\ (\beta_{K_r+1},\ C_{K_r})$$

and, $\beta_{K_m} = \sigma_1\ (\beta_{K_r+1},\ C_{K_r})$

Since, according to (5.7b) above, an increase in C_i in the function σ_1 leads to an increase in the value of β_i, therefore

$$\beta'_{K_r} > \beta_{K_r} \qquad (5.14)$$

Now, $\beta'_{K_r-1} = \sigma_1 (\beta'_{K_r}, C'_{K_r-1})$

Even if $C'_{K_r-1} = C_{K_r-1}$, i.e. no-fault at section K_r-1

$$\beta'_{K_r-1} > \beta_{K_r-1} \qquad (5.15)$$

because $\beta'_{K_r} > \beta_{K_r}$ from (5.14) above.

If $C'_{K_r-1} > C_{K_r-1}$

then, β'_{K_r-1} will be further greater than β_{K_r-1}.

Thus, $\beta'_{K_r-1} > \beta_{K_r-2}$, and so on.

Hence, $\beta'_i \geq \beta_i$ for all i (5.16)

II- In case the last fault falls on the last section of the train-line,

$K_r = N$.

Then, $\beta'_N = \sigma_2(C'_N)$, with $C'_N > C_N$.

According to (5.7b), $\frac{\partial \beta_N}{\partial C_N} > 0$.

Hence, $\beta'_N > \beta_N$

Thus, $\beta'_i \geq \beta_i$ for all i (5.17)

Proof (b)

According to the definition of E in Eqn (5.9)

$$E_i = \prod_{j=1}^{i} \left(\frac{\beta'_i}{\beta_j}\right)^{1/2} = E_{i-1} \left(\frac{\beta'_i}{\beta_i}\right)^{1/2}$$

When there is no fault in section i, $C'_i = C_i$. Therefore,

$$(E_{i-1})_0 = E_i \left(\frac{\beta_i}{\beta'_i}\right)^{1/2}$$

$$= E_i \left[\frac{\sigma_1 (\beta_{i+1}, C_i)}{\sigma_1 (\beta'_{i+1}, C'_i)}\right]^{1/2} = E_i \left[\frac{\sigma_1 (\beta_{i+1}, C_i)}{\sigma_1 (\beta'_{i+1}, C_i)}\right]^{1/2} \quad (5.18)$$

Since from (5.16)

$\beta'_i \geq \beta_i$ for all i, therefore $(E_{i-1})_0 \leq E_i$ (5.19)

This completes the first part of Theorem 1, that the pressure-ratio at any section of a faulty train-line is at least as greater as that at any section upstream of it.

Proof (c)

When a fault is located at section i, $C_i' > C_i$, then

$$\sigma_1 \ (\beta_{i+1}', \ C_i') > \sigma_1 \ (\beta_{i+1}, \ C_i) \qquad (5.20)$$

Consequently,

$$(E_{i-1})_1 = E_i \left[\frac{\sigma_1 \ (\beta_{i+1}, \ C_i)}{\sigma_1 \ (\beta_{i+1}', \ C_i')}\right]^{1/2}$$

$$< E_i \left[\frac{\sigma_1 \ (\beta_{i+1}, \ C_i)}{\sigma_1 \ (\beta_{i+1}', \ C_i)}\right]^{1/2}$$

This together with (5.14) and (5.15) above, yields,

$$(E_{i-1})_1 < (E_{i-1})_0 \leq E_i \qquad (5.21)$$

Hence a bend of the E-curve occurs at section i where there is a faulty leak, completing the proof for the second part of Theorem 1.

A ratio-method for locating faulty leak of a train-line may be formulated as follows:-

"Compare the pressure readings of the train-line, section by section, before and after the faulty situation has developed, i.e. compute E_i for each i. On a plot of E_i vs.i, where there exists a sudden change of slope, a

fault leak exists".

Note that with this method,

1- knowledge of the physical parameters of the train-line is not required.

2- there is no limit to the number of faults that can be detected and located.

Fig. 5.2 shows 2 examples of a train-line with leakages with the following characteristics

Example I: $C_i = 0$; in other words, no initial leakage. Faults are located at sections 3, 6 and 9.

Example II: Some initial leakage. Faults are located at sections 3, 5 and 9.

In each case, the digital computer model using the theory outlined in section (5.2) successfully locates the position of the faults. Using a laboratory train-line

model, the details of which are given in section (3.2), the author has also been able to locate the position of faults with adequate accuracy.

The values of R_i, as defined in Eqn (5.3), characterizing the pipe resistance, are determined experimentally. The values are shown in Fig. 5.3. For a computer calculations, an average of $\bar{R}^* = 12.8$ is assumed.

It has been observed in the course of experimentation that difficulties do arise when pressure changes are too small compared to the sensitivity of the transducers available (typically at 0.05%). For this reason, it is recommended that a finite difference method be applied to the test data to obtain the 2nd order difference. This is based on the fact that since the E-curves are bent at the location of a fault, there is a discontinuity of the first differential (or difference) at these locations. Fig. 5.4 shows that applying this method to the data in Fig. 5.2 yields amplified "leaks" at the locations of faulty leaks. The second difference is formulated according to the following scheme:

$$G_0 = 0.0$$

$$G_i = \delta_i^2 = 2 \cdot E_i - \left[E_{i-1} + E_{i+1}\right] \qquad 1 \leq i \leq N$$

$$G_N = E_N - E_{N-1} \qquad i = N$$

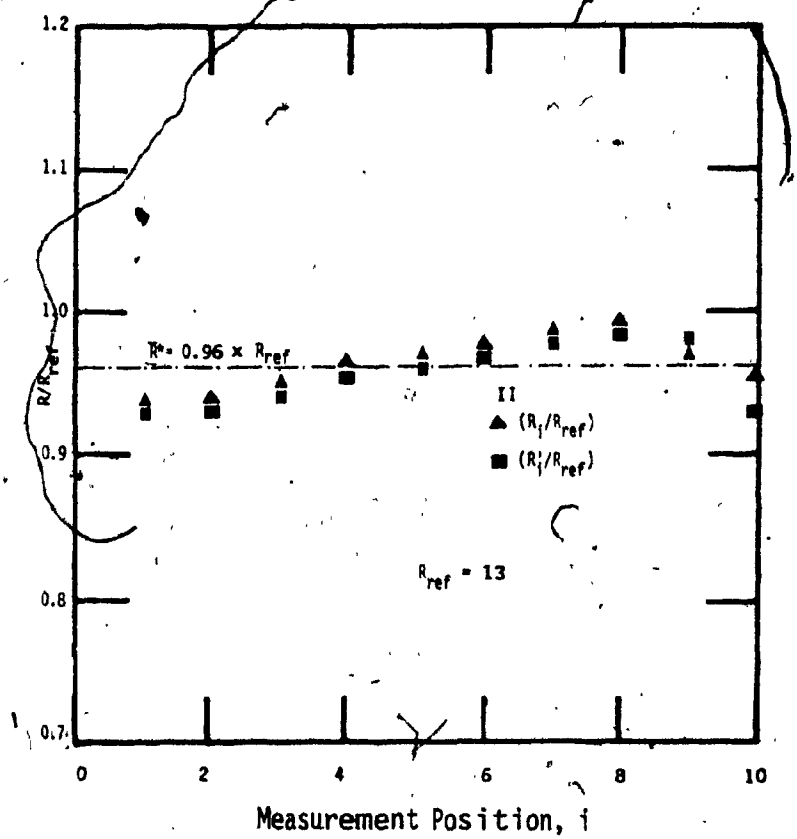

Fig. 5.3 Experimental Values of In-line Resistance R_i (normalized)

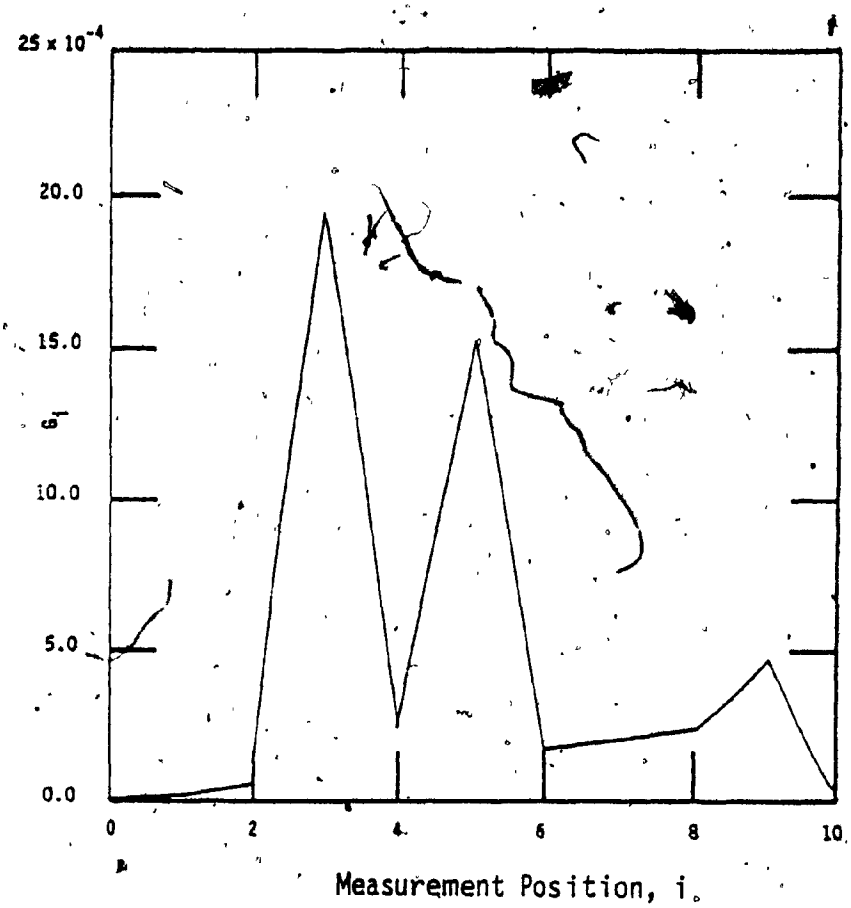

Fig. 5.4 Central Difference of E_i for Example II

5.4 Pressure-Difference Method for Multiple-Leak Location

Trick and Chien [27] proved that for any positive resistor network, if one and only one resistor changes its value for the nominal one, then the voltage changes across that resistor will be greater than or equal to the voltage changes across any other resistor in the circuit.

A theorem may be similarly formulated for a train-line with leakage, even though the train-line is a nonlinear ladder network:-

Theorem 2

> **"In a train-line with leakage, if one and only fault develops, then the change in the pressure reading at the faulty section is universally greater than the pressure change at any other section".**

Previously, Aula et al [21] successfully applied this theorem, without proof, for a single fault location in a train-line with leakage. Fig. 5.5 is an excerpt of the result from Ref. 21, showing 2 examples of a train-line with a fault in section 2 in one case, and in section 8 in the other.

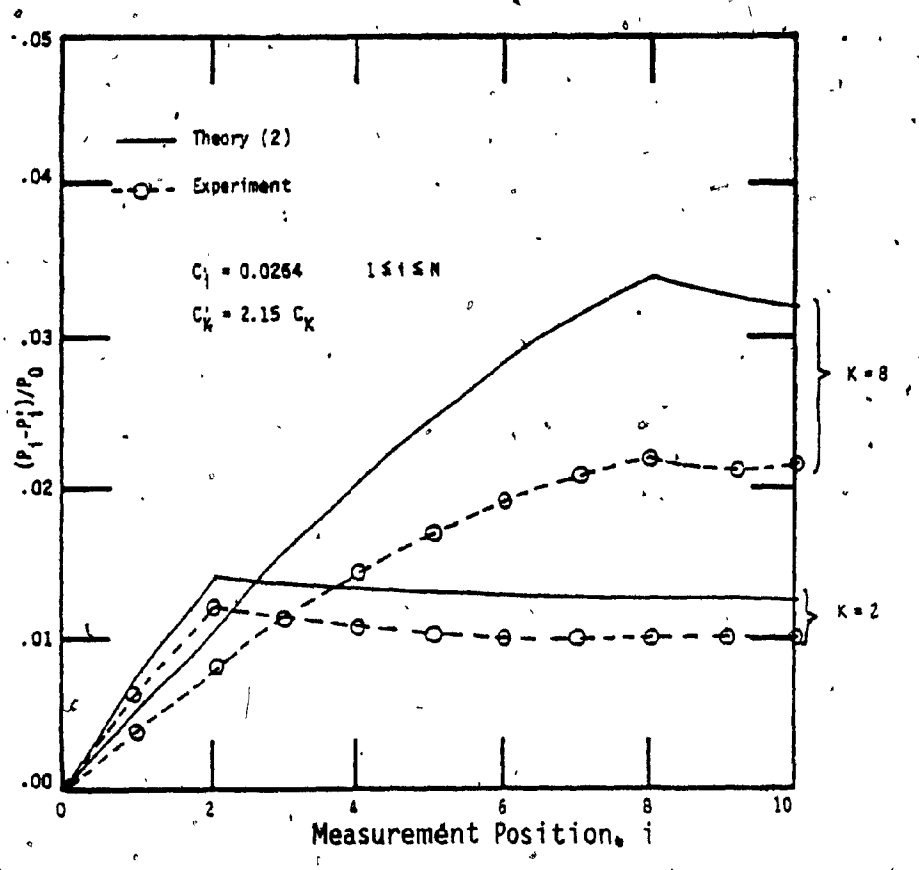

Fig. 5.5 Experimental and Simulated Results of the Difference Method (according to Aula et al [21])

This section presents a formal proof of this theorem for a single faulty leakage. Further on, the concept of pressure-difference is extended to multiple-leakage locations, without proof.

Proof

Let Δ be defined as the pressure difference,

$$\Delta_i \stackrel{\Delta}{=} P_i - P_i' \tag{5.22}$$

Let the single faulty leak be located in section K. Retracting the argument leading to Eqn (5.19),

$$E_K = E_i \qquad K \leq i < N \tag{5.23}$$

By definition of E,

$$\frac{P_K}{P_K'} = \frac{P_i}{P_i'}$$

and so,

$$\frac{P_K - P_K'}{P_K'} = \frac{P_i - P_i'}{P_i'} \tag{5.24}$$

From Equation (5.6a)

$$\beta_i' = \sigma_1 (\beta_{i+1}', C_i')$$

$$= 1 + \left[\frac{1}{D_i} \left(1 - \frac{1}{\beta_{i+1}'}\right)^{1/2} + C_i'\right]^2$$

The second term of the right-hand side of the equation is positive. Therefore,

$\beta_i' > 1$ for all i

i.e. $P_{i-1}' > P_i'$ by definition of β_i' for all i

Thus,

$P_K' > P_i'$ as long as $i \geq K + 1$

Substituting this into (5.24)

$$P_K - P_K' > P_i - P_i' \qquad i > K + 1$$

In other words,

$$\Delta_K > \Delta_i \qquad K + 1 \leq i \leq N \qquad (5.25)$$

Stated in words, the pressure difference Δ at the faulty section is larger than that at any section downstream of it.

It remains to prove that this pressure change is also

larger than that at any section upstream of it as well, i.e. $\Delta_K > \Delta_{K-1} > \ldots > \Delta_1 > \Delta_0$.

It has been proven in Theorem 1 that

$$E_{i-1} < E_i \tag{5.21}$$

as long as i is upstream of the fault.

For i=1

$$E_0 < E_1 \tag{5.26}$$

Since the head-end pressure remains constant,

$$P_0' = P_0$$

Therefore,

$$\left.\begin{aligned} E_0 &\triangleq \frac{P_0}{P_0'} = 1 \\ \Delta_0 &\triangleq P_0 - P_0' = 0 \end{aligned}\right\} \tag{5.27}$$

Hence, from Eqn (5.26),

$$\begin{aligned} &E_1 > 1 \\ &\text{i.e. } P_1 > P_1' \end{aligned} \tag{5.28}$$

Also $\Delta_1 > 0$ (5.29a)

or $\Delta_1 > \Delta_0$

i.e. $P_1 - P_1' > P_0 - P_0'$ (5.29b)

In general, from (5.21)

$$E_i > E_0 \qquad 1 \leq i \leq K - 1$$

Therefore,

$$E_i > 1, \text{ since } E_0 = 1 \text{ from (5.27).}$$

Therefore,

$$P_i > P_i' \tag{5.30}$$

Similarly,

$$P_{i-1} > P_{i-1}'$$

Adding these two inequalities,

$$P_i + P_{i-1} > P_i' + P_{i-1} \tag{5.31}$$

Rearranging the terms of Eqn (5.29b)

$$P_1 - P_0 > P_1' - P_0'$$

and multiplying with Eqn (5.31) for i= 1,

$$P_1^2 - P_0^2 > (P_1')^2 - (P_0')^2$$

i.e. $$(P_0')^2 - (P_1')^2 > P_0^2 - P_1^2 \qquad (5.32)$$

Now upstream of the single fault located at section K,

$$C_i = C_i' \qquad 1 \leq i \leq K - 1$$

Recalling (5.3a)

$$P_i > P_i'$$

therefore

$$C_i P_i > C_i' P_i' \qquad (5.33)$$

Let us now reexamine Eqn (5.6a)

$$\beta_i \triangleq \left(\frac{P_{i-1}}{P_i}\right)^2$$

$$= 1 + \left[\frac{1}{D_i}\left(1 - \frac{1}{\beta_{i+1}}\right)^{1/2} + C_i\right]^2$$

This can be re-arranged to become,

$$\left[P_i^2 - P_{i+1}^2\right]^{1/2} = \left[P_{i-1} - P_i^2\right]^{1/2} - C_i P_i \qquad (5.34a)$$

Compare this with its "faulty" counterpart,

$$\left[(P_i')^2 - (P_{i+1}')^2\right]^{1/2} = \left[(P_{i-1}')^2 - (P_i')^2\right]^{1/2} - C_i' P_i' \qquad (5.34b)$$

It is seen that the right-hand side of each equation is made up of the difference of 2 terms. Reiterating them for i =1

$$\left[P_1^2 - P_2^2\right]^{1/2} = \left[P_0^2 - P_1^2\right]^{1/2} - C_1 P_1 \qquad (5.35a)$$

$$\left[(P_1')^2 - (P_2')^2\right]^{1/2} = \left[(P_0')^2 - (P_1')^2\right]^{1/2} - C_1' P_1' \qquad (5.35b)$$

The first term of the RHS of Eqn (5.35a) is smaller than that of Eqn (5.35b), as previously proven in Eqn (5.32), while the second term is larger according to Eqn (5.33). Hence the difference of these two terms of Eqn (5.35a) is smaller than that of Eqn (5.35b). In other words,

$$P_1^2 - P_2^2 < (P_1')^2 - (P_2')^2 \qquad (5.36)$$

But,

$P_1 + P_2 > P_1' + P_2'$, according to (5.31).

Dividing the smaller LHS of Eqn (5.36) by the larger LHS of Eqn (3.37) and so on, results in again a smaller

LHS:-

$$P_1 - P_2 < P_1' - P_2'$$

Rearranging this

$$\left.\begin{aligned} P_2 - P_2' &> P_1 - P_1' \\ \Delta_2 &> \Delta_1 \end{aligned}\right\} \quad (5.38)$$

Repeating the proof for the higher values of i (i < K-1), yields

$$\Delta_K > \Delta_{K-1}, \ldots, \Delta_2 > \Delta_1 > \Delta_0 \quad (5.39)$$

thus completing the proof of Theorem 2.

At this point, there is no theorem available for pressure difference for a train-line with multiple faulty leaks. However, it is worth noting that by merely plotting Δ for all i in the case of a multiple-leaks train-line, one can obtain results similar to those illustrated in Fig. 5.6. The curve Δ_i is similar in appearance to the E-curve in Fig. 5.2. It rises monotonically from i =0 onwards, exhibiting sharp changes in slope at sections where a faulty leak is known to be located.

Thus a pressure-difference method for locating

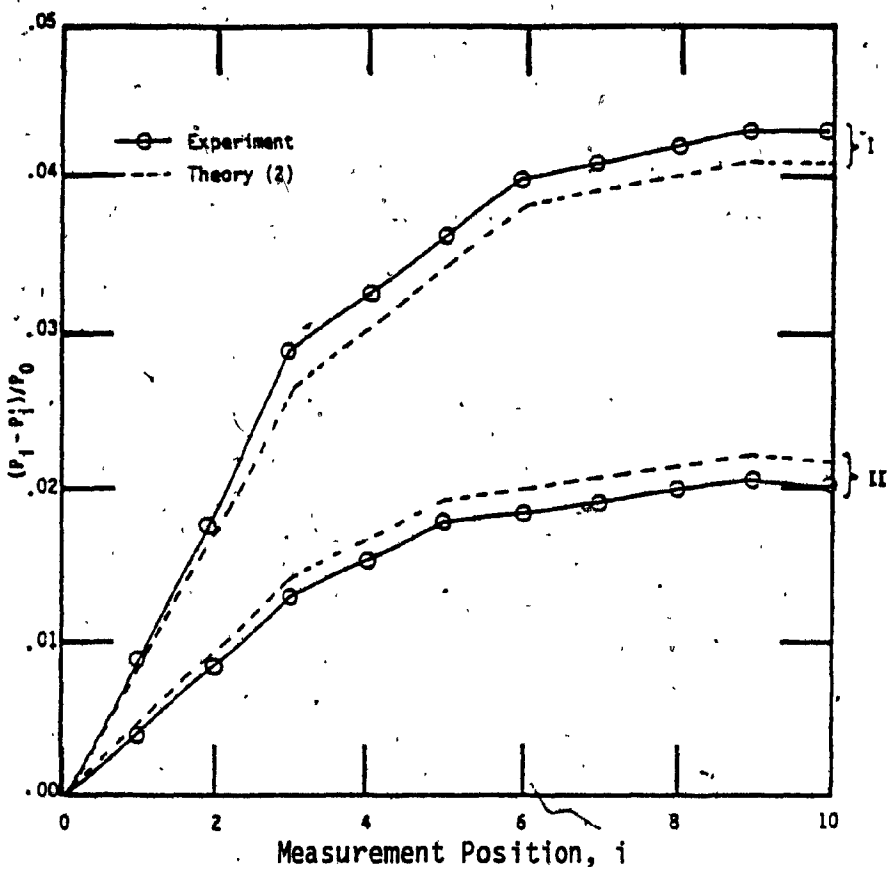

Fig. 5.6 Experimental and Simulated Results of the Difference Method

multiple faulty leaks may be formulated.

5.5 Summary

In this chapter, two theorems have been formulated. Theorem 1 (Sec. 5.3) explains the behaviour of the ratio between the no-fault pressure reading at a section and the faulty pressure reading for a train-line with multiple leaks. This Theorem can be stated as:

> **"In a faulty train-line, the ratio between the no-fault pressure reading at a section and the faulty pressure reading of the same section, E_i ,is smaller than, or at most equal to, the pressure-ratio of any other section downstream of it. Furthermore, the curve E_i exhibits an abrupt change in slope (a bend) at a section of the train-line where there exists a faulty leak."**

Theorem 2 (Sec. 5.4) explains the behaviour of the pressure-difference for a train-line with a single faulty leakage only. This theory can be stated as:

- **In a train-line with leakage, if only one fault develops, then the change in the pressure reading at the faulty section is universally greater than the pressure change at any other section".**

Both theorems have been utilized as the basis of determining the location of the faulty leaks in a train-line. Both methods show similar characteristic when the pressure-ratio or the pressure-difference is ploted against the section number: namely, the plot rises monotonically and exhibits sharp changes in slope where there is a faulty leak.

It has been observed in the course of experimentation that the difficulties arise when the pressure changes are too small compared with the sensitivity of the transducers available (typically at .05%). For this reason, the finite difference is applied to the test data to obtain the 2nd order difference (Sec. 5.3).

In conclusion, the two methods proposed in this chapter have been shown to be satisfactory in achieving their goal of fault-location. However, in case of limited accuracy from the transducers, the difference method seems to offer some slight advantage over the ratio method.

CHAPTER 6

CONCLUSION

6.1 Introduction

As mentioned in Chapter 1, this thesis has been divided into two parts. Part One has described the train-line mathematical model. Then, two finite difference schemes were proposed to provide the solution for the mathematical model. Finally, the effects of the leakage and other factors on the train-line behaviour have been investigated. Then, two methods for locating multiple faulty leaks have been developed in Part Two. The summary in this chapter is also divided into two parts. Part One (Sec. (6.2)) summarizes and discusses the effects of the leakage and some other factors on the train-line behaviour. This section contains two topics, the first one deals with the steady-state behaviour, whereas the other deals with the transient behaviour. Part Two (Sec. (6.3)) summarizes the two multi-leak methods. Finally, Sec. (6.4) gives suggestions for further work.

PART ONE

6.2 Train-Line Behaviour-Summary and Discussion

In Chapter 2, the train-line mathematical model has been developed to simulate the physical model. Then, two finite difference schemes (Sec. (2.4)) have been proposed to provide a solution for this mathematical model (sec (2.3)). First scheme was the explicit scheme (refered as the method of lines), which has been used before by Funk and Robe [17], and Ho [16]. The other method was the implicit scheme. Then, the computational results using these two schemes and the experimental results, using the train-line laboratory model (Sec. (2.2)) and Westinghouse model (2.5), were compared with one another (sec (2.5)). The comparison has shown that the implicit scheme is more accurate than the explicit scheme solution, and it requires less computer time because its time increment (ΔT) is larger than that for the explicit scheme time increment. As a result of these comparisons, the implicit scheme is chosen to provide the solution for the mathematical model.

6.2.1 Train-Line Steady-State Behaviour

In Chapter 3, two test set-ups have been chosen to study the effects of the leakage size ($S \leq 3.57\%$) and leakage location (regions I, II and III) on the steady-state pressure and velocity of the train-line. In Sec. (2.3), both train-line laboratory and mathematical model have been employed to accomplish this task. The theoretical pressure results agreed with the corresponding experimental results. The discrepancy between these results goes as low as 3%. This agreement proved that the train-line mathematical model can be successfully used to simulate the physical model. Then, the mathematical model has been exclusively used to explain the two steady-state phenomena. The first one is the pressure distribution phenomenon, which may be described as follows:

1- If there is a leakage in region III only, the pressure in this region will be lower than the pressure in the same region if the leakage was located in region II.

2- If the leakage is located in region III, the pressure in region I will be higher than the pressure in the same region if the leakage was located in region II.

On the other hand, the velocity distribution phenomenon may be described as follows:

If there is a leakage at a distance X_e , the velocity U_i slightly increases as the distance X_i ($0 < X_i \leq X_e$) increases. Furthermore, the velocity U_i sharply decreases to zero as the distance X_i ($X_e < X_i \leq X_f$) increases, if there is no leakage at a distance greater than X_f .

Finally, the mathematical model was used to study the effects of the leakage (location and size) on the pressure gradient (Δ P) and the steady-state inlet velocity (U(0)). This study can only be applied to a train-line with d_p/l equal to .003%, provided that the flow inside this line can be treated as one-dimensional problem. Fig. 3.3 shows that the train-line pressure gradient and inlet velocity are sensitive to the change of the leakage location as well as the leakage size, whereas, for a small leakage size ($S \leq 2.0\%$), the inlet velocity does not vary with the leakage location,but it varies with the leakage size, of leakage location, but it is sensitive to the leakage size.

6.2.2 Train-Line Transient Behaviour

Chapter 4 has proven that the train-line mathematical model can be successfully used to study the transient response of the train-line. This chapter has also

investigated the effects of leakage among other parameters on the rear-end pressure and velocity transient behaviour of the train-line. These factors were leakage size and location, the changes in the direction of the pressure step applied at the head-end, threshold sensitivity of the transducer D, and the amplitude of the pressure applied at the head-end $P_r(0)$. Sec. (4.2) has described three test cases. The tests were the dry charging test, the discharging test, and the recharging test. Sec. (4.3) has discussed in general the effects of the leakage size and location on the pressure and velocity transient response. It has been observed that for any one of the test cases as the leakage size increases or the leakage goes toward the rear-end, the steady-state time increases and the gain coefficient decreases. Then, Sec. (4.4) has discussed in detail the effects of the leakage and the threshold sensitivity on the transient behaviour of the last section velocity ($U(1-\frac{1}{N}, T)$) of the train-line which was refered as the peak time T_p, and peak velocity U_p. In general, it can be concluded that the peak velocity and the peak time decreases with the increase of the leakage size, and the peak velocity increases while the peak time decreases, as the leakage goes towards the rear-end of the train-line. In Sec. (4.5), the theoretical results are compared with the experimental results, and the discrepancy between these results is found to be less than 10%. Then, the mathematical model has been exclusively used to study the

effects of the above mentioned factors on the rear-end pressure transient behaviour, which was refered as the propagation speed V. In this section, the discussion showed that the train-line may be linearized and simulated as a blocked transmission line provided

1- the leakage is concentrated at the rear-end.

2- large pressure amplitude applied at the head-end of the line ($P_r(0) \geq .68$ or 10 psi).

However, Appendix F has desribed the linearized model while Appendix G has provided the analytical solution for this model. This linearization approach did reduce the number of parameters affecting the propagation speed (l, d_p, d_i), to only one parameter (N_K).

In general, one can conclude that the decrease of the propagation speed may be caused by the existence of one of the following possibilities:

1- The increase of the leakage size, S.

2- The leakage is located at the rear-end

3- The increase of the threshold sensitivity, D.

4- The decrease of the head-end pressure amplitude, $P_r(0)$.

This analysis shows the effects of the leakage on the propagation speed, and points out that the leakage is the most important factor among the others. Because of this reason, it is very important to develope a method for locating this leakage and eliminate it if possible.

PART TWO

6.3 Multi-Leak Location Methods-Summary and Discussion

Based on ladder network model proposed for a train-line with leakage in Sec. (5.2), Theorem 1 has been formulated with rigorous proof in Sec. (5.3). Theorem 1 (the ratio method) can be stated as,

> **" In a faulty train-line, the ratio between the no-fault pressure reading at a section and the faulty pressure reading of the same section, E_i ,is smaller than, or at most equal to, the pressure-ratio of any other section downstream of it. Furthermore, the curve E_i exhibits an abrupt change in slope (a bend) at a section of the train-line where there exists a faulty leak."**

Theorem 2 (Sec. 5.4) explains the behaviour of the pressure-difference for a train-line with a single faulty leakage only. Theorem 2 can be stated as:

> **"In a train-line with leakage, if one and only one fault develops, then the change in pressure reading at the fault section is universally greater than the pressure change at any other section".**

Both theorems have been utilized as the basis of determining the location of the faulty leaks in a train-line. Both methods show similar characteristic when the pressure-ratio (or pressure-difference as the case may be) is plotted against the section number, namely, the plot rises monotonically and exhibts sharp changes in slope where there is a faulty leak. Hence both methods can be utilized to advantage, provided the train-line is accessible for pressure measurements at all points or at points that are sufficiently close.

It has been observed in the course of experimentation that difficulties do arise when the pressure changes are too small compared to the sensitivity of the transducers available (typically at .05%). For this reason, it was

recommended that a finite difference method could be applied to the test data, the E- or Δ- curves are bent at the locations of a fault, there is a discontinuity of the first differential (or difference) at these locations. Figure (5.3) shows that applying this method to the data in figure (5.2) yields amplified "leaks" at the locations of faulty leaks.

In conclusion, the two methods proposed in this thesis have been shown to be satisfactory in achieving their goal of fault-location.

However, in case of limiting accuracy attained from the transducers, the difference method (subtraction) seems to offer a slight advantage over the ratio method.

6.4 Suggestions for Further Work

PART ONE

In Part One of this research thesis, a mathematical model for the train-line was proposed using the finite difference in the space. Then, two finite difference schemes were developed to provide the solution for this model. However, there is a discrepancy between the calculated and observed pressure (especially at the beginning of the transient response period) which indicated

that further work is required to be done. The following suggestion should be given serious consideration:

1- to include the heat transfer effects in the formulation of the mathematical model.

2- to account for the temporal variation in density by the truncation of the full transient one-dimentional energy equation.

3- to assume that the flow is isoentropic at the beginningng of the transient period. Then, it is isothermal for the rest of the transient period.

4- to apply the mathematical model to real train-line of a freight train (different train-line dimensions).

Finally, the author also suggests that the e linearization technique may be used to study and explain the transient behaviour of the train-line.

PART TWO

In Part Two of this thesis, two methods were developed for locating multiple-leak in the train-line.

Test results were found satisfactory for the train-line laboratory model.

Further applications for these methods could include the following.

1- To extend the test for different numbers of leakage, different numbers of sections, and different leakage sizes.

2- Finally, tests should be carried out in train-line racks and ultimately on typical train.

REFERENCES

1. Blaine, D.G. and Hengel, M.F., "Brake-System Operation and Testing Procedure and Their Effects on Train Performance", ASME Paper No.71-WA/RT-9 Dec.1971.

2. Normu, Y., Matsui, S., Takami, Y., Kikuch, T.Iwaki, T. and Nakamure, M., "Development of High Performance Air Brake System", Quarterly Reports, Vol. 12, No. 1, Railway Technical Research Institute, Japanese National Railways, pp 449, 1971.

3. Association of American Railroads' Interchange Rules, 1971.

4. Schuder, C.B and Binder, R.C, "The Response of Pneumatic Transmission Lines to Step Inputs", Transaction of the ASME Journal of Basic Engineering, Vol. 81, Series D, No. 4, Dec 1959, pp.578-584.

5. Nichols, N.B., "The Linear Properties of Pneumatic Transmission Lines", Transactions of The Instruments Socity of America, Vol. 1, No.1, January 1962, pp 5-14.

6. Brown, F.T, "The Transient Response of Fluid Lines", Transactions of The ASME Journal of Basic Engineering, Vol. 84, Series D, No.4,1962, pp 547-553.

7. Brown, F.T, "Pneumatic Pulse Transmission With Bistable-Jet-Relay Reception and Amplification", Sc.D.Thesis, M.I.T, May 1962.

8. Cheng, R.M.H., Katz, S. and Abdol-Hamid, K., "Apparent Sub-Acoustic Propagation of Pneumatic Braking Systems in Trains", ASME Paper 82-WA/DSC-11, Nov-1982.

9. Kantola, R., "Transient Response of Fluid Lines Including Frequency Modulated Inputs", Transactions of the ASME Journal of Basic Engineering, Vol. 93, Series D, No. 2,1971.

10. Karam, J.T.Jr., "A Simple but Complete Solution for the Step Response of a Semi-infinite Circular Fluid Transmission Line", Transaction of the ASME Journal of Basic Engineering, Series D, Vol. 94, No.2,1972.

11. Brown, F.T. and Nelson, S.E., "Step Responses of Liquid Lines with Frequency-Dependent Effects of Viscosity", Transactions of the ASME Journal of Basic Engineering, Vol. 87, Series D, No.2, 1965, pp.504-510.

12. Katz, S., "Transient Response of Terminated Pneumatic

Transmission Lines by Frequency Response Conversion", ASME Paper 75-WA/Flcs-4, Dec 1975.

13. Zielke, W., "Frequency Dependent Friction in Transient Pipe Flow", Transactions of the ASME, Journal of Basic Engineering, Vol. 90, Series D, No. 1, 1968, pp 109-115.

14. Brown, F.T, "A Quasi-Method of Characteristics with Application to Fluid Lines with Frequency Dependent Wall Shear and Heat Transfe", Transactions of the ASME, Journal of Basic Engineering, Vol. 91, Series D, No. 2, 1969, pp. 217-227.

15. Krishner, J.M. and Katz, S., **"Design Theory of Fluidic Components"**, Academic Press Inc., pp 123-124, 1975.

16. Ho, A.K., "A Study on The Effects of Leakage for Scaled-Down Brakepipe Model", Master's Thesis, Concordia University, Montreal, September 1981.

17. Funk, J.F. and Robe, T.R., "Transient in Pneumatic Transimission Lines Subjected to Large Pressure Changes", ASME Paper 69-FLCS-42,1969.

18. Katz, S. and Cheng, R.M.H., "A Network Approach to Brakepipe Leakage", Asme Paper 77-WA/FLCS-10, 1977.

19. Katz, S., Cheng, R.M.H. and Aula, V., "Locating a Single Shunt Fault in Resistor Ladder Networks", International Journal of Circuit Theory and Application , Vol. 7, pp 399-412, 1979.

20. Katz, S., Aula, V. and Cheng, R.M.H., "Some Single Fault Detection Methods in Nonlinear Resistor Ladder Network", Fourth International Symposium on Network Theory, Bled,Yugoslavia, Sept. 1979.

21. Aula, V., Cheng, R.M.H and Katz, S., "Single Leak Detection Methods Applied to a Brake Pipe Model", ASME Paper 79-WA/RT-11, December 1979.

22. Sakes, R.and Liberty, S.R. (Eds.), "Rational Fault Analysis, Texas Technical University, August 1974, Puplished by Marcel Dekker,Newyork, 1977.

23. Rault, J.C., Garzia, R., and Bedrosian, S.D., "Fault Detection and Location in Analog Circuits- a Bibliography",Rational Fault Analysis, 165-175, Marcel Dekker, Newyork 1977.

24. Berkowitz, R.S., "Conditions for Network-Element Value Solvability ", IRE Transactions on Circuit Theory, Vol.CT-9,March 1962.

25. Shekel, J., "Some Properties of Network with One Variable Element", IEEE Transactions on Circuit Theory, Vol.CT-14, 1967.

26. Gefferth, L., "Fault Identification on Resistive and Reactive Networks", International Journal of Circuit Theory and Application, Vol. 2, 1974.

27. Trick, T.N and Chein, R.T, "A Note on Single Fault Detection on Positive Resistor Circuit", IEEE Transaction on Circuit and Systems, Vol.CAS-25, No. 1, 1978.

28. Shute, B.W, Wright, E.C, Taft, C.K and Banister, W.N, "The Effect of Leakage Distribution on Brake Pipe Gradient and Brake Pipe Flow", ASME Paper 79-WA/RT-16.

29. Chuen-Yen Chow, **"An Introduction to Computational Fluid Mechanics"**, John Wiley & Sons, Chapters 2 and 3, New York 1979.

30. Rudinger, G., **"Wave Diagram for Unsteady Flow in Ducts"** D.Vannostránd Company Inc, pp 9-17 and pp 46-49, New York 1954.

31. Owczarek, J.A, **"Fundametals of Gas Dynamics"** International Textbook Company, pp 550-560, 1964.

32. Yuan, S.W, **"Foundations of Fluid Mechanics"** Prentice-Hall Inc., pp 265-269, 1967.

33. Roach. P J. **"Computational Fluid Dynamics"** Hermosa Publishers, Chapters III and V, 1972.

34. Chirlian, P.M., **"Signals, Systems and the Computer"**, Intext Education Publishers, Chapter 10, 1973.

APPENDIXES

APPENDIX A

A.1 The Continuity Equation

The Continuity Equation shows the principle of mass conservation. Consider a volume element of the duct Adx (shaded area in Fig. A.1a). Fluid is entering and leaving this element and also may leave the duct through the walls. Where μ is the mass flow leaving the element through the walls per unit length. The mass which is entering and leaving the element during the time interval dt as shown in Fig.A.1a. During this time, the mass contained in the element increases from ρ Adx to ρ Adx + $\frac{\partial \rho u}{\partial x}$ dtdx, where ρ is the density. In this case, the area of the duct can be taken out of the differentiation process since it is not varied with the time or the distance. The excess of the inflow over the outflow must be equal to the increase of the mass contained in the element and the continuity equation thus becomes.

$$\frac{\partial \rho}{\partial t} + \frac{\partial \rho u}{\partial x} + \mu = 0 \qquad \text{(A.1)}$$

A.2 The Momentum Equation

The Momentum Equation expresses Newton's Law, that is

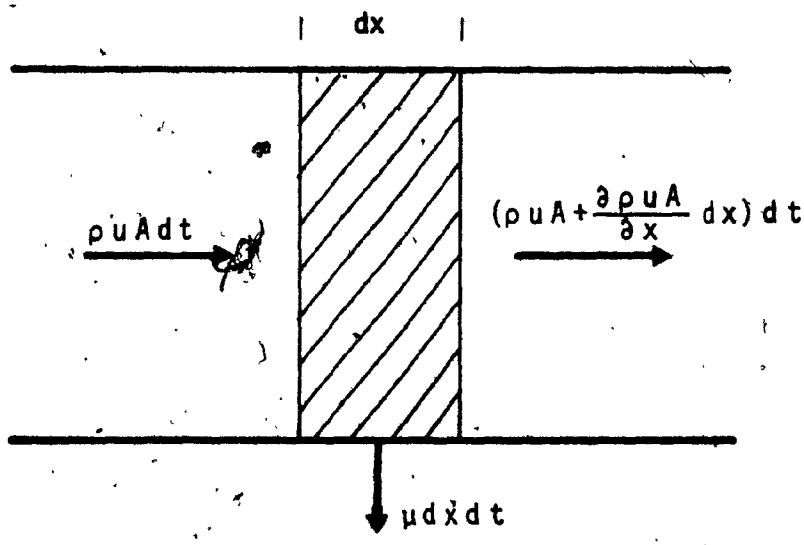

Fig. A.1 Mass Flows Into and Out of a Volume Element

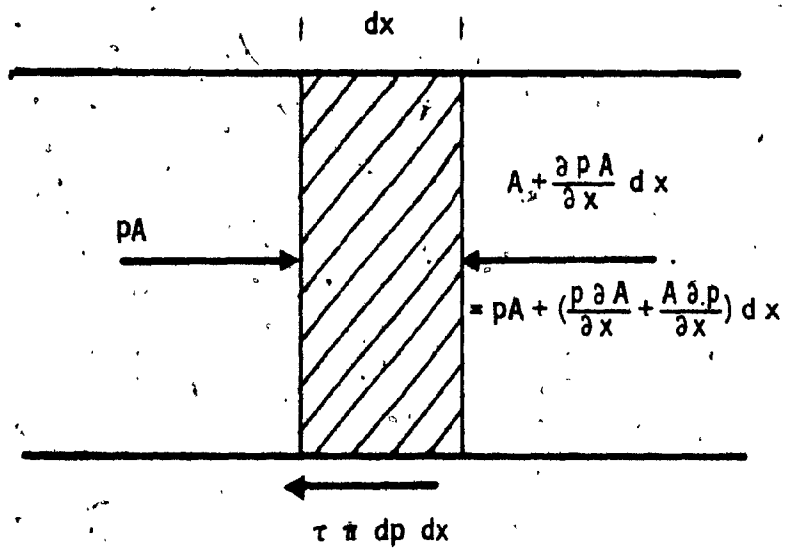

Fig. A.2 Forces Acting on a Fluid Element

the acceleration of a particle equals the sum of the forces acting on it divided by its mass. Consider a fluid element between two adjacent sections (shaded in Fig. A.1b). The mass of this element is equal to $\rho A dx$ and the forces acting on it are indicated in the figure. Where τ is the wall shear stress per unit area. The acceleration of the particle is given by the substantial derivative $\frac{Du}{Dt}$, and the momentum equation can be written in this form:

$$\frac{Du}{Dt} = \frac{\partial u}{\partial t} + u\frac{\partial u}{\partial x} = -\frac{1}{\rho}\frac{\partial P}{\partial X} - \frac{4\tau}{\rho d_p} \qquad (A.2)$$

APPENDIX B

B.1 Relationships between the Friction Factor, f, and the Reynolds Number Re.

In Eqn. (2.5), f has taken a different form, for each of three conditions on the value of the Reynolds number, Re.

1- **Re ≤ 2000 (laminar).** in this region the flow is assumed to be laminar. From the Poiseuille Law

$$f = \frac{64}{Re} = \frac{64}{Re^{*}\overline{P}\,U} \qquad (B.1)$$

where,

$$Re^{*} = \frac{a\,d_p}{\nu_a} \qquad (B.2)$$

2- **Re > 4000 (Turbulent).** From Eqn. (5.4), f is related to the pressures (P_i and P_{i-1}) at two neighboring nodes (i and i-1) as follows:

$$f = \left(\frac{P_{i-1}^2 - P_i^2}{M_{i-1}^2}\right)\left(\frac{d_p}{\gamma\, l\, \Delta X}\right) \qquad (B.3)$$

Fig. B.1 shows the experimental results from the laboratory train-line model for different lengths ($l\,\Delta X$) using Eqn. (B.3). Assuming

that the data is exponentially related in the form as:

$$f = a\ Re^{b} \qquad (B.4)$$

Using the least squares method, one can find the exponential relation as follows:

$$f = 0.15\ Re^{-0.14} \qquad (B.5)$$

3- 2000 < Re ≤ 4000 (Transition).

$$f = 3.8 \times 10^{-4}\ Re^{0.57} \qquad (B.6)$$

This relation is obtained by connecting the friction factor f at Re = 2000 to that at Re = 4000, with a straight line on the log-log scale (Fig. B.1).

Fig. B.1 shows the agreement between the experimental data and the result from Eqn. (B.5), whereas Fig. B.2 shows

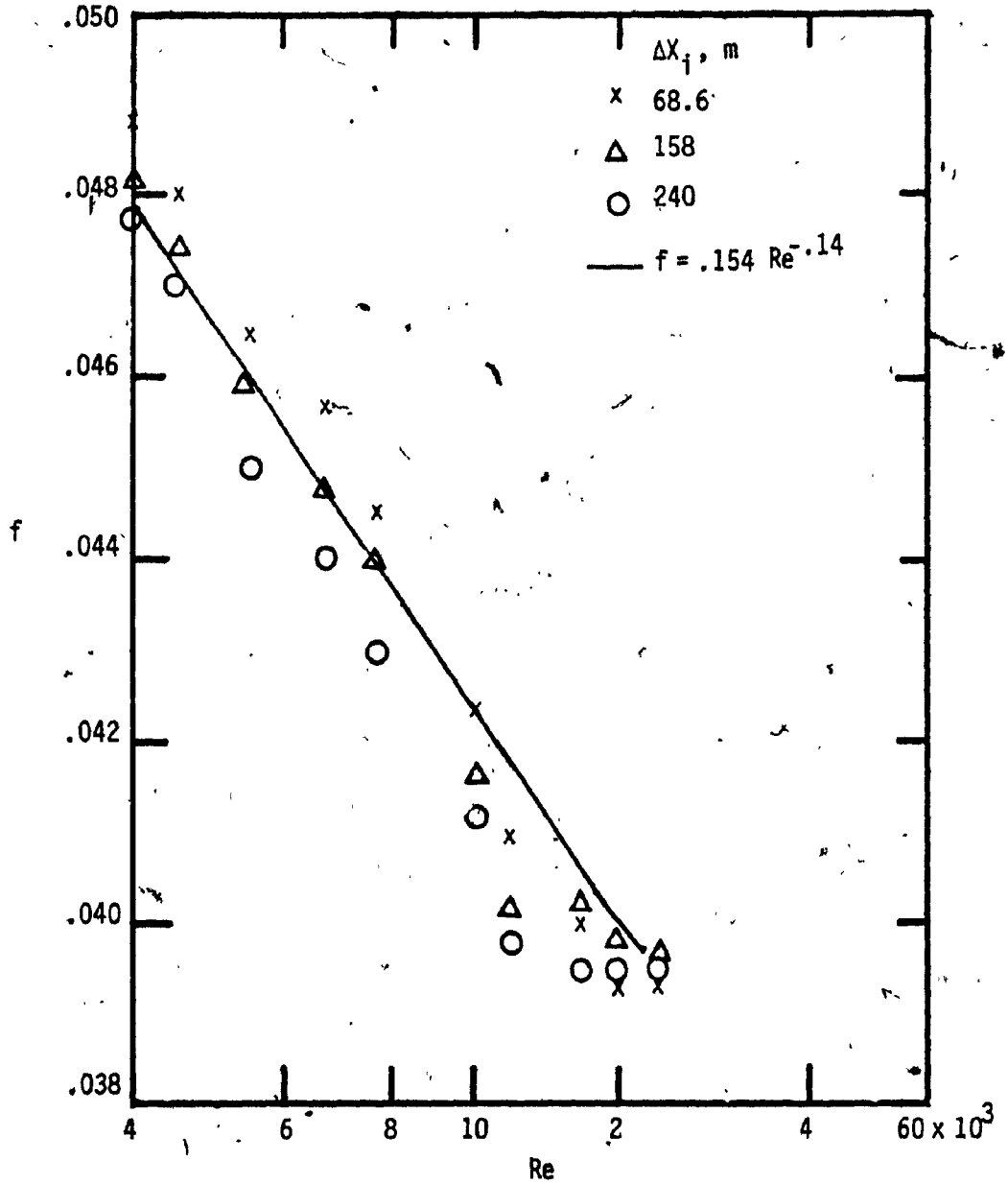

Fig. B.1 Experimental and Theoretical Values of the Friction Factor f (Turbulent)

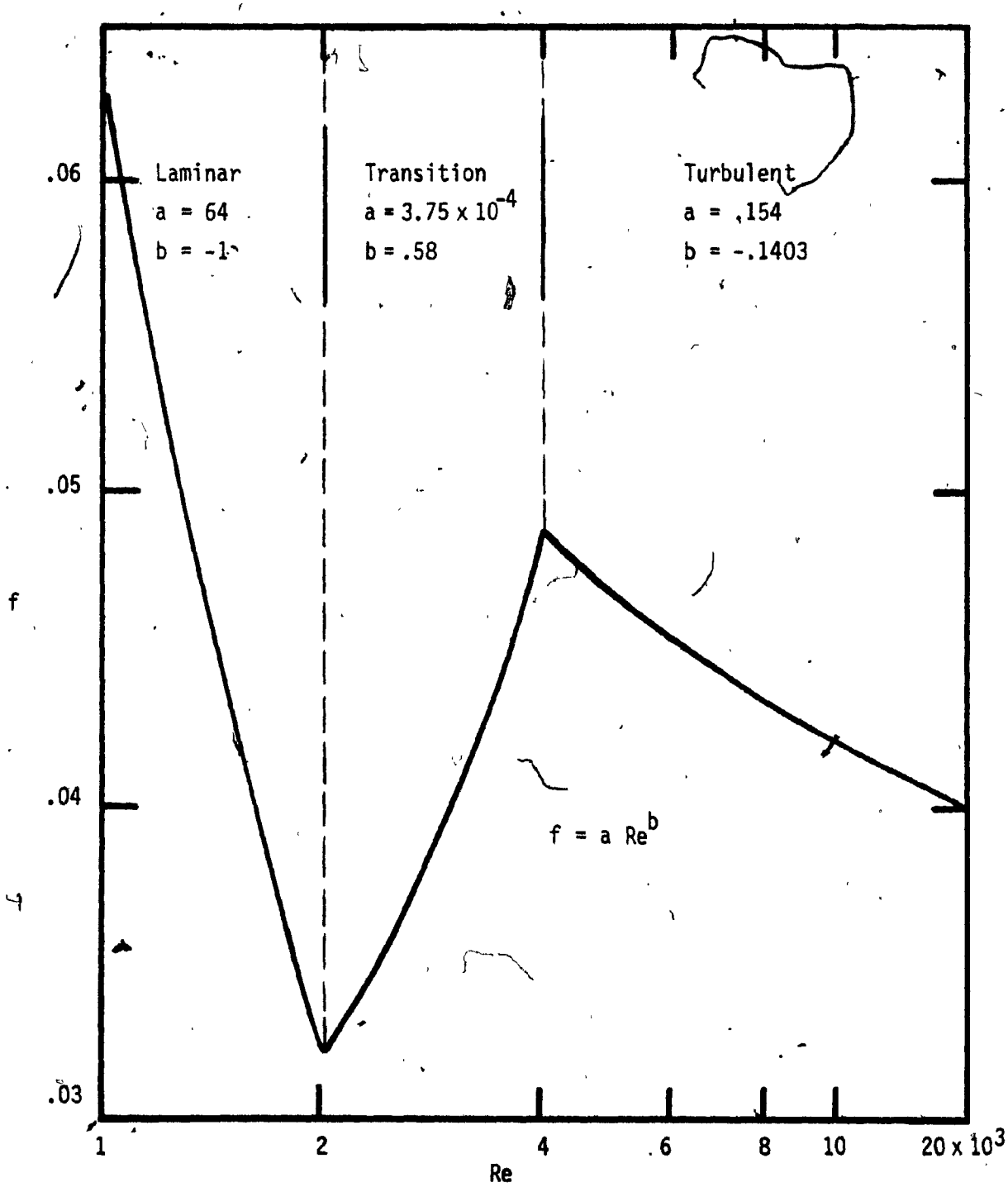

Fig. B.2 Theoretical Values of the Friction Factor f (Laminar - Transition - Turbulent)

the result of f from Eqns. (B.1), (B.5) and (B.6).

B.2 Relationships between the Pressure and the Mass Flow Through Section i

The relationships between the pressure at the two neighboring nodes (i and i-1) and the normalized mass flow through the ith section. It may be shown from Eqn. (5.4) that,

$$M_{i-1} = \left[\frac{Z_i}{f} \right]^{1/2} \qquad (B.7)$$

where, $$Z_i = (P_{i-1}^2 - P_i^2)\left(\frac{d_p}{\gamma\, l\, \Delta X}\right) \qquad (B.8)$$

It may be shown from Eqn. (B.1) above that.

1- Re ≤ 2000 (Laminar) or $Z_i \leq 1.6 \times 10^{-5}$

$$M_{i-1} = 1.69 \times 10^{-3}\, Z_i \qquad (B.9)$$

2-2000 < Re ≤ 4000 (Transition) or $10^{-5} < Z_i \leq 6.6 \times 10^{-5}$

$$M_{i-1} = \left[3.02\, Z_i\right]^{0.386} \qquad (B.10)$$

3- Re > 4000 (Turbulent) or $Z_i > 6.6 \times 10^{-5}$

$$M_{i-1} = \left[32.98\ Z_i\right]^{0.538} \qquad (B.11)$$

Fig. B.3 shows the experimental result and the result using Eqn. (B.11), whereas Fig. B.4 shows the result of Z_i using Eqn. (B.9), (B.10) and (B.11) vs. the normalized mass flow M_i through the ith section.

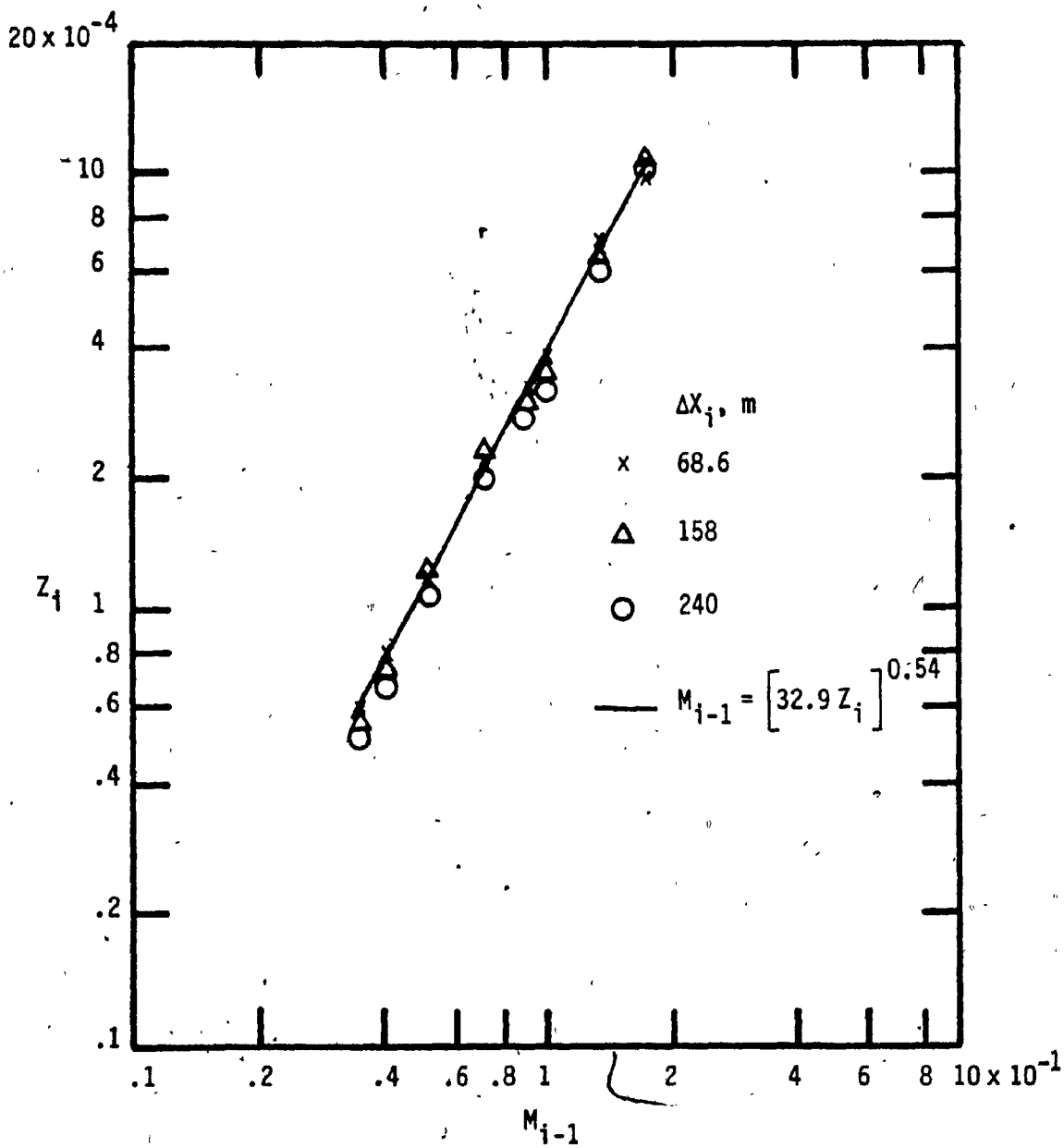

Fig. B.3 Experimental and Theoretical Values of Z_i (Turbulent)

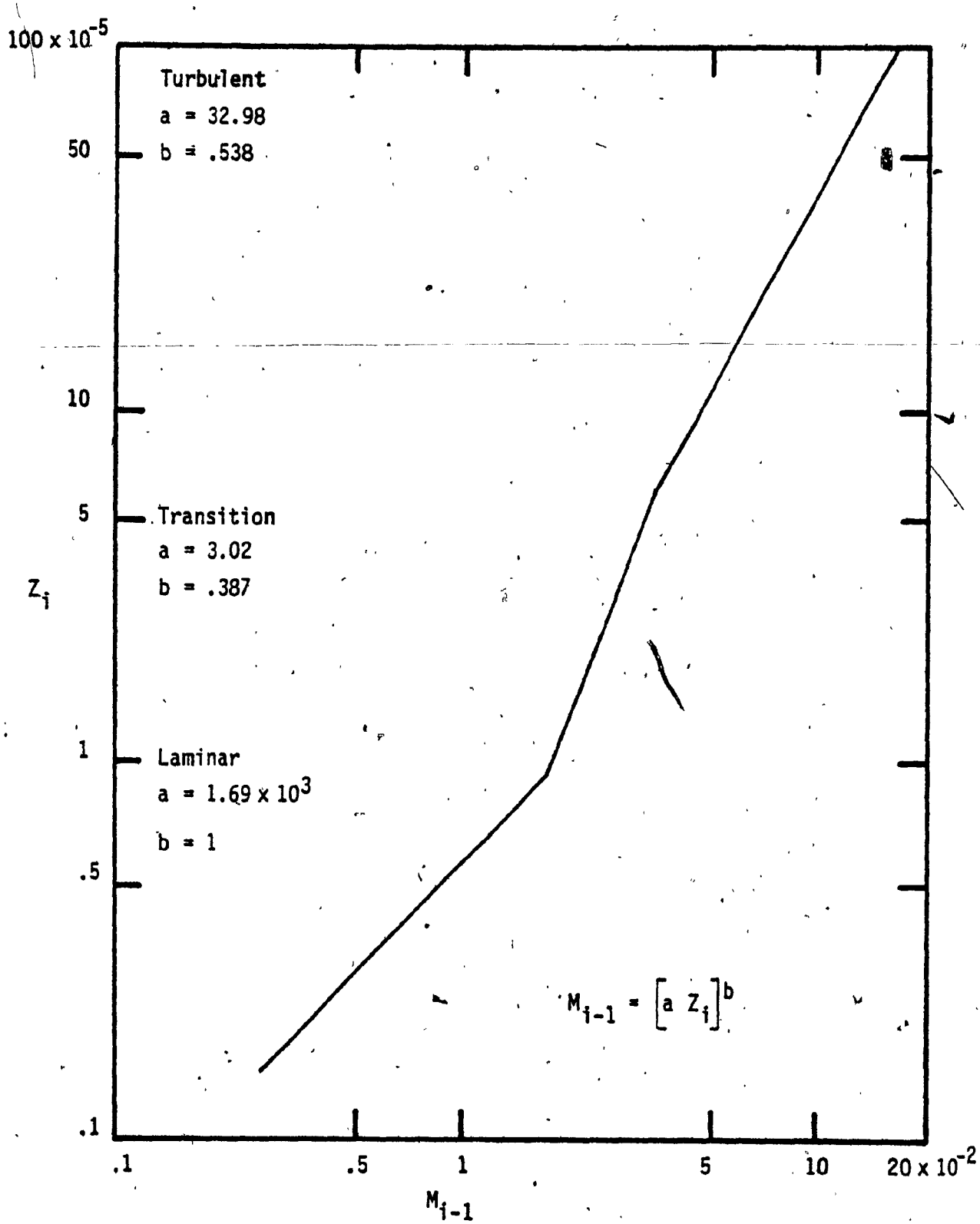

Fig. B.4 Theoretical Values of Z_i (Laminar - Transition - Turbulent)

APPENDIX C

DERIVATION OF EQUATION (2.19b)

When air flows through an orifice of diameter d_e to atmosphere p_a, and upstream pressure is p_i. From to the continuity Eqn. (5.3), the inflow η_i equals the outflow η_e as follows:

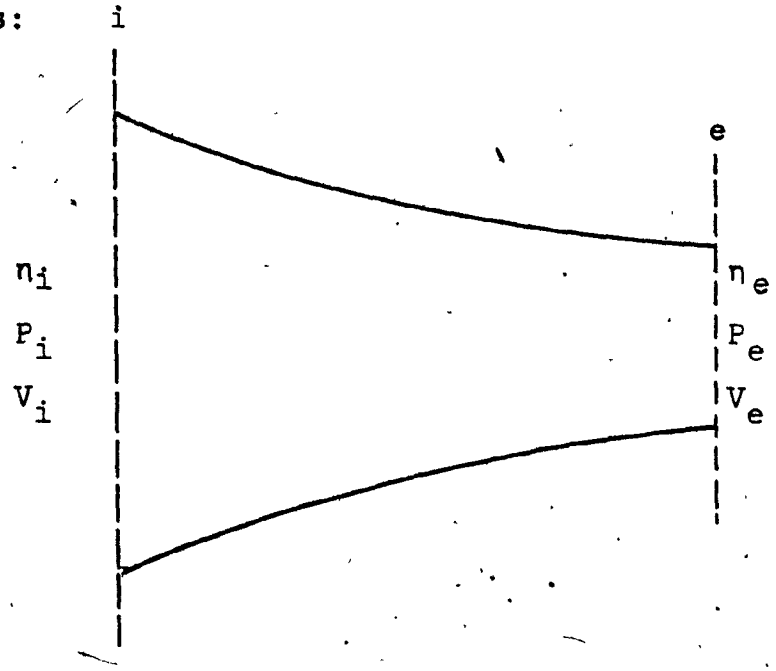

$$\eta_i = \eta_e = \rho_e V_e A_e \qquad (C.1)$$

where,

$\rho_e \triangleq$ the density of exit e, Kg/m^3.

$V_e \triangleq$ the velocity through exit e, m/s.

$A_e \triangleq$ the cross-sectional area of exit e, m^2.

and,

$$\left.\begin{aligned} \rho_e &= \frac{P_e}{R_g \theta_e} \\ V_e &= M_e \sqrt{\gamma R_g \theta_e} \end{aligned}\right\} \qquad (C.2)$$

The air flow through the orifice is assumed to be adiabatic, and the relation between the mach number M_e at exit e and the pressure ratio $\frac{p_i}{p_e}$ can be written in this form:

$$M_e = \left\{ \left[\left(\frac{p_i}{p_e}\right)^{\frac{\gamma-1}{\gamma}} - 1 \right] \frac{2}{\gamma-1} \right\}^{1/2} \qquad (C.3)$$

It may be shown from (C.1) above that

$$\eta_i = \frac{\pi}{4}\sqrt{\frac{\gamma}{R_g\ \theta_i}}\ p_i\ d_e^2 \sqrt{\frac{2}{\gamma-1}} \left\{ \left(\frac{p_e}{p_i}\right)^{\frac{2}{\gamma}} - \left(\frac{p_e}{p_i}\right)^{\frac{\gamma+1}{\gamma}} \right\}^{1/2} \qquad (C.4)$$

Eqn. (C.4) is nondimensionalized by means of the following definitions

$$\phi_i = \frac{\eta_i}{\rho_a\ A a}, \qquad P_i = \frac{p_i}{p_a}, \qquad \rho_a = \frac{p_a}{R_g \theta} \qquad (C.5)$$

where,

$\rho_a \triangleq$ The density at the atmospheric condition, Kg/m

$p_a \triangleq$ The atmospheric pressure, kPa

Now, the relation between the normalized mass flow ϕ_i and pressure P_i can be expressed in this form

$$\left.\begin{aligned} \phi_i &= K_i \left(\frac{d_e}{d_p}\right)^2 P_i \\ &= P_i / r_i \end{aligned}\right\} \qquad (C.6)$$

where r_i is the orifice or leakage resistance, the relation between r_i, K_i and the normalized pressure P_i can be shown from Eqn. (C.6) and above as, in the case of subsonic flow ($p_e = p_a$)

$$K_i = \sqrt{\frac{2}{\gamma-1}} \left\langle P_i^{-\frac{2}{\gamma}} - P_i^{-\frac{\gamma+1}{\gamma}} \right\rangle^{1/2} \qquad (C.7a)$$

and in the case of sonic flow ($p_e = .5283\ p_i$)

$$K_i = 0.579 \qquad (C.7b)$$

and the relationships between r_i and K_i can be expressed in this form

$$r_i = \frac{1}{K_i} \left(\frac{d_p}{d_e}\right)^2$$

It is more convenient to rename d_e to d_i in the main text.

APPENDIX D

Equation (2.30) represents a tridiagonal system,

$$\{B\}\{Y\} = \{Q\}$$

$$\begin{bmatrix} b_{1,2} & b_{1,3} & 0 \ldots\ldots 0 & 0 & 0 \\ b_{2,1} & b_{2,2} & b_{2,3} \ldots 0 & 0 & 0 \\ \vdots & \vdots & \vdots & & \\ 0 & 0 & 0 \ldots\ldots b_{2N-1,1} & b_{2N-1,2} & b_{2N-1,3} \\ 0 & 0 & 0 \ldots\ldots 0 & b_{2N,1} & b_{2N,2} \end{bmatrix} \begin{bmatrix} y_1 \\ y_2 \\ \vdots \\ y_{2N-1} \\ y_{2N} \end{bmatrix} = \begin{bmatrix} b_{1,4} \\ b_{2,4} \\ \vdots \\ b_{2N-1,4} \\ b_{2N,4} \end{bmatrix} \tag{D.1}$$

and the matrix {B} is called tridiagonal matrix, whose non-vanishing elements form a band of three elements wide along the diagonal. This particular set of equations can be solved by using Gaussian elimination method. According to this method, by multiplying the second equation in (D.1) by $b_{1,2}$ and the first by $b_{2,1}$ and then by taking the difference of the two equations to eliminate y_1. The resulting equation is

$$(b_{2,2}\, b_{1,2} - b_{2,1}\, b_{1,3})\, y_2 + b_{2,3}\, b_{1,2}\, y_3 = b_{2,4}\, b_{1,4} - b_{2,1}\, b_{1,4} \tag{D.2}$$

In this equation, the coefficient of y_2 is called $b_{2,2}$, and of y_3 is called $b_{2,3}$, the group in the right hand side is called $b_{2,4}$, and the final equation is used to replace the second equation in (D.1). The form of Eqn. (D.1) will remain unchanged except that $b_{2,1}$ is replaced by zero. The same process is repeated until $b_{2N-1,1}$ is eliminated. In summary, the elimination processes are achieved by successively renaming the coefficients according to the following assignments:

$$\left.\begin{aligned} b_{K,2} &\longleftrightarrow (b_{K,2}\, b_{K-1,2} - b_{K,1}\, b_{K-1,3}) \\ b_{K,3} &\longleftrightarrow (b_{K,3}\, b_{K-1,2}) \\ b_{K,4} &\longleftrightarrow (b_{K,4}\, b_{K-2} - b_{K,1}\, b_{K-1,4}) \end{aligned}\right\} K = 2,3,\ldots 2N-1 \qquad (D.3)$$

At this stage all the equations in (D.1) are in the simple form of having only two terms on the left hand side. The value of y_{2N} can be immediately found by solving simultaneously the last two equations in (D.1).

Therefore

$$y_{2N} = \frac{b_{2N,4}\, b_{2N-1,2} - b_{2N,1}\, b_{2N-1,4}}{b_{2N,2}\, b_{2N-1,2} - b_{2N,1}\, b_{2N-1,3}} \qquad (D.4)$$

It can easily be verified that the remaining unknowns can be calculated in a backward order, from the following recurrence formula:

$$y_K = \frac{b_{K,4} - b_{K,3}\, y_{K+1}}{b_{K,2}} \qquad (D.5)$$

APPENDIX E

A METHOD TO PREDICT THE VELOCITY TRANSIENT RESPONSE USING THE PRESSURE DIFFERENCE

This method is applied for the last section of the train-line. The equation describing the velocity at the time level T_{j+1} may be written in this form (see Eqn. (2.25a)).

$$U_{N-1,j+1}(1 + G_2 U_{N-1,j} \Delta X) + \frac{G_1}{P_{N,j}} (P_{N,j+1} - P_{N-1,j+1})$$

$$= U^2_{N-1,j} + U_{N-1,j} \qquad (E.1)$$

The theoretical results of the velocity $U_{N-1,j+1}$ in Fig. 4.5, show that the value of the velocity $U_{N-1,j+1}$ does not exceed .006, that means the flow is always laminar in the last section. Based on this fact, the term $U^2_{N-1,j}$ can be neglected in comparison with the other terms in Eqn. (E.1). The difference between the terms $U_{N-1,j+1}$ and $U_{N-1,j}$ can also be neglected. Now Eqn. (E.1) may be rewritten in this form:

$$U_{N-1,j+1} = \frac{G_1}{G_2 \bar{P}_{N,j} \Delta X} \qquad (E.2)$$

But from Eqn (2.19)

$$\frac{G_1}{G_2} = \frac{2\, d_p\, \gamma}{l\, f} \tag{E.3}$$

and from Eqn. (B.1)

$$f = \frac{64}{Re^{*}\, \bar{P}_{N,j}\, U_{N-1,j}} \tag{E.4}$$

Substituting $\frac{G_1}{G_2}$ from Eqn. (E.3) to (E.2) and f from Eqn. (E.4) to (E.2) leads to

$$U_{N-1,j+1} = Y \left[P_{N-1,j+1} - P_{N,j+1}\right] \tag{E.5}$$

where,

$$Y = \frac{\gamma\, d_p\, Re^{*}}{32\, l\, \Delta X} \tag{E.6}$$

or

$$\left.\begin{aligned} U_{N-1,j+1} &\propto \left[P_{N-1,j+1} - P_{N,j+1}\right] \\ &\propto \delta \end{aligned}\right\} \tag{E.7}$$

That mean by measuring the pressure difference δ between two neighbouring nodes N and N-1, one can be able to predict the velocity transient response of

the last section of the train-line from Eqn. (E.5). The value of Y for this train-line model is equal to .367.

APPENDIX F

LINEARIZED TRAIN-LINE MATHEMATICAL MODEL

F.1 Transmission Line Model

If the leakage is concentrated towards the rear-end of the line, the train-line may be linearized and simulated as RLC blocked transmission line [8], assuming that the influence of the leakage does only affect the in-line resistance. Fig. F.1 shows an infinitisimal section of the line, the parameters are 2 in-line impedance, Z, and the shunt admittance, Y. The in-line parameters are the distributed resistance per unit length R, and the inductance per unit length L. The shunt parameter is the capacitance per unit length C.

In the Laplace domain s, the in-line impedance Z and the shunt admittance Y of the linearized train-line model are:

$$\left.\begin{aligned} Z(s) &= R + Ls \\ &= Cs \end{aligned}\right\} \qquad (F.1)$$

where,

s = complex number

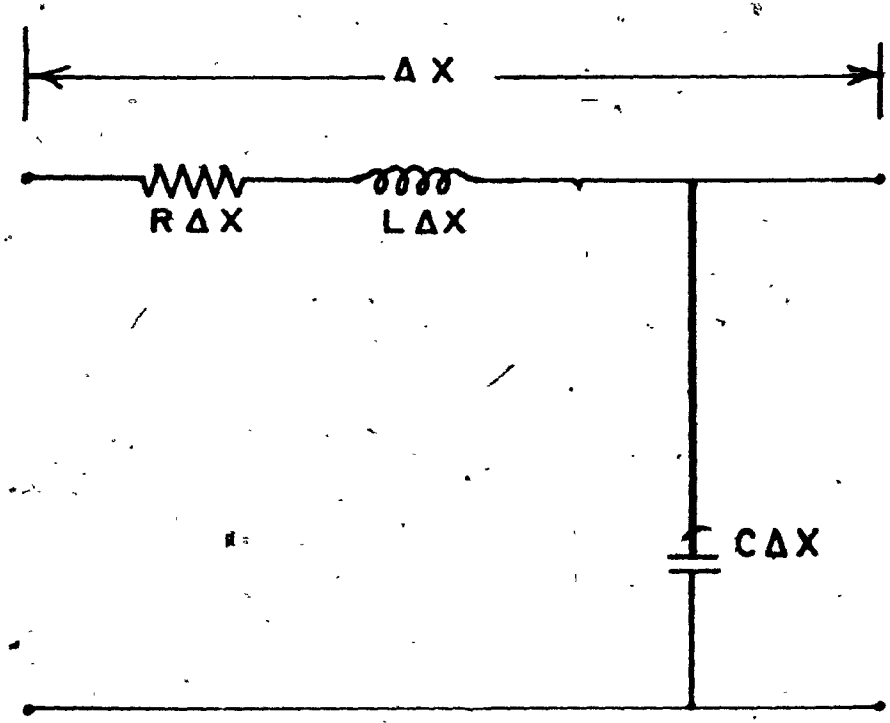

Fig. F.1 The RLC Transmission Line Section

An important parameter is the propagation function per unit length, defined as

$$\Gamma(s) \triangleq \left[Z(s) \cdot Y(s)\right]^{1/2} = \frac{1}{a}\left[s(\omega_f + s)\right]^{1/2} \qquad (F.2)$$

where,

a =acoustic speed (adiabatic)

$$= \frac{1}{\sqrt{LC}},$$

and where ω_f is defined as the friction characteristic frequency (=R/L). For convenience the following non-dimensional characteristic number is defined as:

$$N_K = \frac{a}{\omega_f \, l}$$

For a semi-infinite line, the ratio between the pressure at the head-end P(0,s) and the pressure at the rear-end P(l,s) is

$$\left.\frac{P(l,s)}{P(0,s)}\right|_{\text{semi-infinite}} = e^{-l\Gamma(s)} \qquad (F.3)$$

On the other hand, the blocked line presents a different situation as can be seen below

$$\left.\frac{P(l,s)}{P(0,s)}\right|_{\text{Blocked Line}} = 1 \;/\; \cosh\,(l\Gamma(s) \qquad (F.4)$$

F.2 Line Parameters

The most appropriate signal variables for compressible flow lines are pressure difference (Δ p) and mass flow (m). With these variables the time dependent parameters per unit length, inertance and capacitance may be expressed as:

$$L = \frac{1}{A} \tag{F.5}$$

$$C = \frac{A}{\gamma R_g \theta} \tag{F.6}$$

where A is the cross-sectional area of the line, R_g is the gas constant, θ is the absolute temperature, and γ is the ratio of specific heats, assuming that the polytropic exponent has a constant value during the signal propagation period. In terms of these parameters the acoustic propagation speed is:

$$a \triangleq \frac{1}{\sqrt{LC}} = \sqrt{\gamma R_g \theta} \tag{F.7}$$

The in-line resistance parameter is the most crucial one in causing this delay. An expression for the turbulent resistance can be obtained from the Dracy-Weisbach equation [15] and the equation of state. A small pressure change (Δ p) along an infinitesimal section of the line (Δ x) has the form:

$$\Delta p = \frac{F \ \Delta x \ m^2}{2 \ p(x)}$$

where, $F = \frac{f \ R_g \ \theta}{d \ A^2}$, f is the friction factor, d is the line diameter, l is the total length of the transmission line and p(x) is the pressure at the section of line. There is a continuous mass flow through the line. The in-line resistance will depend on the magnitude of the through-flow. The pressure along the line may be expressed in terms of a constant supply pressure at the entrance of the line p(0) and the mass flow as follows:

$$p(x) = \left[p(0) - F \ x \ m^2\right]^{1/2} \qquad (F.9)$$

Now the resistance per unit length along the line is defined as:

$$R \equiv \frac{1}{\Delta x} \cdot \frac{d\Delta p}{dm} \qquad (F.10)$$

If Eqns. (F.8) and (F.9) are used in conjunction with Eqn. (F.10), the resistance per unit length may be written as:

$$\frac{R}{Fm/p(0)} = \frac{1}{2} \left\{ \left[\frac{p(0)}{p(x)}\right]^3 - \left[\frac{p(0)}{p(x)}\right] \right\} \qquad (F.11)$$

Fig. F.2 is a schematic drawing showing the typical

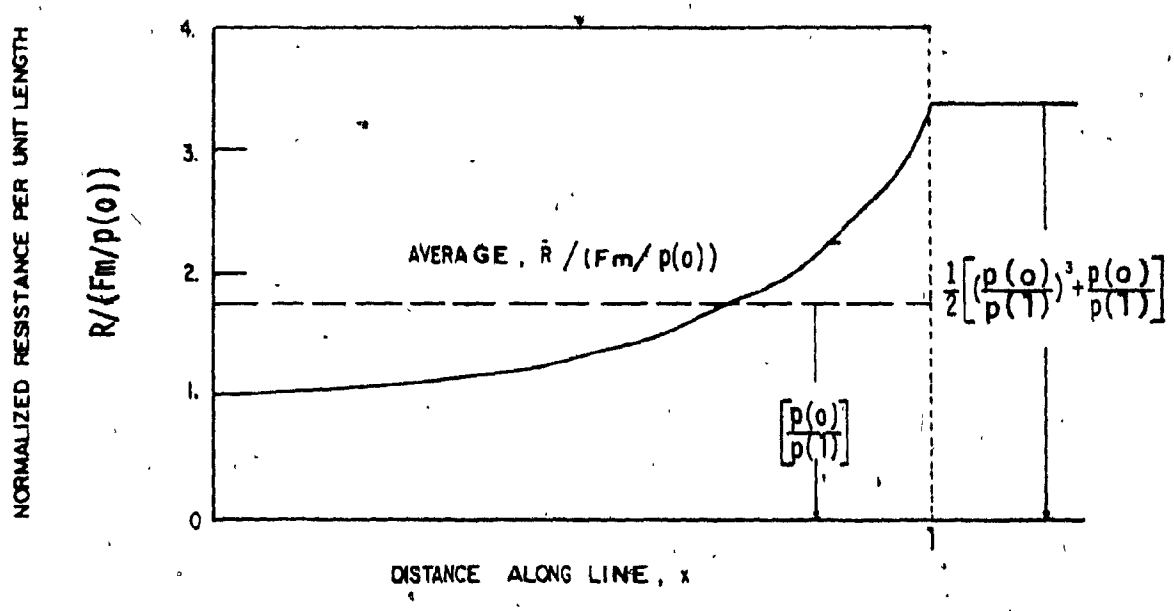

Fig. F.2 Schematic Drawing of Resistance Along the Line

relation between unit resistance and position along the line. The resistance increases monotonically from the front to the rear of the line as the pressure decreases. An average unit resistance, $\bar{R}$, may be defined as:

$$\bar{R} = \frac{1}{l}\int_0^l R\ dx \tag{F.12}$$

If Eqns. (F.9), and (F.11) are substituted into Eqn. (F.12), the integration yields:

$$\frac{\bar{R}}{Fm/p(0)} = \frac{p(0)}{p(l)} \tag{F.13}$$

or

$$\bar{R} = \frac{p^2(0) - p^2(l)}{m\ l\ p(l)}$$

where p(l) is the pressure at the end of the line. The average value of the resistance is shown in Fig. F.2. This was an attempt to linearize the train-line mathematical model, if the leakage is concentrated towards the rear-end.

F.3 Experimental Determination of Line Resistance

In the experiments the head-end pressure is maintained constant, while the valve at the rear-end is adjusted in discrete increments to provide increasing flow through the line. At each valve setting the rotameter and the rear-end pressure transducer readings are recorded. It

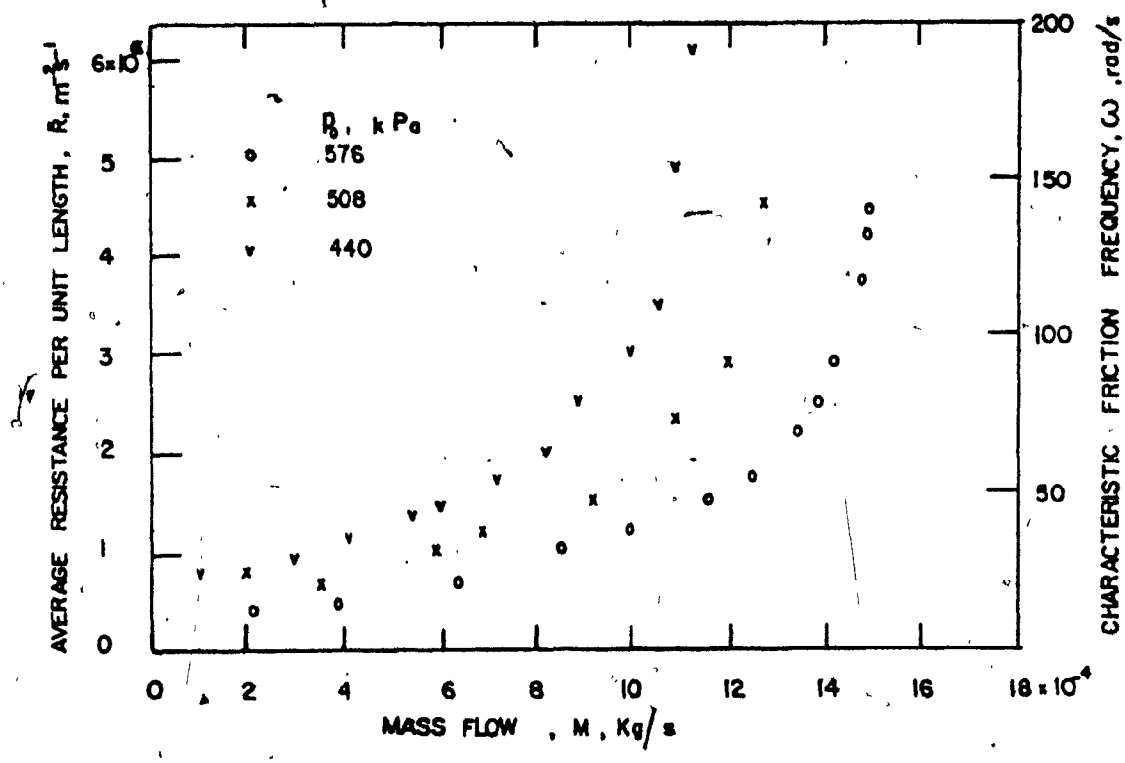

Fig. F.3 Resistance and Characteristic Frequency vs. Mass Flow (l = 257)

should be emphasized that the generation of the through-flow in the line is only used to obtain a highly resistive line. In addition, the velocity of the throughflow is always less than 12 percent of the acoustic velocity.

The resistance tests are performed at three head-end pressure levels, 575, 508 and 440 kPa abs. At each level the resistance could be determined from the slope of the least-square pressure difference-flow characteristic calculated from the data. However it seemed more systematic to use the data points directly in Eqn. (F.10). For the lower flows the difference in the two methods is not appreciable. However there is a considerable discrepancy at the higher flows where the slope of the characteristic is quite steep.

Fig. F.3 shows the average unit resistance versus mass flow for the 257 m line. At all head-end pressures, the resistance increases with the increase of the mass flow. For the higher flows the pressure setting has an inverse effect on the resistance. As the head-end pressure increases the resistance decreases. This is the consequence of the increase in density with pressure. The right hand ordinate of Fig. F.3 is the characteristic friction frequency. This is related to resistance by an area scale factor ($\omega_f = R\ A$). The friction frequencies are all larger than the viscous characteristic frequency (laminar flow, for

which this pipe size would be ω_v = 10 rad/s.

The friction frequencies that are determined from the average resistance concept, are then used in the calculation of the corresponding values of N_k.

APPENDIX G

ANALYTICAL SOLUTION

OF

THE LINEARIZED TRAIN-LINE MATHEMATICAL MODEL

(BLOCKED TRANSMISSION LINE)

The step response of a semi-infinite transmission line has been very well documented by Chirlain [34]. It can be derived by taking the Laplace inverse of Eqn. (F.3). From this solution, the final steady state value of the pressure at a 100% of the total length down the line is,

$$P(1,\infty) = P(1) \tag{G.1}$$

The step response solution may be written as:

$$\left.\frac{p(1,T)}{p(1)}\right|_{SI} = H(T-1)\left[e^{-\frac{1}{2N_k}} + \frac{1}{4N_K^2}\int_1^T \frac{e^{-\frac{1}{2N_K}}\, I_1(\nu)}{\nu}\, dZ\right] \tag{G.2}$$

where,

Z = a dummy variable of the integration.

$$\nu = \sqrt{\frac{Z^2 - 1}{2N_K}}$$

$$T = \frac{ta}{I}$$

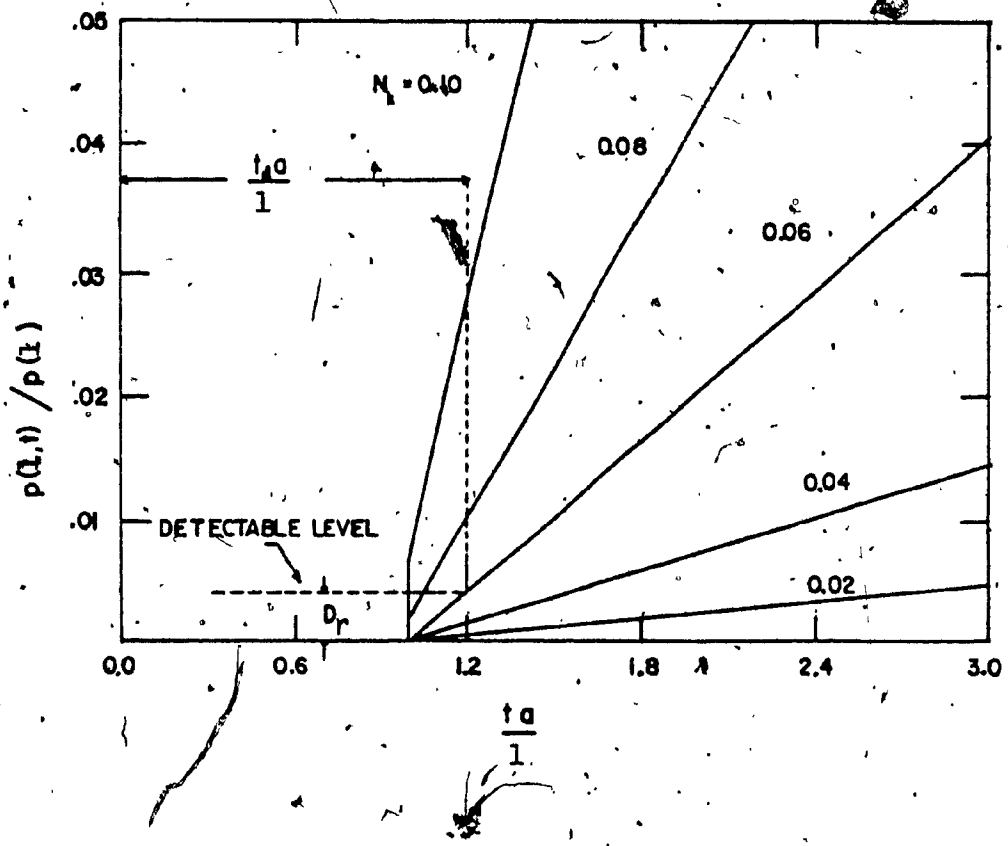

Fig. G.1. Pressure vs. Time with Different N_K as a Parameter for Semi-infinite Line

T = ratio of time to acoustic delay.

$H(T) = 1$ for $T > 0$

$= 0$ for $T \leq 0$

$I_1(\nu)$ = modified Bessel function of the first kind and of order 1.

For cases where $N_k = 0.1$ and smaller, Eqn. (G.2) is illustrated in Fig. G.1. In all cases acoustic delay is experienced, after which pressure begins to rise more or less linearly with T. However, this response will be observed experimentally only if a given transducer is infinitely sensitive. In practice, as in the case of the sensing part of a pneumatic brake valve, the transducer threshold (D_r) is finite (i.e. not infinitesimal). The result is that the pressure at point x = 1 is observed to have a delay greater than the acoustic delay (T = 1). In fact, as seen from Fig. G.1, the greater the threshold, the larger the operative delay. Similarly, it is also larger for a smaller value of N_k. Analytically, this delay is obtained by solving for T_D, such that

$$p(1,T_D) = D, \qquad D_r = \frac{D}{p(1,1)} \tag{G.3}$$

A similar representation of the step response can be

developed for a blocked line, starting from Eqn. (F.4). However, by applying the Taylor expansion to this expression, and taking the inverse Laplace transformation term by term. It can be shown that as the first term contains H(T-1) the following terms contain H(T-3), H(T-5), and so on. Since the objective is to investigate the propagation delay rather than the entire transient, it is quite sufficient to include in the solution the first term only, while ignoring the rest of the series solution which commences only to take effect after 3 times the acoustic delay. This yields a rather convenient solution which can be shown to be,

$$\left.\frac{p(1,T)}{p(1)}\right|_B = 2\left.\frac{p(1,T)}{p(1)}\right|_{SI} \qquad (G.4)$$

On the other hand, in the present context, it is quite sufficient to study a semi-infinite line to analytically predict the propagation speed (V) of the blocked line (Linearized train-line). The propagation speed is defined as:

$$\frac{V}{a} \triangleq \frac{1}{T_D} \qquad (G.5)$$

with respect to a transducer threshold of D_r, where T_D is obtained by solving,

$$\frac{p(1,T_D)}{p(1)} = 2\left.\frac{p(1,T_D)}{p(1)}\right|_{SI} = D_r \qquad (G.6)$$

The solution is implicit in T_D, and hence best handled either by numerical re-iteration or graphically. Fig. G.2 shows the relation of the propagation speed and N_k for various values of the relative transducer threshold sensitivities D_r of 0.001, 0.002 and 0.01. In each case, the propagation speed increases with N_k. Furthermore it approaches acoustic speed in the limit.

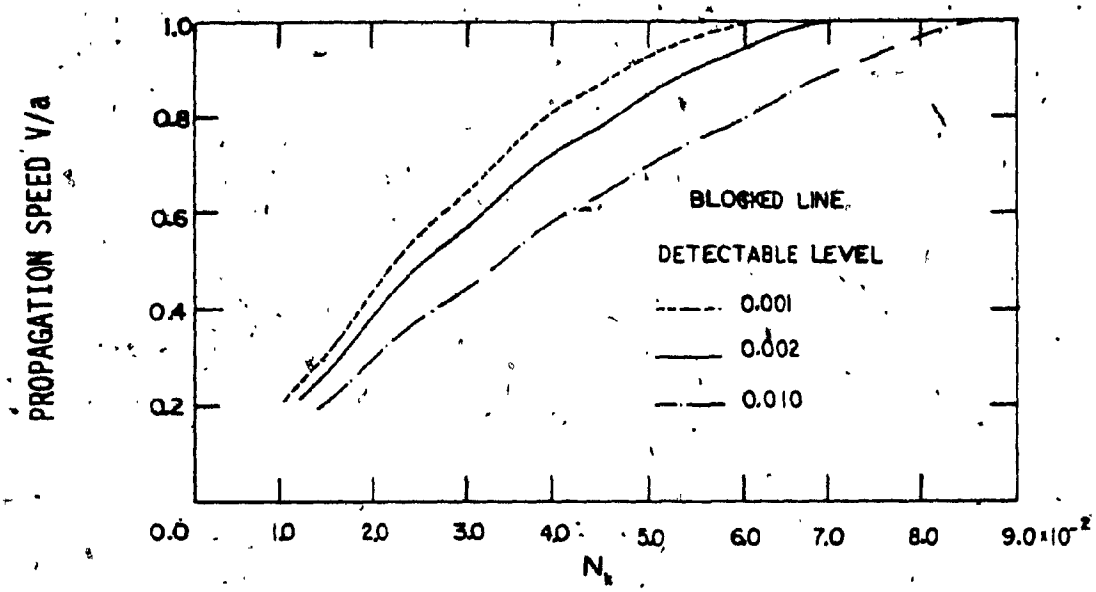

Fig. G.2 Propagation Speed vs. N_K with Different Detectable Level for Blocked Line

APPENDIX H

EXPERIMENTAL DETERMINATION OF PROPAGATION SPEED FOR BLOCKED TRANSMISSION LINE

The theory developed in Appendix (G), is independent of the direction of the step change. (See Eqns. (G.3) and (G.6)). Nevertheless, in the experiments both types of changes are investigated. To produce a negative change simulating a pressure reduction in brake application, a valve at the head-end is suddenly opened to vent the line to atmosphere. To produce a positive step, similar to a recharge signal in brake release, the head-end is suddenly switched to a source of higher pressure by means of a 3-way valve. The result is that a compression wave travels down the line.

Experimentally, the time delay is obtained by displaying the output of the 2 pressure transducers, one is located at the head-end and the other is located at the rear-end, on a storage oscilloscope. The head-end pressure rises sharply, and so the response is independent of the sensitivity threshold of the transducer. The rear-end tranducer responds slowly. The delay is strongly influenced by the sensitivity threshold. In the experiments, a threshold of $D_r = 0.001$ is assumed. The time delay is scaled directly from the oscilloscope. The propagation is

then calculated accordingly.

The results are shown in Fig. H.1 for a pressure reduction (discharging) from different initial pressures; and Fig. H.2 for charging and discharging from the same initial pressure. In all cases, the propagation speed V/a is plotted against N_k. The values of N_k used are determined from the experimental measurements and some theoretical consideration that are developed in Appendix G. The solid line in Fig. H.1 and H.2 represents the theoretical values of $D_r = 0.001$ for a blocked line (See Appendix G). There is considerable spread among the data points, and discrepancy with the theory probably goes as high as 30%. It may even be observed from Fig. H.2 that the results from the charging tests are in better agreement with the solid line. Nevertheless, the trend is firmly established by the theoretical curve in all the cases.

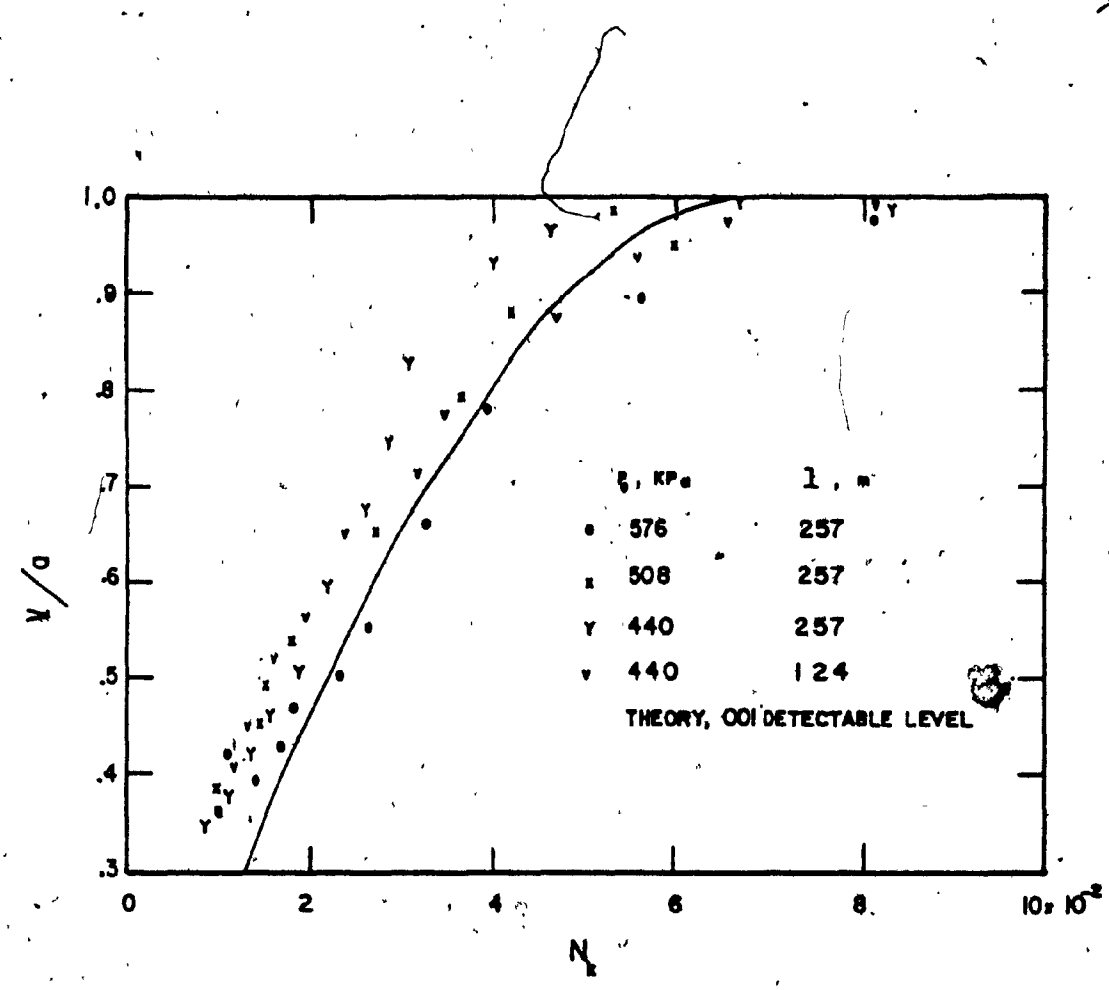

Fig. H.1 Propagation Speed vs. N_K for Discharging Line

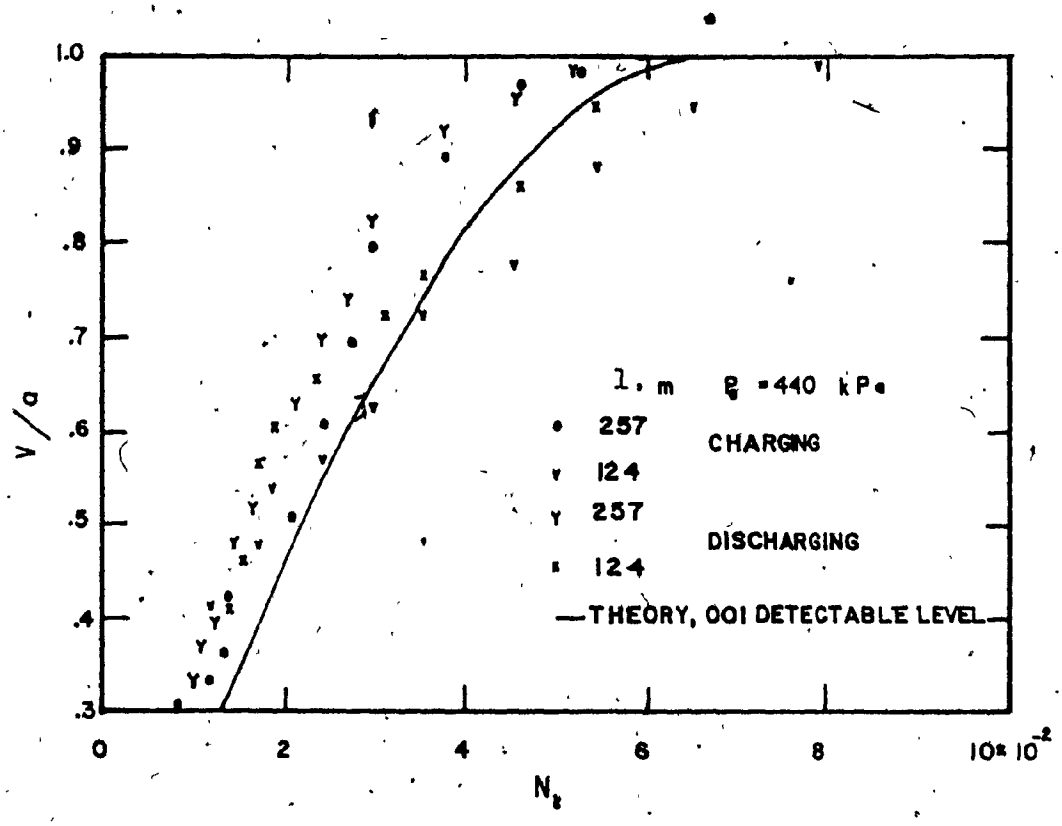

Fig. H.2 Propagation Speed vs. N_K (P_o = 440 kPa) for Charging and Discharging